Functionalization, bio-conjugation and toxicity studies of quantum dots

Lucia Mattera

Communauté
UNIVERSITÉ Grenoble Alpes

THÈSE

Pour obtenir le grade de

DOCTEUR DE LA COMMUNAUTÉ UNIVERSITÉ GRENOBLE ALPES

Spécialité : **CSV/Chimie-Biologie**

Arrêté ministériel : 7 août 2006

Présentée par

Lucia MATTERA

Thèse dirigée par **Peter REISS**
Et co-encadrée par **David Djurado**

préparée au sein du **Laboratoire INAC/SPrAM UMR5819/LEMOH**
dans **l'École Doctorale Chimie et Sciences du Vivant**

Fonctionnalisation, bio-conjugaison et études toxicologiques de quantum dots

Thèse soutenue publiquement le **10 juin 2016**
devant le jury composé de :

Prof. Frédérique LOISEAU
Professeur à l'Université Grenoble-Alpes, Présidente du jury
Dr. Michel de WAARD
Directeur de recherche INSERM, Rapporteur
Dr. Thomas PONS
Chargé de recherche INSERM, Rapporteur
Dr. Loïc CHARBONNIERE
Directeur de recherche CNRS, Examinateur
Prof. Niko HILDEBRANDT
Professeur à l'Université Paris Sud, Examinateur
Dr. David DJURADO
Directeur de recherche CNRS, Co-encadrant de thèse
Dr. Peter REISS
Chercheur au CEA Grenoble, Directeur de thèse
Dr. Claudia TORTIGLIONE
Chercheur au CNR, Pozzuoli, Invitée

To my beloved parents and Massimo

for their everlasting love and support….

Remerciements

A ce moment, ce sera que désormais je sens l'odeur des changements, fermant les yeux pour un moment, je revins mentalement le long voyage qui m'a conduit ici. Je me suis souvenu de toutes les années, je me suis souvenu des visages, des situations, les contre-charmes habituels, les appels téléphoniques désespérés, des sourires béats, le temps formidable que j'ai passé. Encore, le jour fantastique de ma soutenance, la présence de toutes les personnes qui sont restées jusqu'au but de la discussion. Les personnes de prêt et da loin qui m'ont suivi pendant ce voyage sont impressionnant et je n'aurai pas les paroles pour exprimer ma gratitude et mon remerciement à leur égard.

Je vais essayer de remercier tous en espérant de n'oublier personne, vous êtes beaucoup !!

Tout d'abord je souhaiterais commencer à adresser mes sentiments de gratitude à mon directeur de thèse, Peter Reiss pour m'avoir donné l'opportunité d'entreprendre ce voyage. Il a eu beaucoup de confiance en moi et j'ai eu la possibilité de m'améliorer et d'apprendre des domaines différents, de participer à des conférences nationales et internationales, formations, écoles thématiques, etc. Tout ça étaient des expériences formidables et uniques que je garderai toujours comme un don précieux dans ma vie. Peter, tu es formidable, c'était un plaisir et un honneur d'être étudiante dans ton laboratoire et ma gratitude est si grande. Merci aussi pour le temps précieux que tu as dédié à corriger mon manuscrit et pour tous les conseils.

Je remercie vivement mon co-encadrant David Djurado, il a eu aussi beaucoup de confiance en moi, David, merci pour les discussions pas seulement scientifique mais aussi de danse et de vie ;) et surtout pour tous le support soit moral soit scientifique, que tu m'as toujours donné et encore plus marqué dans le dernier période. Merci pour les remarques si précieux qui était de conseil fondamental pour l'écriture et pour avoir dédié aussi toi beaucoup de temps pour les corrections. Merci pour ta bonne humeur et pour la personne formidable que tu es !

Je tiens à remercier Michel de Waard et Thomas Pons d'avoir accepté d'être rapporteurs pour cette thèse et de leur intérêt marqué pour ce travail, d'avoir eu la patience de lire en détail mon manuscrit. Je suis honoré d'avoir été examiné par ce comité si prestigieux et je suis flattée pour ses appréciations sur mon travail. J'ai particulièrement appréciée l'intense et enrichissante discussion que nous avons eu lors de la soutenance. Merci beaucoup.

Mes remerciements vont également aux autres membres de mon jury Loïc Charbonnière et Niko Hildebrandt qui ont eu la gentillesse de faire partie aussi de mon comité de suivi de thèse durant ces trois années, et qui m'ont apporté de précieux conseils dans les directions à prendre sur ce sujet et pour l'enthousiasme que vous avez démontré pour mon travail. Merci beaucoup aussi à Frédérique Loiseau d'avoir accepté d'être présidente du jury.

Je tiens aussi à adresser mes plus sincères remerciements à Claudia Tortiglione (CNR, Pozzuoli Italy) pour le temps qu'elle m'a généreusement consacré toujours depuis que j'étais étudiante de master dans son laboratoire. Pour m'avoir donné l'opportunité aussi d'entreprendre ce voyage et pour m'avoir poussée à partir, pour l'amour, l'estime... Merci pour être venu à Grenoble et d'avoir faire partie de mon jury de thèse aussi, pour avoir accepté de collaborer alors que j'ai pu amplifier mon projet de recherche avec des données superbes de nanotoxicologie et pour le temps que tu m'as toujours dédiée. Je vais remercier également ta co-bureau Angela Tino pour m'avoir toujours stimulé d'améliorer et d'envisager tout dans une vision critique. Merci à vous deux pour tout, pour m'avoir encouragé, pour les conseils judicieux, pour votre disponibilité et l'intérêt et grâce à eux que j'ai pu aussi conquérir une nouvelle étape ici à Grenoble. Grazie infinite! Je leur souhaite beaucoup de bonheur et in bocca al lupo per tutto !

Mon travail de thèse a été accompli dans le cadre de l'ANR NanoFret, que je vais remercier pour avoir financier cette thèse et je voudrais remercier tous ceux qui en font partie : Shashi Bhuckory, David Wegner, Niko Hildebrandt (Nano Bio Photonics. Institut d'Electronique Fondamentale. Université Paris-Sud). Merci pour m'avoir accueillie dans votre laboratoire et pour le travail fait ensemble!), Loïc Charbonnière (IPHC, Strasbourg), Emmanuel Bois et Valerie Vallois (Cezanne ThermoFisher, Nîmes). Merci pour ce projet si passionnant, intéressant et multidisciplinaire, pour les réunions et pour votre professionnalité et bon humour. C'était un plaisir collaborer et travailler avec vous et je suis reconnaissante pour avoir eu l'occasion d'aborder différents domaines.

Un remercîment spécial en plus à Niko Hildebrandt et sa famille qui m'ont accueilli chez eux pendant mon séjour dans l'équipe NanoBio Photonics, pour les bons moments passés ensemble et en particulier la conférence à Paris « 30 years of colloidal quantum dots » pendant laquelle tu m'as pris photo avec presque tous les plus grands chercheurs (y compris toi et Peter ;)) sur le QDs ☺ Je ne pourrais pas oublier tous ces bons moments passés ensemble et je vous remercie encore pour tous.

Remerciements

Un clin d'œil pour Shashi car on a traversée ensemble le gros de notre projet, merci pour tous le soutien aussi avant les conférences et pour tous nos discussions scientifiques et non-scientifiques ☺. Tu es un grand et bravo jeune chercheur. Grazie infinite Shashi….Je te souhaite le mieux pour le futur. A toi de jouer maintenant. ;)

Je tiens également à remercier toutes les personnes qui ont corrigé une partie de ma thèse, ainsi que toutes les autres personnes avec qui j'ai eu l'occasion de collaborer au cours de ma thèse.

Alors, un remerciement spécial au NanoBiomolecular group en Italie et tout particulier à Mariateresa Allocca et Alfredo Ambrosone pour la collaboration et l'échange avec le projet de nanotoxicologie. Siete fortissimi e vi auguro il meglio nella vita e nel futuro professionale. Un grande in bocca al lupo soprattutto a te Mariateresa ;). Un grande merci à les petit Hydra aussi :p.

Un vif remerciement à Adeline Tarantini et Marie Carrière pour le projet de nanotoxicologie aussi. Marie, merci pour ton sourire, ton soutien et tes conseils. Adeline c'était un grand plaisir travailler avec toi, merci pour tous le bon moment passé ensemble, notre discussion pendant les manips, la danse et pour le soutienne morale, tu es devenu une vraie amie. Je te souhaite tant bonne humeur pour la suite et bon courage pour tous ☺ Un grand merci aussi à ta co-bureau Anne Vonkoschembahr pour tout le soutien aussi.

Un grand merci très spécial à Maria Moula-Karimdjy pour la collaboration avec son projet sur le sonde bimodale quantum dot/IRM qu'a enrichi mon manuscrit et pour le bon moment passé ensemble, pour ta gentillesse et bon humour et soutien unique et spéciale, spéciale comme toi. Il me manque déjà travailler en « causalité » avec toi :D. Garde toujours ton bon humour et la magnifique personne que tu es. Je t'adore.

Un remerciement spécial est obligatoire le faire à un autre collaborateur Fabio Annunziata. Grazie per tutto, pour les imagines TEM, pour le temps passée ensemble au travail et en dehors et pour m'avoir faire prouver l'expérience de l'escalade; e a proposito della scalata, non posso non ringraziare anche Luca De Trizio (IIT, Istituto Italiano di Tecnologia, Genova) per la collaborazione, per la scalata e per tutto….Grazie di cuore capo ☺.

Je remercie Emile Rustique, pour m'avoir ouvert les portes de son laboratoire (NanoBio-LETI) lorsque j'en ai eu besoin pour les mesures du diamètre hydrodynamique et du potentiel zeta, et merci aussi à tous les components en particulier, à Arnaud Lemelle, Lisa Racine, Marie Escude et Mathieu Varche pour la patience et l'aide que vous m'avez toujours donnée quand je vous "coloniser" la machine pours les mesures. :D

Merci particulièrement aigu va à mes collègues de laboratoire qui m'ont accompagné lors de ce voyage, anciens (Olga Burchak, Franz Fuchs, Tim Senden (thanks for your excellent quantum dots), Axel Maurice, Aurélie Lefrançois, Ashley Gaulding, Luca Assumma, Jinhyung Park, Mohammad Jouni, Reback Matthew, Maria MendezMalaga) et presente, Louis Vaure, Clement Thomassé, Dorian Gaboriau, Florent Caffy (mon petit frère), Martina Sandroni, Christophe Linchenau, Maxime Godfroy, Cyril Aumaitre, Mathilde Bouchard, Maria Moulakarimdjy, Sebastiano Di Pietro (il grande chimico), Fanny Laporte, Jennifer Molloy pour avoir transformé les jours de laboratoire dans les moments de loisirs et de plaisir, mais surtout pour l'amitié que vous m'avez montrée. Ils m'ont encouragé dans les moments de désespoir et ils ont essayé par tous les moyens de me calmer! Merci aussi pour m'avoir appris la beauté de la langue française ☺. Grazie infinite vi adoro ragazzi !

Et je n'oublie pas tous les gens avec qui on a partagé quotidiennement les couloirs, les déjeuners et les pauses café.

Merci Olga, tu as illuminé mes journées, tu es une femme et chercheur formidable. Nos discussions ont constitué une aide précieuse à mes yeux. Merci pour tous, gardes toujours ton bon humour et ton esprit unique et que donne toujours beaucoup de conforte à tout le monde qu'est à côté de toi. Grazie di cuore, ne pas changer, resta sempre la splendida persona che sei !

Un remerciement très très spécial à mon co-bureau depuis trois ans, Louis, pour m'avoir soutenu depuis toujours, pour la grande patience, l'intérêt et la disponibilité avec laquelle il m'a suivi au cours de ces année, pour l'aide dans le travail, avec le français, pour les précieux conseils et le soutien moral que aussi tous les composants de laboratoire ils ont jamais me faire manqué. Encore pour le truc rigolo que tous, en particulier avec Florent, mon petit frère, vous avez me faire croire tout le temps. C'était des moments formidables. Je vous adore.

Grazie mille Christope j'ai appris plein de choses en travaillant avec toi et j'ai beaucoup aimé toutes les nos discussions scientifiques et non, toujours accompagnées par une très bonne humeur. Grazie mille à ta femme aussi Jennifer, pour tous tes bons conseils et pour tous les bonnes moments passé ensemble. Grazie di cuore, vi auguro tutto il bene di questo mondo.

Remerciements

Un remerciement spécial est également adressé à Charlie Picot soleil moi ☺ pour m'avoir donné toujours beaucoup d'attention, pour m'avoir écouté et compris tous mon humeur et que, avec peu de mots, mais de grands gestes a toujours réussi à me remonter le moral. Grazie infinite ☺

Je remercie également tout le groupe de chercheurs que pendant la pause déjeuner et dans la vie du labo ont contribué à rendre les jours sans soucis et joyeux, en particulier, Frédéric Chandezon (notre grand Chef, merci pour votre chaleureux accueil), Jérôme Planès, Benjamin Grévin, Renaud Demadrille, Pascale Chenevier, Jean-Pierre Travers, Jérôme Faure-Vincent, Dmitry Aldakov, David Aradilla, Yann Kervella…..Merci pour le temps que vous m'avez accordé, pour tout ce que vous m'avez appris, pour votre gentillesse et votre soutien tant sur le plan matériel qu'humain, vos conseils et tous les très bons moments passés ensemble qui ont rendu ces trois années beau, serein et très agréables à vivre au quotidien.

Avec ces gens, j'ai partagé les plus beaux moments, mais aussi le plus dur de cette expérience, j'ai appris à les connaître et à l'aimer : je vous remercie pour tout. Vous êtes spécial, et grâce à tous vous je suis arrivée à la fin de ce voyage ... Je vous adore !

Enfin, je remercie tous ceux qui ont contribué à faire de ces années plus heureuses, partageant avec moi les joies mais aussi les petites déceptions en dehors du laboratoire.

Donc je remercie tous les amis de Grenoble, grâce à eux l'éloignement de la maison était parfois imperceptible, en particulier, Bastien, Carlos, François, Guillaume, Charles, Romuald, Monkrane, Johanna, Simone et i paesani: Stefano, Alessandra, Lisa, Dario. Vi voglio bene Guagliù' !!..et tous mes colloques passée et présent en particulier Onintza (que comme une maman m'as pris à la main et m'aidée à faire mes premier pas dans un pays estranger) et Florent, pour leur patience et soutien de toujours. Tous les membres de mon association de tango ECOS DEL PLATA, en particulier mes prof. José Artigas et Verónica Cordero, et copine Narae Jung et Jeanne Alacoque.

*J'ai un penser spécial pour toi, Narae, « mon petit grande angelo » qui par tes prières, tes encouragements, ton esprit formidable, unique et spécial m'a épaulé moralement tous les jours. Je t'adore. Un grand merci à Hugo aussi^^*

Je remercie également tous mes oncles, cousins et cousines, en particulier Arianna que, avec une patience extrême, comme une sœur, a toujours réussi à me donner la force dans les heures les plus sombres. Je remercie en particulier Zia Anna et Zio Bernhard et Zio Nello pour leur amour énorme pour moi et pour tous les conseils que m'ont toujours donné.

Je remercie tous mes amis pour me mettre en place dans les moments de nervosité, sans eux, tout serait plus difficile. I miei amici di sempre di Ischia, lontani ma vicini : Cristina, Paoluccio, Claudia, Terenz, Marisa et Maria, per avermi sempre sostenuta e mai criticata, hanno condiviso con me emozioni, ansie, successi e insuccessi. Vi voglio bene.

Dans ce voyage, la présence permanente de chaque étape étaient mes parents, mon guide, mon père, le mythe de ma vie, ma mère, femme merveilleuse, ils m'ont donnée beaucoup de courage et elle a eu la force, malgré les difficultés, à être aussi présente lorsque de ma soutenance. Sans eux, je ne l'aurais pas fait même la moitié de ce que maintenant je vais célébrer, ils m'ont répété sans cesse au fil des ans de croire beaucoup en moi-même et m'ont poussée à faire face avec confiance tout ce qui se passerait sans jamais me faire peser tous qu'ils ont dû affronter pédant ces trois années. Grazie di cuore siete la mia vita. <3 Mio fratello, mia cognata e sua madre Anita che mi sono state sempre vicine e la mia dolce nipotina, Sara, sei la più bella del mondo. Ti amo amore di zia !.

Ringrazio inoltre "il mio angioletto" Sonia che veglia sempre su di me dall'alto e Sally che con la sua dolcezza dipinge i giorni bui con fantastici colori ; Gaetano Ponzano, caro amico scrittore e poeta, semplicemente grazie per la tua dolcezza e per il tuo fantastico spirito poetico!

Enfin, je remercie tous ceux avec qui j'ai partagé les petites étapes de ce long voyage, tous ceux qui pour un certain temps, ou bien plus qu'un certain temps, marchait à côté de moi et qui a été en mesure de me faire sentir des émotions fortes, chacune d'eux était un élément fondamental de ce puzzle.

Dulcis in fundo, Massimo, vita mia, je dis merci, merci d'être là, tout simplement. Ti amo!

A tutti voi un grazie di cuore....

Lucia

Table of contents

1 General introduction

1.1 Colloidal semiconductor quantum dots (QDs)

Over the last 30 years, following the pioneering work of Efros, Emikov, Brus and Henglein great advancements have been achieved in the field of colloidal nanocrystals (NCs) synthesis and engineering.[1-4] While early studies focused primarily on CdS and CdSe based NCs and the study of their size-dependent optical properties, the field has now expanded to include various classes of materials with different types of core, shell or passivation chemistry for manifold applications, spanning form biology, optoelectronics to solar and thermal energy conversion.[5] Fluorescent QDs are mainly characterized by their unique optical properties, which make them appealing alternatives to conventional organic dyes in a number of applications, in particular in biological labeling and signaling.[6] Organic dyes are characterized by asymmetric emission spectra and narrow absorption spectra, which means that they can only be excited within a narrow window of wavelengths. QDs instead exhibit narrow, symmetrical and tunable emission spectra according to their size and composition. This allows a closer spacing of different probes without substantial spectral overlap. Furthermore, they also have broad absorption spectra, allowing the excitation of all colors of QDs simultaneously with a single excitation light source and the minimization of sample auto-fluorescence of biological background by choosing an appropriate excitation wavelength.[7, 8] Moreover, they exhibit excellent photostability compared to most organic dyes that suffer of photobleaching,[6] as evidenced in **Figure 1-1.** For all these reasons, a part of our work will be focus on the synthesis and functionalization of QDs in order to replace traditional luminescent probes in biological detection.

Another interesting asset of the QDs is their large surface area giving the possibility to introduce numerous additional functionalities by surface functionalization. The facile linking of multiple functionalities enables the production of multimodal diagnostic and therapeutic agents, including in addition to the possibility of fluorescence detection for example active species and their controlled release, contrast agents for other imaging modes like MRI, molecules for tumor targeting, cell penetration, and so on. These later advantages make QDs ideal candidates for biological sensing and imaging as demonstrated in different studies.[9-11]

For biological purpose, the efforts of researchers to develop QD as probe has focused in particular on the synthesis, solubilization and bioconjugation of highly luminescent and stable QDs, and this part we will discuss in **section 1.2.**

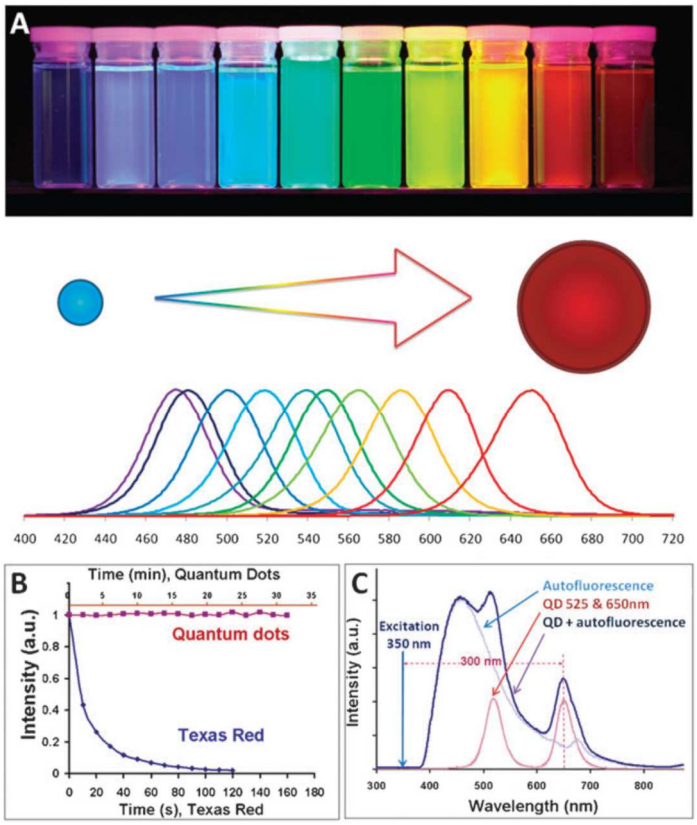

Figure 1-1. Images taken from Ref.[6, 10], representing the unique photo-physical properties of QD probes. **A)** Narrow size-tunable light emission profile enables precise control over the probe color by varying the nanoparticles size. **B)** Photobleaching curves showing that QDs are several thousand time more photostable than organic dyes under the same condition, whereas their quick photobleaching limits accurate quantitative analysis. **C)** Comparison of mouse skin and QD emission spectra, demonstrating the capability of absorbing high-energy (UV-blue) light of QDs allow efficient separation of the QD signal over fluorescent background.

1.1.1 Definition and photophysical properties of QDs

Colloidal semiconductor NCs or QDs are crystalline particles of dimensions between 1 and 10 nm, i.e. in most cases significantly smaller than the exciton Bohr diameters of the associated semiconductors. In this case, the electron-hole pair (exciton) is “squeezed” in the particle and the optical properties of the QDs are depending on their size. The biggest particles experience the lowest spatial confinement hence the longest emission wavelength and vice versa. Beside the influence on the band gap, which is a function of the QD diameter, the quantum confinement effect also leads to the discretization of the electron and hole energy levels (**Figure 1-2**). The relative positions of the highest occupied state and lowest unoccupied state, equivalent to the highest occupied molecular orbital (HOMO) and lowest unoccupied molecular orbital (LUMO) for molecular dyes, and corresponding to the top of the valence band and the bottom of the conduction band of the bulk material, are determined by the size of the QD.

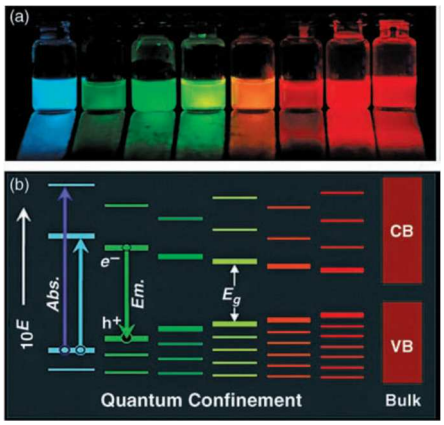

Figure 1-2. Quantum confinement effect: **a)** size-dependent emission of CdSe QDs under UV light **b)** Discretization of the valence and conduction bands (VB, CB) into discrete energy levels. Absorption (Abs.) takes place of photons with larger energy than the band gap energy (Eg), fluorescence emission (Em.) occurs from the lowest excited level to the highest ground state level.[12]

One of the challenges in QD synthesis is that their optical properties can be dramatically affected by surface trap sites. Unpassivated surface atoms can act as recombination centers for photoexcited carriers and diminish or even extinct fluorescence emission. In order to passivate them and increase the fluorescence intensity of the QDs, the most widespread approach consists in coating them with shells of semiconductors of different nature (**Figure 1-3**).[13] In such core/shell NCs the emissive core is surrounded by a shell of a few atomic layers of a larger band gap semiconductor. The shell greatly improves the photoluminescence quantum yield (PL QY) as well as the photo- and chemical stability of the QDs, while the size of the core determines the emission wavelength of the QD.

Figure 1-3. Illustration of core, core/shell and core/shell/shell QDs.[14]

In this case, the band alignment of the core and shell materials is chosen in a way that the conduction band edge of the shell (the higher band gap material) is of higher energy than that the core (the lower band gap material), and the valence band edge of the shell has lower energy than that the core (type I alignment). Consequently, both electrons and holes are confined in the core. CdSe/ZnS and InP/ZnS core/shell NCs are typical examples. There are also other core/shell systems, in which one of the carriers is localized in the

core and the other one in the shell, namely in cases of staggered (type II) band alignment. CdSe/ZnTe and InP/CdSe are examples where the electron (hole) is confined in the core and the opposite carrier in the shell.[15] Interestingly, the resulting band gap of such type II systems is narrower than the gap of each of the constituting materials. On the other hand, generally an additional outer shell of a large band gap material is required as the carrier localized in the shell can easily be trapped on surface states. Such core/shell/shell systems find also widespread use in type I systems, the most intensively investigated being CdSe/CdS/ZnS. In this case, the intermediate shell serves as "lattice adapter", i.e. its purpose is to reduce crystallographic strain at the interface between the core and outer shell material. Even though lattice mismatch is less a problem in 0D QDs than in 2D quantum wells, its value should not exceed 10% (like in CdSe/ZnS) and ideally is below 5% (like in CdSe/CdS and in CdS/ZnS).

Nowadays it is possible to synthesize QDs that emit within the whole visible and NIR spectral regions by tuning the size and/or the composition of the particle. **Figure 1-4** shows the emission ranges reported for different types of QDs. Nonetheless, to date most of the studies focus on cadmium chalcogenide NCs like CdSe, whose intrinsic toxicity restricts their wide-scale application. Indium phosphide (InP) is one of the most promising alternatives.[16] It is a III-V semiconductor (bulk value of $\mathbf{E}_g$: 1.35 eV) with a Bohr exciton radius of ~ 10 nm.[17] Its photoluminescence can be tuned from blue to the near infrared by varying the size of the NCs and the very limited number of toxicological studies indicate a much lower intrinsic toxicity compared with CdSe.[18, 19]

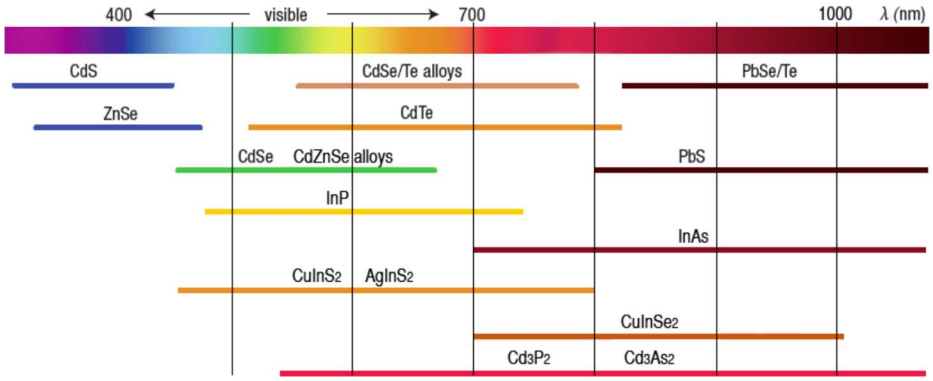

Figure 1-4. PL emission ranges for the most studied types of semiconductor nanocrystals.[20]

Although the optical properties of InP-based NCs in terms of PL line width and QY are (still) inferior to the best reported Cd-containing QDs, significant progress in their chemical synthesis has been made in the past decade. While InP core NCs have a QY of less than 1%, values above 50% have been reported for InP/ZnS core@shell NCs.[21, 22] Our team reported the single-step synthesis of InPZnS alloy NCs reaching a PL QY >60%.[23, 24] Using Zn in the synthesis of the core InP NCs, leading to InZnP alloy QDs, also enables to greatly

enhance the emission efficacy.[25] The best value reported today (85%) has been obtained by using a thin GaP interfacial layer between the InZnP core and the ZnS shell.[26]

1.2 QDs in biotechnology

1.2.1 Surface functionalization

The use of semiconductor QDs as biological fluorescents probes requires that they (**a**) are water soluble, (**b**) present long-term colloidal stability without aggregation and precipitation, (**c**) offer reactive groups on their surface, and (**d**) maintain their photophysical properties when transferred into aqueous buffer. NC surface functionalization is a process consisting in the introduction of amphiphilic or hydrophilic organic molecules or macromolecules, peptides or other bioactive molecules on the surface of the QDs in order to induce water solubility, prevent their aggregation, enhance their resistance to oxidation, reduce their toxicity, optimize their behavior (e.g. circulation, uptake) in biological environment and allow their link with specific targets.[27]

High quality QDs are mostly synthesized in non-polar organic solvents; their hydrophobic surface must be converted to a hydrophilic one in order to solubilize them in aqueous buffer. This solubilization procedure of QDs in aqueous media while maintaining their emission properties and achieving high colloidal stability is a great challenge. It can be achieved by either (**a**) *ligand exchange*, a process primarily driven by mass-action in which the native hydrophobic ligand is substituted with bifunctional ligands or by (**b**) *encapsulation* of the original hydrophobic QD within a heterofunctional amphiphilic coating. In the latter case the strategy is based on compounds capable of assembling with the QD surface via hydrophobic interactions and bearing amphiphilic moieties leading to the desired change of solubility (**Figure 1-5**). The hydrophobic domain allows for the encapsulation of QDs by a hydrophobic cavity whereas the hydrophilic domain enables the dispersion of QDs in aqueous solution. The coating molecules include phospholipids, bock copolymer, liposomes and appropriate precursors for generating a silica shell around the particles.[10, 28] This solubilization strategy can easily be extended to insert additional functionalities on the QD surface. Another appealing feature of the encapsulation strategy is the conservation of the PL QY as the initial surface state is not modified.

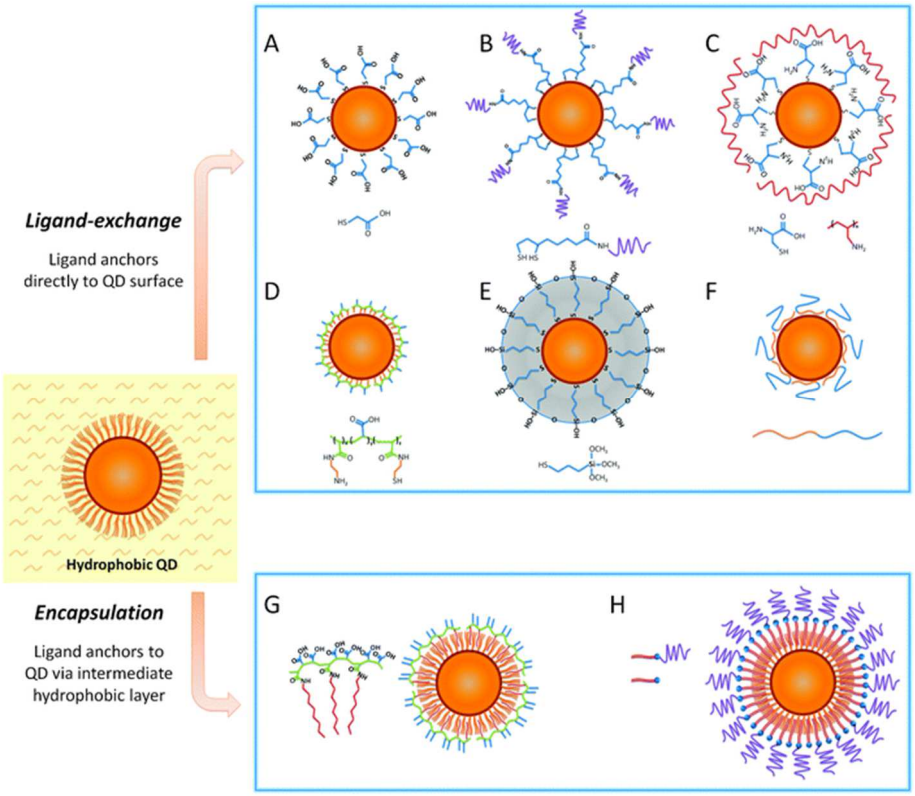

Figure 1-5. Scheme illustrating different strategies for the water solubilization of hydrophobic QDs. **A-F**: Ligand-exchange procedures; **G-H**: encapsulation procedures.[10]

In contrast, ligand exchange with bifunctional molecules containing an anchoring site for the QD surface and a hydrophilic site assuring dispersibility of the QDs in aqueous media is a method that radically changes the surface of the NCs. By consequence this strategy bears a high risk of diminishing the PL QY through the generation of surface trap states. These can trap charge carriers despite a protective inorganic shell because the latter is generally only a few atomic layers thick and therefore the escape of the carriers to surface states, e.g. via tunnelling, is still possible. On the other hand, the ligand exchange strategy has a strong potential for providing QDs that are smaller in size than the encapsulation technique, which can be of importance for some applications (see below). It also offers the possibility of coupling biological entities.[29]

Most procedures for ligand exchange use bifunctional thiol-based molecules for the incubation with the hydrophobic QDs, which are usually coated with fatty acid or trioctylphosphine oxide (TOPO) ligands.[30] Thiols can strongly interact with ZnS, which is the most widely applied shell material for QDs. Common examples of such ligands are thioalkyl acids containing a carboxylate terminal group such as mercaptoacetic acid (MAA), mercaptopropionic acid (MPA), or mercaptoundecanoic acid (MUA). In their thiolate form these molecules interact strongly with the ZnS surface of the QDs, exposing the polar carboxylate group to the surrounding solution and imparting aqueous solubility (**Figure 1-6**).[31]

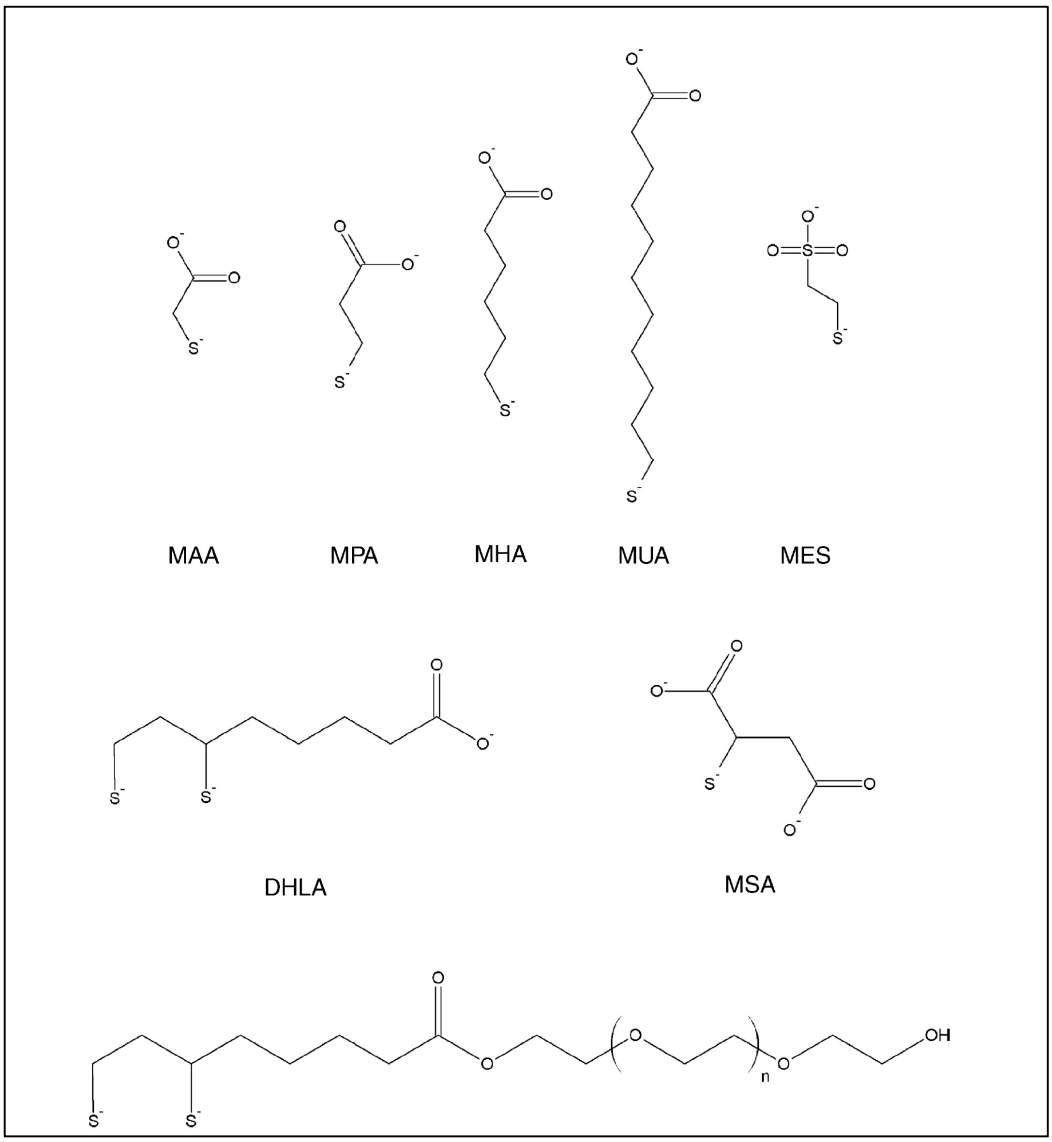

Figure 1-6. Commonly used thioalkyl acid ligands for aqueous solubilization of QDs: mercaptoacetic acid (MAA), mercaptopropionic acid (MPA), mercaptohexanoic acid (MHA), mercaptoundecanoic acid (MUA), dihydrolipoic acid (DHLA), mercaptosuccinic acid (MSA), mercapthoethane sulfonate (MES) and DHLA appended with poly(ethylene glycol) (PEG).[31]

In summary, two major methods for engineering the surface chemistry exist in view of the use of QDs in biological media. Encapsulation approaches are very efficient but they imply a large increase in the hydrodynamic diameter of the QDs, from less than 10 nm to 15-25 nm in most cases. Maintaining a small hydrodynamic diameter is crucial for some biological applications. This is particularly true for those relying on Förster resonance energy transfer (FRET) because the FRET efficiency is strongly dependent on the distance between the donor and the acceptor (***cf.*** **1.2.3.1**). Therefore, we focused in this work on the aqueous phase transfer of QDs by means of ligand exchange with small zwitteronic molecules that offer several advantages for bioapplications (***cf.*** **Chapter 2**).

1.2.2 Bioconjugation strategies

As discussed in **section 1.1**, most organic dyes generally used as fluorescent probes suffer from photobleaching, a low brightness above background fluorescence, a wide overlap of the absorption and the emission spectra of different dye molecules, and so on.[7, 32] These shortcomings severely limit the use of organic dyes for detection of rare events or multiplexed imaging and analysis. In contrast, QDs are characterized by bright, stable fluorescence and, hence, are particularly interesting as tools for biological imaging and diagnostics.[33] Moreover, all visible and NIR emitting QDs can be excited at the same wavelength in the UV/blue, which can be very far from their respective emission bands, removing the need of several excitation sources and filtering systems. Despite these advantages QDs issues related to the reproducibility, stability and toxicity of QD-bioconjugates still negatively impact their widespread utilization in biotechnologies.[34]

The first proof-of-principle applications of QDs in biological imaging have been reported by Bruchez *et al*. and Chan *et al*. in 1998.[7, 8] Since then the optical properties of QDs have been greatly exploited in a variety of cell imaging experiments, *in vivo* imaging, fluoroimmunoassays, DNA sequencing, and other types of bioconjugation.[35] Different conjugation protocols have been developed to specifically bind biomolecules to QDs, such as peptides, lipids, polysaccharides or nucleic acids, creating divers bio-non-bio interactions. Given the versatility of the QD surface for bioconjugation, the possibility of applications is enormous. For example, QDs can be labeled with tumor-targeting antibodies and traced with fluorescence imaging techniques or can be employed in tracking cancer cells in metastasis. However, the efficiency of a fluorescence based probe in biomedical imaging highly depends on the fate of the photons propagating in and out of the living tissue and for diagnostics the stability of the probe in biological serum. Due to the large sizes of antibodies (*ca.* 10 nm in length for IgG), AB conjugation to QDs is a challenging task (see **section 1.2**).

Among the large number of bioconjugation strategies we only discuss the most widely used in the following.[36] Among them, amine-reactive chemistry using N-hydroxysuccinimid (NHS-) esters, carboxyl-reactive chemistry using carbodiimide (1-ethyl-3-(3-dimethylaminopropyl)carbodiimide – EDC crosslinking for coupling with an amine-containing compound), and sulfhydryl-reactive chemistry using maleic acid imides are the most prominent. Since a heterobifunctional crosslinker has different reactive groups on either end of the molecule, each side can be directed specifically toward different functional groups on proteins or other molecules. Therefore, heterobifunctional reagents are commonly used to crosslink proteins and other molecules in a two- or three-step process that limits the degree of polymerization often obtained using homobifunctional crosslinkers.[36] The most popular heterobifunctional reagents are those which contain amine-reactive and sulfhydryl-reactive ends (**Figure 1-7**). The amine-reactive group is usually

an active ester, most often an NHS ester, while the sulfhydryl-reactive group may be one of several different functional groups. Succinimidyl 4-(N-maleimidomethyl)cyclohexane-1-carboxylate (SMCC) is a hetero-bifunctional reagent of utmost utility in protein conjugation processes. The NHS ester end of the reagent can react with a primary amine group to form stable amine bonds. The maleimide end of SMCC is specific for the coupling to sulfhydryls when the reaction pH is in the range of 6.5-7.5. However, this compound suffers from a cross-bridge that is both water-insoluble and immunogenic. Redesigning this crosslinker to have a PEG cross-bridge provides enhanced water solubility for modified proteins or other molecules as well as displaying very low immunogenicity. Moreover, a PEG group used as a cross-bridge in a heterobifunctional reagent to prepare immunogen conjugates will result in non-immunogenic modifications on the carrier protein and thus no antibody production against the polyether linker.[37]

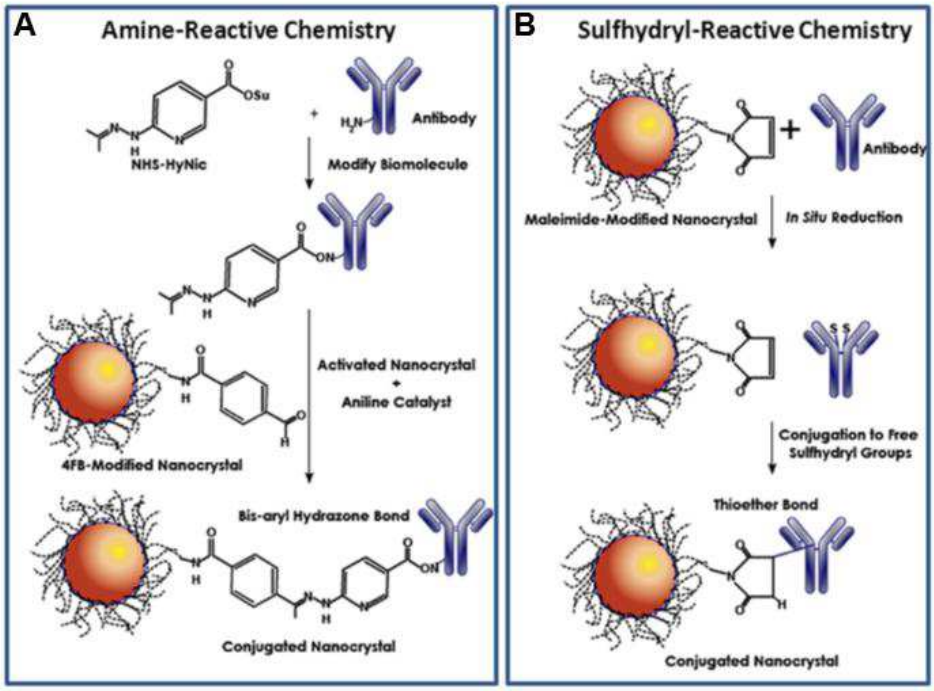

Figure 1-7. Principles of nanoparticles bioconjugation. **A)** Amine-reactive chemistry: primary amines on the antibody are modified with N-hydroxysuccinimide (NHS) esters that conjugate in solution with activated QDs (functionalized with 4-formylbenzamide). **B)** Sulfhydryl-reactive chemistry: maleimide-functionalized QDs conjugate with antibodies via *in situ* reduced disulfide bonds.[38]

In this work we have focused our attention on the conjugation of maleimide-functionalized QDs to antibody sulfhydryl groups and therefore we review some strategies using the sulfhydryl chemistry in the following.

Min *et al*. demonstrated a method to efficiently capture and quantify circulating tumor cells (CTCs) using Anti-EpCAM antibody-conjugated QDs.[39] The QD-attached CTCs are isolated using anti-IgG-modified magnetic beads. The antibody was thiolated using succinimidyl-S-acetylthioacetate (SATA) and the QDs were coated with DSPE-PEG 2000 and DSPE-PEG2000-amine (**Figure 1-8**). Anti-EpCAM antibody was successful conjugated using a heterobifunctional linker, sulfo-SMCC.

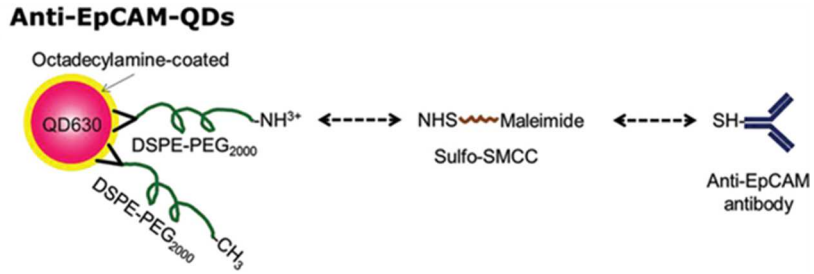

Figure 1-8. Construction of anti-EpCAM antibody-conjugated quantum dots (anti-EpCAM-QDs) as primary nanoparticles. DSPE-PEG 2000-methoxy and DSPE-PEG 2000-amine were grafted onto the surface of the QDs and the resulting QDs and antibodies were conjugated using a sulfo-SMCC linker.[39]

In another example of sulfhydryl coupling chemistry, the conjugation of anti-interleukin-10 antibodies to CdSe/ZnS QDs by means of a SMCC was demonstrated (***cf.*** **Figure 1-9**).[40] Interleukin-10 molecules participate in the inter-cellular communication. A commercially available conjugation kit from Invitrogen was used to perform the attachment of the antibodies to the QDs.

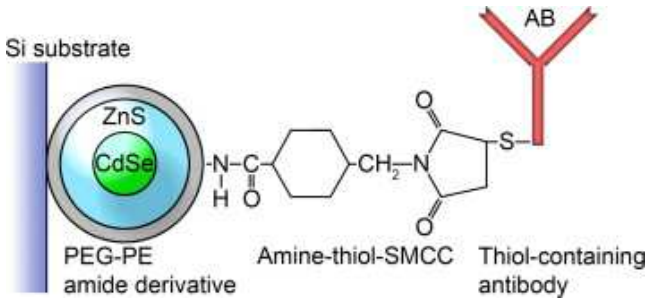

Figure 1-9. Conjugation of CdSe/ZnS QD PEG amide to thiol-containing anti-interleukin-10 antibodies using SMCC as linker.[40]

Recently, a new strategy for the preparation of near-infrared (NIR) emitting protein-functionalized QDs at room temperature was presented (**Figure 1-10**).[41] $Zn_xHg_{1-x}Se$ QDs were synthetized in aqueous solution and directly protein-functionalized as the protein molecules and small hydrophilic thiols (*e.g.* mercaptopropionic acid) are both used simultaneously as ligands during the reaction. According to the authors, protein molecules will bind to the QDs through the coordination of amino acid residues with Zn^{2+} ions on QD surface and the small thiol-containing MPA molecules would serve as additional surface ligands.

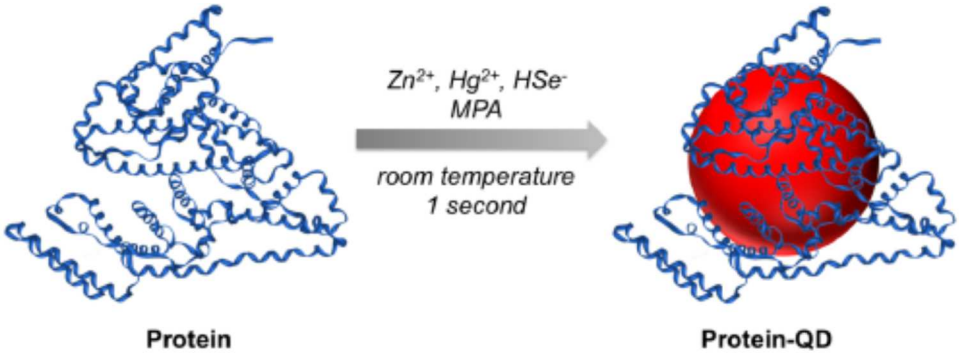

Figure 1-10. One-step synthesis of protein-functionalized NIR emitting $Zn_xHg_{1-x}Se$ QDs using Zn^{2+}, Hg^{2+}, and HSe^- ions as precursors in aqueous solution and MPA and the protein as ligands.[41]

The instructive review article of Montenegro *et al.* summarizes strategies of controlled bioconjugation of nanoparticles with special emphasize on the questions of how to precisely adjust the number of biomolecules per NP precisely and how to attach ABs on NPs in an oriented way (***cf.* Figure 1-11**).[42] Controlling the AB orientation on the NC surface is of crucial importance to ensure its optimal interaction with antigens.

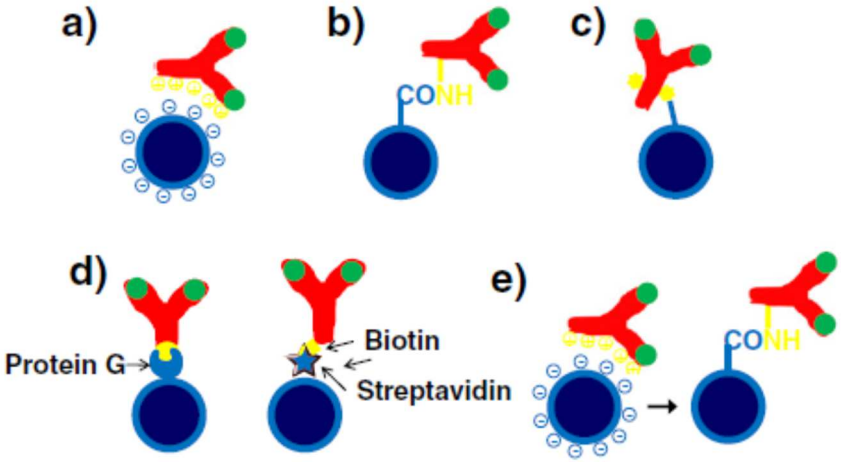

Figure 1-11. Schematic representation of strategies AB conjugation on NCS and for controlling their orientation.[42] The different methods are discussed in the text.

Figure 1-11a shows the electrostatic adsorption between the antibody and the surface of the NP. It is based on the electrostatic interactions, eventually enforced by hydrophobic, hydrogen binding, and van der Waals attractive forces. Using this method causes denaturation of the immobilized ABs, thus yielding poor reproducibility.[43, 44] Strategy **b)** is less straightforward as it involves the covalent binding of ABs on the NC surface, which needs generally to be preceded by the insertion of functional groups on the NP surface. It also relies on the use of chemical linkers/crosslinkers, and/or chemical modification of the AB. Method **c)**

involves binding through sugar moieties of the AB, which guarantees an oriented immobilization on the NCs' surface. Carbohydrate chains on the Fc region of the AB are mildly oxidized to CHO (reactive aldehydes) and can be directly reacted with primary amines on the NC surface or to NCs that have been activated with hydrazide groups. Strategy **d)** uses appropriate crosslinking biomolecules to obtain oriented immobilization of ABs. These biomolecules are directly coupled on the NP surface. Finally, method **e)** combines ionic adsorption plus covalent binding to promote oriented immobilization. To achieve this, bifunctional NPs are prepared containing both ionizable groups and reactive groups at their surface.

In summary, different strategies based on sulfhydryl chemistry using SMCC or EDC/NHS crosslinkers for bioconjugation of proteins to NCs have been developed over the last years. In this study we are focusing on the development of compact QD-AB conjugates. As mentioned we will use the maleimide/sulfhydryl bioconjugation strategy. With the goal to further reduce the size of our probes we will apply antibody fragments instead of full ABs. The use of fragmented ABs is also advantageous because their conjugates display less interference with various Fc binding proteins, less immunogenicity (due to lack of the Fc region), and lower nonspecific binding to surfaces or membranes. Enzymatic digests of IgG can result in two particularly useful fragments called Fab and $F(ab')_2$, prepared by action of papain and pepsin, respectively (**Figure 1-12**).

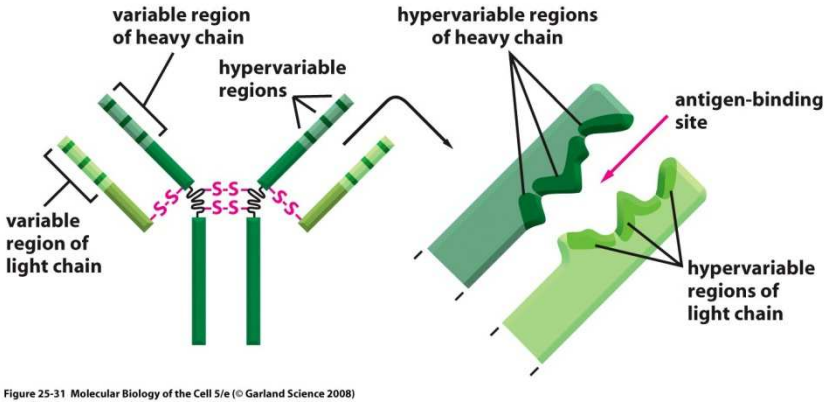

Figure 1-12. Antibody hypervariable regions. Schematized drawing of how the three hypervariable regions in each light and heavy chain together form the antigen-binding site of the AB.[45]

1.2.3 QDs for *in vitro* diagnostics (*IVD*)

One of the most popular biotechnological applications with high potential for the use of QDs is *in vitro* diagnostics (IVD). A good IVD agent should be highly luminescent, stable, capable of bioconjugation and yield a very high sensitivity, *i.e*. a very low detection limit (LOD). Among the large number of different immunoassays in clinical diagnosis, we will focus here on those based on FRET, and in particular time-gated Tb-to-QD FRET. Indeed, a rapid, sensitive and specific immunoassay for protein markers in whole blood or plasma would largely improve the early diagnosis as well as monitoring therapy and disease progression. Important parameters for the immunoassay are that it must be fast, simple of use and inexpensive allowing for uncomplicated diagnosis and better treatment. Homogeneous assays based on FRET are an ideal basis to meet the challenging requirements of IVD. They do not require any washing or separation steps (homogeneous), the fast solution-phase kinetics allow short incubation times and time-resolved detection permits nearly background-free measurements. Moreover, the ratiometric format (luminescence detection of FRET from a donor to an acceptor) offers an instantaneous suppression of sample or measurement fluctuations resulting in an extremely good reproducibility. Since the first proof-of-concept study in 2005,[46] which used biotin-streptavidin as biological binging model, there have been many applications that used Ln-to-QD FRET for versatile, multiplexed, and sensitive bioanalysis.

1.2.3.1 *Homogeneous Tb-to-QD Förster Resonance Energy Transfer (FRET) immunoassays*

Homogeneous FRET sandwich immunoassays, which use donors and acceptors labeled with antibodies that bind to different epitopes of a biomarker, are a smart solution to perform the rapid and separation-free biomarker detection. Since several years Ln-donor-based time-gated FRET immunoassays using organic dyes as acceptors have been applied in commercial diagnostic kits. Indeed, this technology can also be found on many commercial fluorescence plate readers for biological and biochemical analysis. Geißler *et al.* achieved picomolar detection limits for five different lung cancer tumor markers by combining 15 different biomolecules (10 antibodies interacting with 5 tumor markers) in a 5-fold multiplexed FRET immunoassay using Tb-to-dye time-gated FRET.[47] Nonetheless spectral crosstalk in such multiplex assays using dyes is unavoidable and therefore computational treatment of the data is required. Initial studies on biotin-streptavidin binding systems showed the advantages of Tb-to-QD FRET over Tb-to-dye FRET concerning multiplexing and sensitivity.[48] However, the implementation of Tb-to-QD FRET in immunoassays has been limited, due to the much larger sizes of the antibodies, compared to biotin-streptavidin and the difficulty to create reproducibly stable and highly luminescent QD-AB conjugates. Only very recently, different

examples have demonstrated the efficient use of this system. Wegner and collaborators used TG-FRET immunoassays against prostate specific antigen (PSA). **Figure 1-13** shows the principle of the QD-based homogeneous FRET immunoassay that explored all different combinations of conjugates. It showed that the combination of Tb-IgG conjugates and QD-F(ab) conjugates provided the best sensitivity compared to the other possible combinations of donor and acceptor antibody conjugates.[11] In other words, the best immunoassay systems combining maximum sensitivity (minimum LOD), minimum antibody modification (no IgG reduction for the Tb conjugates), and maximum separation efficiency was the (Tb-IgG)+(QD-F(ab)) system. LODs down to 1.6 ng/mL in 50 µL serum samples demonstrated the relevance of these assays for clinical diagnostics. It should be noted that these Tb-to-QD FRET immunoassays used a commercial QD-antibody conjugation kit from eBioscience, which is not available anymore. We will see in **Chapter 3** that we developed a strategy for the synthesis of much more compact QD-AB conjugates which allowed to achieve a further twofold improvement of the LOD.

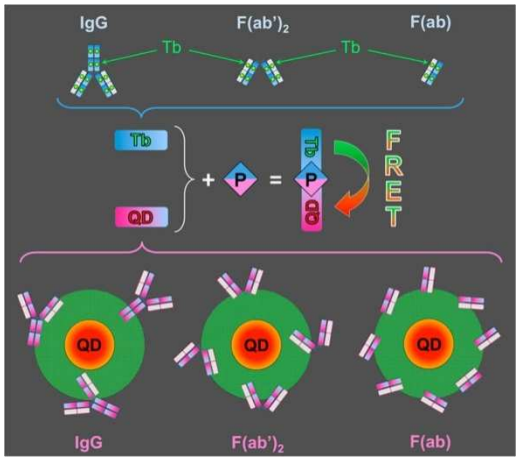

Figure 1-13. Top: Tb-AB conjugates; bottom: QD-AB conjugates. Each containing different primary antibodies against PSA.[11]

Very recently, Bhuckory *et al*. investigated currently commercially available QDs (Qdot-ITK from Thermo Fisher – Life Technologies), which were conjugated to free sulfhydryls of reduced anti-PSA IgG antibodies using sulfo-EMCS crosslinkers (**Figure 1-14**). Tb-complexes were conjugated to anti-PSA IgG antibodies (specific to a different PSA epitope than the F(ab)) using amino-reactive chemistry. The performance of the resulting FRET immunoassay will be discussed in comparison with our results in **Chapter 3**.

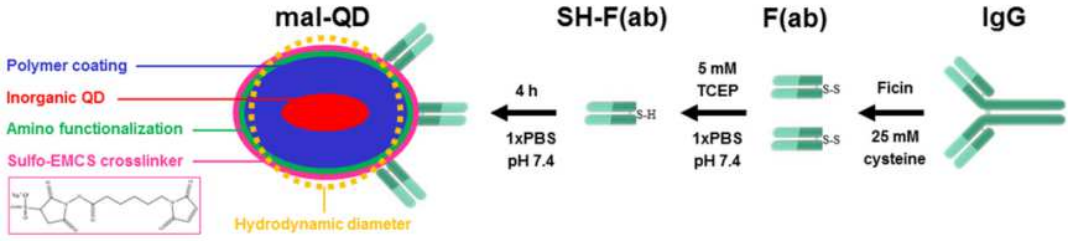

Figure 1-14. Scheme showing the reduction of IgG antibodies followed by the sulfhydryl coupling reaction with maleimide-functionalized QDs.[49]

1.2.3.2 Principle of FRET detection

Förster Resonance Energy Transfer is the non-radiative transfer of energy between a donor and an acceptor, forming the FRET pair, via a dipole-dipole coupling mechanism.[50] The distance between the donor and the acceptor molecules is typically in the range of 1-10 nm, in extraordinary conditions FRET at larger distances up to 20 nm has been reported. Ln-to-QD FRET allows for a complete suppression of the emission of photoexcited QDs by using time-gated PL detection, *i.e.* by using a pulsed excitation source and applying a delay (in the microsecond range) between excitation and detection. This is possible due to the large differences in the excited state lifetimes of both fluorophores, nanoseconds in the case of QDs, milliseconds in the case of Ln complexes. As a result, the observed QD PL is a pure FRET signal that is generated by sensitization from the Ln. This acceptor-background-free FRET has some influence on the FRET efficiency (ηFRET, eq.3), which is generally defined by the donor-acceptor distance (r) and the Förster radius (or Förster distance) R_0. The Förster radius (R_0) is the distance between donor and acceptor where the energy transfer is 50% efficient (**Figure 1-15**). R_0 can be calculated using the spectral overlap integral of donor luminescence and acceptor absorption, as defined by **eq. 1**.

$$R_0^{\,6} = \frac{9\ \ln(10)\ \kappa^2\ \Phi_D}{128\ \pi^5\ n_r^4\ N_A} J(\lambda) \qquad \textbf{(1)}$$

where K^2 is the orientation factor between the two dipole moments, Φ_D is the donor luminescence quantum yield, n is the refractive index of the solvent, N_A is Avogadro's number, and $J(\lambda)$ is the spectral overlap integral defined by **eq. 2.**

$$J(\lambda) = \int F_D(\lambda)\varepsilon(\lambda)\lambda^4 d\lambda \qquad \textbf{(2)}$$

J is dependent on the acceptor molar absorptivity (ε) and the donor area-normalized emission spectrum (F_D).

Finally, the FRET efficiency ηFRET can be calculated using **eq. 3**, displaying the characteristic r^{-6} distance dependence:

$$\eta_{FRET} = 1 - \frac{\tau_{DA}}{\tau_D} = \frac{R_0^6}{R_0^6 + r^6} \qquad (3)$$

where τ are the decay times of the donor in absence (subscript "D") and in presence (subscript "DA") of the acceptor. The sensitivity of ηFRET to the D-A distance is shown in **Figure 1-15.**

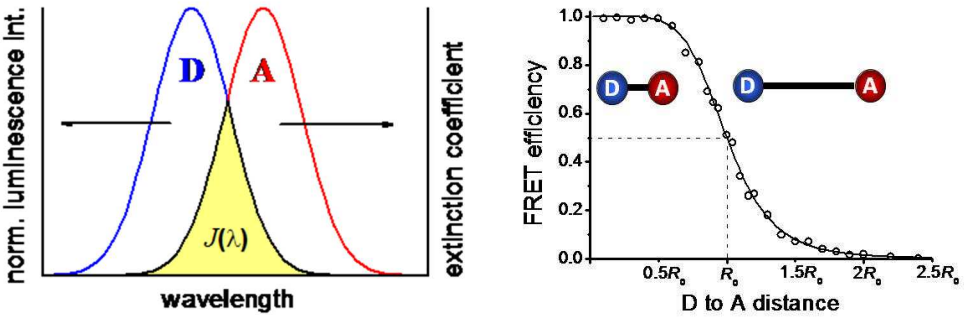

Figure 1-15. Left: Visualization of the spectral overlap integral *J(λ)* between the donor D and acceptor A. Right: Relationship between the Förster radius and the FRET efficiency where the FRET efficiency is inversely proportional to the sixth power of the D-A distance.

In this Figure it becomes clear that the largest dynamic range lies in a region between 0.5 $R_0 < r < 2.0\ R_0$. Beyond this region, FRET is either too efficient (100%) or negligible (0%), making it insensitive to distance changes, which is important for applications relying on the use of FRET as so-called "molecular ruler".

After donor excitation, FRET is in competition with radiative and non-radiative deactivation of the donor. Upon acceptor excitation via FRET, it can again return to its energetic ground state by radiative or non-radiative transitions (***cf.* Figure 1-16**).

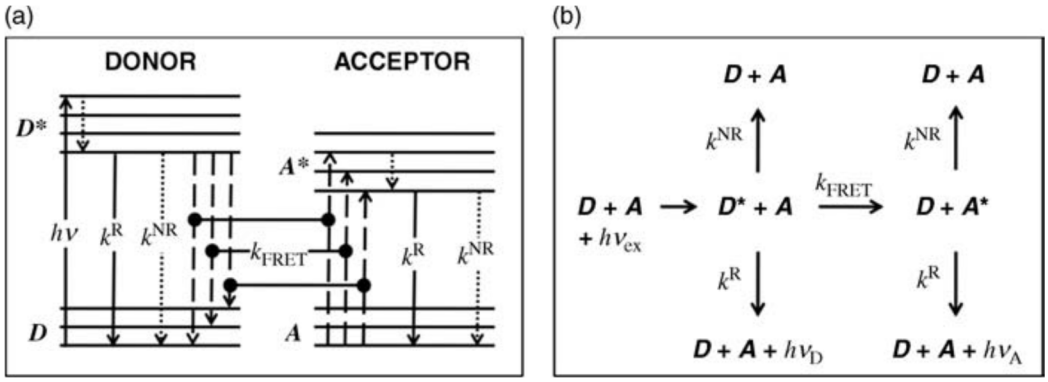

Figure 1-16. Principle of donor / acceptor interaction in FRET. (**a**) Simplified energy-level diagram (Jablonski diagram) representing the excitation of the donor (*hν)* from an electronic ground state (D) to an excited state (D*), subsequent inner relaxation (dotted arrow), followed by radiative decay (k^R), non-radiative decay (k^{NR}) or FRET (k_{FRET}). For FRET occurring from D to A, the difference between the respective energy levels needs to be equal (resonance condition). After FRET, the acceptor is in an excited state (A*), followed by radiative or non-radiative decay to its ground state (A). (**b**) Summary of the different decay pathways after donor excitation ($h\nu_{ex}$).

1.2.3.3 FRET using QDs as energy donors or as acceptors

QDs can be used as both FRET donors and acceptors. The main advantages of the QDs used as donor are 1) their size tunability, which allows to adjust a spectral overlap with almost any acceptor, 2) their broad absorption spectra which allow excitation at almost any wavelength, 3) the attachment of several acceptors to the large surface of QDs, which allows an increase of the FRET efficiency.

Using QDs as acceptors there is efficient direct excitation of the QDs at almost any wavelength used for donor excitation, due to their broad absorption spectrum. This will lead to inefficient FRET, as a result of the small ratio of excited Tb donors to ground state QD acceptors. To avoid this problem, the use of long-lived luminescent lanthanide complexes (LLCs) as donors, pulsed excitation and time-gated detection is the best solution (***cf.*** **Figure 1-17**). Indeed, several microseconds after the excitation pulse, all QDs have decayed back to their ground states, whereas most of the LLCs have remained in their excited states leading to efficient FRET. Moreover, due to the large spectral overlap between Ln emission and QD absorption, these FRET systems result in very long Förster distances of >10 nm.[51]

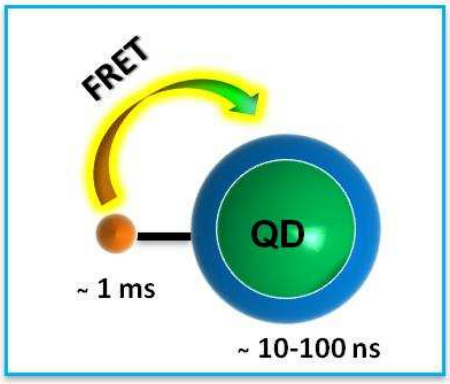

Figure 1-17. Scheme of the FRET pair composed of Tb donors and QD acceptors indicating the ranges of excited state lifetimes.

1.3 Cancer and nanomedicine: a brief introduction

Nanomedicine is a cutting-edge area of biomedical research that exploits the application of nanotechnology to medical science. It involves the design and development of novel nanostructured material that, once engineered, promise a profound impact in prevention, diagnosis, and treatment of several diseases.[52]

Cancer, due to an abnormal accumulation of cells, is one of the diseases that have the strongest impact on the population. It is estimated that 80% of cancer related deaths are due to metastases. Indeed, morbidity and mortality associated with tumors mostly result from the invasion of adjacent and distant tissue given rise to metastases. This dismal scenario is primarily due to the fact that most patients are diagnosed when the cancer has reached an advanced stage, which often is the result of a lack of specific symptoms and limitation in diagnostics that allow the disease to elude detection during its formative stage. Thus, it is clear that further progress needs a deeper understanding of tumor initiation and progression and methods for monitoring tumor development. Tumor cells gain advantages in initial growth through dysfunction of growth factor responses that are mediated by receptor proteins expressed on cell membranes.[53] Thus, methods to detect, identify and quantify cell surface proteins or marker proteins in a sensible way may potentially facilitate reliable early-stage cancer diagnostics. We have already addressed this topic in section 1.2.2, and we highlighted that one of the promising methods in this context is based on FRET-immunoassays, to directly quantify the biomarker concentration in serum samples. Among the myriad of biomarkers, in this thesis we use the prostate specific antigen (PSA) as biomarker specific for prostate cancer. This cancer is common, a frequent cause of cancer death and, has surpassed lung cancer as the most common cancer in men.[54] PSA is a glycoprotein and is expressed by both normal and neoplastic prostate tissue. The measurement of its absolute value in serum is useful for determining early stage of prostate cancer. The American Cancer society systematically reviews the literature assessing PSA performance.[54] This analysis estimated the sensitivity of a PSA cut-off level of 4.0 ng/mL was 21% for

detecting any prostate cancer and 51% for detecting high-grade cancers (Gleason ≥8). Using a cut-off value of 3.0 ng/mL increased these sensitivities to 32 and 68%, respectively. Thus, we note that a lower PSA cut-off value is highly desirable, because a fraction of men with PSA levels below 4 ng/mL were found to have prostate cancer.[55]

This improvement of test sensitivity by lowering the PSA cut-off value is however normally accompanied by a reduced test specificity, leading to far more false-positive test and unnecessary biopsies.[56] To avoid this problem time-gated FRET immunoassays have proven a great potential on the way towards systems for real-time *in vitro* diagnostics. The commercial KRYPTOR compact plus plate reader is a fully automated, closed laboratory analysis system that can be perform various analyses in random-access operations using TRACE (Time Resolved Amplified Cryptate Emission) Technology. Cezanne/Thermo Fisher (partner of my PhD project) employs TRACE technology in the scope of an exclusive license to develop innovative *in vitro* diagnostic reagents.

1.4 Nanotoxicological aspects

In this Introduction we have shown that QDs offer great opportunities for bioapplications. On the other hand, the use of NCs in real-life biological imaging, detection and diagnostics is still very limited. One major drawback which severely limits the potential for clinical translation of QDs is the toxicity concern of commonly used II-VI semiconductors, such as CdSe and CdTe QDs. These semiconductor QDs are easily disintegrated in biological systems if their surfaces are not carefully coated with inert protective shells, biocompatible polymers, and biomolecules. The release of Cd^{2+} ions as a result of degradation of the coatings that surround the NC triggers severe toxicity due to the fact that Cd^{2+} can penetrate the cell using calcium channels and saturate them. It also reduces the availability of antioxidant factors and thus increases the concentration of reactive oxygen species (ROS).[57] Therefore, over the past years, the emphasis has shifted toward the synthesis of non-Cadmium based QDs for bioapplications. In this direction, QDs made up of III-V semiconductors, such as indium phosphide (InP), have drawn considerable attention.
It is hard to give a single explanation for the toxicity of QDs, which appears to depend very much on the chemical composition of the core (or core/shell structure) and the surface, which represents the key interface interaction with biological components. The small size, combined with very high surface:volume ratio, makes NPs very reactive compared to larger particles. In general, particles covered with thick polymer coatings are less damaging to the cells,[58] while the elimination of this protective coating (for example, through irradiation, low pH, lysosomal or metabolic degradation) can induce cell damage and death.[59] Two possible mechanisms have been proposed to explain these toxicity phenomena: the first one is the release

of metal ions from the core of the NC, the second one is the formation of reactive molecules, such as reactive oxygen species (ROS).

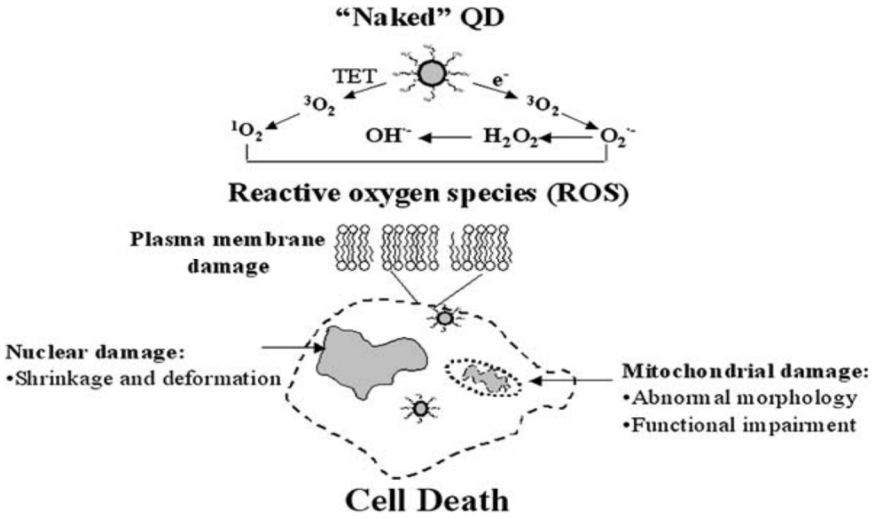

Figure 1-18. ROS produced by QDs can cause damage to organelles. In addition, the precipitation of QDs on the cell surface even without the entry into the cell can damage the function and eventually lead to cell death.[60]

Indeed, NPs often escape the endosomal trafficking and continue their journey into the cytoplasm, in cell organelles, or into the nucleus, affecting the cells' structural or functional integrity. NPs can further induce genotoxic effects either by direct interaction with the genetic material or by indirect action through reactive oxygen species or ions released from the NP core. QDs act as active redox nanoparticles (electron donors)[61] and can generate highly reactive radicals with or without exposure to light.[62] At high concentrations, ROS can cause damage to cellular proteins, lipids, DNA and carbohydrates, causing apoptosis or necrosis.

Toxicological studies of cadmium-free QDs are very scarce in the literature but suggest that InP-based QDs minimize the toxic effects observed with their CdSe-based counterparts. This feature is of course an essential prerequisite for the use of such NCs in the biomedical field. Nanotoxicology studies conducted both *in vitro* and *in vivo* on Drosophila melanogaster show that CdSe/ZnS QDs are more toxic than InP/ZnS QDs despite the similar physicochemical properties and equivalent localization in the cell.[63] The effect is due to the release of core metal ions indicating that the indium toxicity is virtually zero compared to that of cadmium. Other findings in mice confirm that InP/ZnS QDs do not show toxicity *in vivo* during the evaluation period (84 days), suggesting that these NPs are suitable for use in biological systems.[64] Concomitant with the increased use of QDs in consumer products such as sun creams, textile fibers, TV screens and other types of displays, solar cells, etc. there is a strong need to increase the investigation of

potential toxic effects due to unintentional release or contamination of the environment through powder/water waste-streams.[65-68] Furthermore, an urgent evaluation of QD toxicity on human beings is strongly needed.

Actually, most nanotoxicity studies have focused on *in vitro* investigations, representing over-simplification of bio/non-bio interactions and not taking in account the real biological complexity and systemic networking of whole animals; hence, *in vivo* tests are central to achieve an accurate estimation of nanotoxicity in living organisms.[69] The European directives encourage experiments on model systems to minimize testing on vertebrate animals. We will address this point in **Chapter 4** where we present recent studies using a small invertebrate animal, the freshwater polyp *Hydra vulgaris*, and in parallel preliminary studies on keratinocytes from human skin biopsies.

1.5 Aim and motivation of the thesis

The work presented in this PhD thesis is part of the ANR project NanoFRET and our main task was the development of stable, highly luminescent and FRET-compatible QD-antibody conjugates. Such immuno-QDs are together with the AB-labeled Tb donor integral part of FRET immunoassays and of potential interest for the project's industrial partner Cezanne-Thermo Fisher. One of the main motivations of the NanoFRET project is to fill the current lack of stable, functional, highly luminescent and small QD-antibody conjugates that provide a high binding capacity and yield efficient FRET, generating highly sensitive immunoassays.

In my thesis I first focus on the development of a QD functionalization strategy yielding stable, compact and highly luminescent NCs to be conjugated with antibodies and used as FRET acceptor in immunoassays. We will present this strategy in **Chapter 2**, keeping in mind all the main characteristics required. In **Chapter 3** the binding of fragmented antibodies on this nanoprobe as well as the evaluation in FRET immunoassays against PSA will be addressed. In addition, we extend our studies to systems relying on the grafting of paramagnetic (Gd) or luminescent (Tb, Eu, Yb) lanthanide complexes on the QD surface with the goal to design multimodal probes.

Chapter 4 aims at assessing the toxicological impact of the different InP- and CdSe-based QDs used in our study. The main interest of these experiments is the direct comparison of the different QD materials, while using an identical surface chemistry. We have tested them in different biological systems, ranging from *in vitro* cultured human cells to *in vivo* animal models, *Hydra* polyps and keratinocytes from human skin biopsies, respectively.

Each chapter contains its corresponding experimental section in the end.

The manuscript is completed by a Conclusion and Perspectives section, a list of abbreviations and a list of my scientific publications / communications.

2 Phase transfer of QDs from organic solvent to aqueous medium

2.1 Introduction

One of the main goals of this thesis is to develop stable and strongly luminescent immune-QDs for application in FRET immunoassays. In this chapter, we focus on the surface functionalization of QDs making them hydrosoluble and adding functionalities for simple antibody conjugation. Emphasis will be given most particularly on conserving a small hydrodynamic diameter and a maximum of the initial fluorescence intensity. The thickness of the organic coating is of great importance as large hydrodynamic diameters increase the donor−acceptor distance and diminish the FRET efficiency.[37] As already mentioned in **Chapter 1**, the possibility to disperse nanocrystals (NCs) in aqueous medium is a fundamental criterion for their use in biotechnology. Semiconductor NCs prepared in organic solvents are hydrophobic and therefore their phase transfer to aqueous medium is an essential step, for which several strategies have been developed as summarized below (***cf***. **Figure 2-1a**). In view of the utilization of QD in biological applications, the basic requirements are: **a)** colloidal stability in water at physiological pH over an extended period of time in water, **b)** high fluorescence efficiency, **c)** small hydrodynamic diameter (Dh), **d)** low non-specific binding in biological environment.

One strategy for aqueous phase transfer consists of the use of phospholipid micelles[70] or amphiphilic polymers[71] as phase transfer agents. The latter encapsulate the QD, which keeps its initial surface ligands. The amphiphilic molecules stick to the surface via hydrophobic interactions involving their apolar groups. Their polar moieties point to the exterior, giving hydrosolubility and stability to the QDs. In many cases polyethyleneglycol (PEG) moieties of different chain length are applied, which strongly increase the hydrodynamic diameter. It therefore ranges generally in between 15-25 nm for QDs transferred with this method, while the inorganic core may be much smaller than 10 nm. This drawback is counterbalanced by the fact that the encapsulation method typically conserves the initial PL QY. Therefore, this approach is an appealing choice for bio-applications not relying on small size of the QDs. Another approach, which falls also in the range of larger hydrodynamic diameters is the coating of the nanocrystal surface with a silica shell.[72] Silica has many advantageous features such as optical transparency, chemical robustness and there exist also a huge variety of differently substituted silanes facilitating the addition of further functionalities to the QD surface. The silica coating can be achieved by introducing a first layer of appropriate silanes on the QD surface, either by hydrophobic interactions or by chemical grafting, followed by controlled hydrolysis in presence of further silane precursors. Another possibility is the use of micelles as nanoreactors for the silica shell growth, derived from the Stöber method for synthesis of silica nanoparticles. The first

method is preferable if thin silica shells are sought, as the second approach generally leads to particle sizes at least on the order of 40-50 nm.

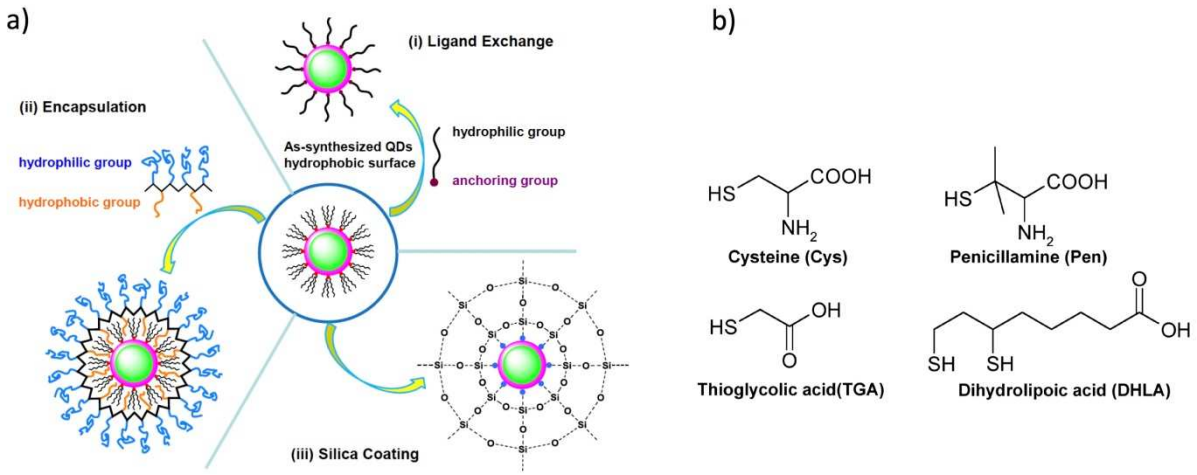

Figure 2-1. a) Most popular methods for the aqueous phase transfer of QDs. **b)** Zwitterionic (Cys, Pen) and anionic (TGA, DHLA) thiol-containing ligands used in ligand exchange phase transfer.

Much smaller hydrodynamic diameters can be obtained by modifying the surfactants on the QD surface using ligand exchange reactions. For this purpose, bifunctional ligands are used which include on one end a functional group assuring hydrosolubility of the QDs, and on the other end an anchorage site, capable of interacting strongly with the QD surface. The anchorage sites can be of different nature, such as amine, phosphine, or thiol based end groups. Thiol anchoring functions offer a high affinity with the surface of many types of QDs, most of which contain an outer ZnS shell. Such an approach consists in reacting the hydrophobic QDs[30] in a solution containing an excess of thiol based ligand. In their thiolate forms, these molecules coordinate strongly with the metal ions on the surface of QDs, which is primordial for the colloidal stability of the QDs.[73]

The detailed solubilization strategies rely also on the nature of the hydrophilic functional group. In general, these are of neutral nature (e.g. methoxy- or hydroxyl-terminated PEG),[29, 74] anionic (e.g. carboxylates) or zwitterionic (e.g. cysteine), while cationic examples (e.g. ammonium) are less common.[33] The use of ionic hydrophilic groups can be problematic for the overall stability of the QDs, which will depend on the pH and the ionic strength of the medium. In the case of anionic and zwitterionic groups, it was demonstrated that the samples were stable over periods ranging from days to months at sufficiently basic pH.[75] The negatively charged carboxylic acid groups provide electrostatic repulsion, which maintains the QDs in colloidal aqueous solution. However, at acidic pH or in solutions of high ionic strength, there is a greater tendency for aggregation due to the charge neutrality of the carboxylic acid groups.[31] It has been shown that more acidic thioalkyl acid ligands yield QDs that are more resistant to aggregation at low pH.[76] For example, mercaptoacetic acid (MAA, pK_a: 3.68) capped QDs aggregate and precipitate more slowly than dihydrolipoic acid (DHLA, pK_a: 4.73) capped QDs, while mercaptosuccinic acid (MSA, pK_{a1}: 3.16, pK_{a2}: 4.67) shows the

least tendency for aggregation.[77] This behaviour was ascribed to the presence of two carboxylate groups on the same molecule, resulting in a higher charge density. Summarizing, these studies have shown that small mercaptocarboxylic acid type ligands offer a library of suitable surfactants, working at different pH values and allowing increasing the pH range of utilization of QDs.

Even if in most of the cases the lack of stability with this kind of ligands is due to the change in the pH or in ionic strength, instability can also be generated by desorption of the thiol anchoring function from the surface of the QD with time. In order to avoid this problem, ligands with a higher affinity for the QD surface have been proposed, such as multi-thiolated compounds. One of the most popular approaches is based on the use of dihydrolipoicacid (DHLA) derivatives. Several studies have shown that the use of bidentate DHLA increases the colloidal stability at neutral pH to periods ranging from several months to a year.[78-80]

However, one of the downsides of direct ligand exchange with hydrophilic thiols is its effect on the optical properties of the QDs. Ligand exchange tends to reduce quantum yields of the QDs in comparison to the initial value in organic solvent. This effect is particularly pronounced in the case of thiol and dithiol anchoring groups. The latter are known to effective hole acceptors and thus to reduce the probability of radiative recombination.[81] In addition, oxidation of the thiols can lead to the formation of the disulfide bonds, which are also efficient PL quenching centers.[75]

In this context, penicillamine (**Pen**) has also drawn strong attention. This small ligand, which is structurally similar to cysteine (***cf.*** **Figure 2-1b**) was found to enhance colloidal stability over a range of physiologically relevant pH values.[82] Furthermore, due to its zwitterionic nature, it provides weak interactions with cell membranes and with other biomolecules, such as serum proteins. In addition, **Pen** offers the opportunity for selective bio-conjugation *via* its carboxylate group or its primary amine group. This superior colloidal stability compared to cysteine-coated QDs was ascribed to steric effects caused by the two methyl groups (instead of protons) at the carbon atom in α position to the thiol group.[75] This structural difference has a strong influence on the reactivity of both molecules. In particular, the sterically hindered thiol group in **Pen** makes it less susceptible to oxidation as compared to cysteine. In the literature, **Pen** has been used as a capping ligand in the aqueous synthesis of QDs[83, 84] and also as a phase transfer agent at pH 7.4.[75, 82] While the stability of the CdSe/ZnS NCs phase transferred with **Pen** at pH 7.4 was high, a rather long reaction time (18h) has been reported. On the other hand, in our team Tamang and coworkers found that the pH value during an aqueous phase transfer procedure played an important role for increasing the stability of the QDs. By adjusting the pH to 9 the phase transfer reaction took place within 2h or less and after purification and transfer to 1xPBS buffer the product was stable for approximately ten weeks before an increase of the hydrodynamic diameter occurred.[75] The thiol group of the **Pen** ligand is deprotonated at elevated pH, and thiolates have been shown to bind the QDs ZnS surface more strongly than thiols.[85] In Tamang's study it was also shown that the QY could be improved by adding tris(carboxyethyl)phosphine (TCEP) as reducing agent during the phase transfer in order to avoid disulfide formation, which is favoured at basic pH.[75]

Concluding, hydrophilic thiols are suitable surface ligands for the preparation of water-soluble QDs of small hydrodynamic diameter. Zwitterionic molecules, such as cysteine or **Pen** are of particular interest as they minimize non-specific interactions in biological media. However, the conditions of the aqueous phase transfer need to be carefully optimized in order to achieve long-term colloidal stability paired with minimized losses of PL QY.

Building to the above-cited studies and with the goal to optimize the synthesis of compact, stable and highly luminescent QDs suitable for subsequent use in FRET immunoassays, in this chapter the phase transfer of InP-based QDs and Cd-based QDs, using the **Pen** ligand will be addressed. Another aspect that will be investigated is the use of a bifunctional crosslinker that enables the subsequent conjugation with proteins.

Aiming at maintaining a small hydrodynamic diameter, we decided to use the heterobifunctional linker **MAL-dPEG3-Lipoic acid**, named here **Mal1**, which is commercially available from Quanta BioDesign (**Figure 2-2**). Using this molecule in a post-functionalization step after phase transfer has several advantages:[36] it contains at one end a dithiol function capable of strongly interacting with the surface of the QDs and replacing **Pen** ligands, and at the other end there is a functional group impairing the chemical functionality, namely a maleimide group allowing for the facile and selective conjugation of sulfhydryl groups present in biomolecules, such as cysteine groups in antibodies, resulting in a stable thioether bond.[86] Both functional moieties are linked by a short polyethylenglycol (PEG) chain that is beneficial for water-solubility of the QDs. It is obvious that a molecule containing both thiol groups and a maleimide function should be very unstable, and therefore as-received **Mal1** contains the dithiol group in its non-reduced disulphide form. Furthermore, the compound has to be kept at low temperature (-20°C) in order to avoid its degradation. We expect several challenging tasks related with the use of **Mal1**: i) during the cleavage of the disulfide bond experimental conditions have to be found which avoid crosslinking due to the head-to-tail binding of ligand molecules; ii) the integrity and reactivity of the maleimide function is strongly pH dependent, and therefore once again the optimum conditions for the post-functionalization and antibody conjugation have to be determined.

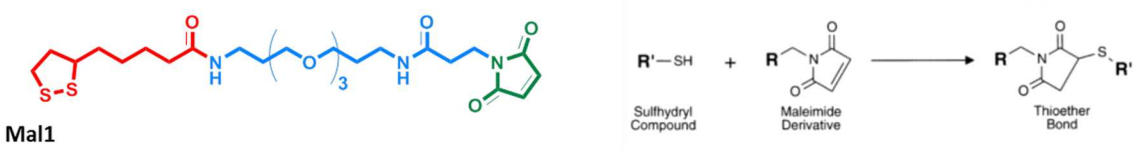

Figure 2-2. Left: ligand **Mal1**, in red the lipoic acid moiety, in blue the PEG spacer and in green the maleimide function. Right: reaction of the maleimide group with a sulfhydryl compound (thiol) leading to the formation of a stable thioether bond.

2.2 Synthesis and properties of InPZnS@ZnSe/ZnS and CdSe@ZnS nanocrystals

As already mentioned in **Chapter 1**, the most important properties of QDs for bio-applications are their size-dependent narrow emission with high fluorescence quantum yield combined with a broad absorption spectrum resulting in a large effective Stokes shift and their long-term resistance against photobleaching.[87, 88] Over the past few years, III-V Nanocrystals are of increasing interest as a replacement for toxic CdSe QDs. Among them Indium phosphide (InP) is one of the most appealing candidates because, with a bulk band gap of 1.35 eV, the photoluminescence can be tuned over the whole the visible range to the near infrared by varying the size. However, in terms of emission line width and PL QY InP still lies behind high quality CdSe QDs. The best values are 40-60 nm FWHM (vs. 20-30 nm for CdSe) and it is challenging to obtain PL QYs exceeding 50%, while with CdSe based QDs virtually unity QY is achieved.

In this study we use alloy InPZnS core QDs,[24, 89] which have been overcoated with a graded Zn (Se,S) shell in order to enhance their photo- and chemical stability. The range of emission of these NCs is 500-620 nm, and the highest QYs of up to 50-60% are obtained with green-emitting QDs (≈530 nm). As this emission wavelength does not overlap with the emission of Tb complexes, the use of **InPZnS@ZnSe/ZnS** (named here **core@shell** or **QD530**) NCs is advantageous for the FRET immunoassays described in **Chapter 3**. For toxicological studies (**Chapter 4**) we also used the InPZnS core QDs emitting at 510 nm (named here **core-only** or **QD510**). The synthesis protocols for **QD510** and **QD530**, described in the experimental section, were optimized by Tim Senden during his master thesis project and by Dr. Christophe Lincheneau during his post-doc. Briefly, for the synthesis of the InPZnS core all precursors except for $P(SiMe_3)_3$ are mixed in octadecene, degassed and heated to 100°C (***cf.* Figure 2-3**). We prefer this procedure over a "real" heat-up synthesis where everything is mixed in the beginning because we have observed that $P(SiMe_3)_3$ undergoes reactions already at room temperature. Therefore here the phosphorus precursor is injected at 100°C and the reaction mixture is immediately heated to 300°C with a large heating ramp (around 50°C/min) and kept at this temperature for 20 min. In a subsequent step, and without intermediate purification, the graded Zn(Se,S) is grown, by injecting first the Zn precursor (Zn oleate) and then the chalcogenide precursors (TOPS, TOPSe) at 220°C, followed by heating to 300°C for 20 min. The optical properties of the obtained **InPZnS@ZnSe/ZnS** QDs will be presented in the following sections.

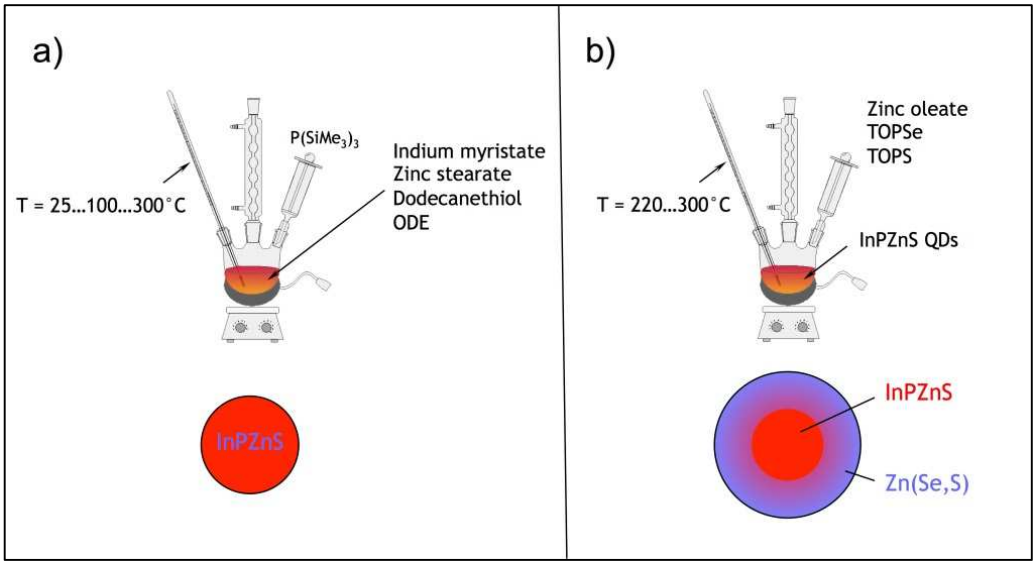

Figure 2-3. Synthesis of InPZnS alloy core NCs (**a**) and subsequent growth of a graded Zn(Se,S) shell (**b**).

In our study we have also used hydrophobic CdSe@ZnS-based QDs emitting at 605, 655 and 705 nm (named here **QD605**, **QD655** and **QD705**) from Life Technologies / Thermo Fisher.[90] The first reason is to have narrow emitters at longer wavelengths where no emission of Tb^{3+} takes place (***cf.*** **Chapter 3**). The second reason is that the QDs of Life Technologies can be considered as "standards" in this field: they show the best and certified emission properties and moreover the identical inorganic QDs (but with hydrophilic polymer coating) are applied in commercial bio-conjugation kits. Therefore we can directly compare our surface functionalization strategy with these commercial products, in particular the performance of the QDs in FRET-based biodetection. Furthermore, by applying the same surface functionalization for aqueous phase transfer on the InP-based and the CdSe-based QDs we can discriminate the influence of the inorganic part of the QD in toxicological studies aiming at the comparison of InP and CdSe (***cf.*** **Chapter 4**).

2.3 Phase transfer and post-functionalization: synthesis of water dispersable, bifunctional QDs

The QDs used in this thesis are coated with hydrophobic organic surfactants (fatty acids in the case of InP, trioctylphosphine oxide in the case of CdSe) rendering them soluble in non-polar solvents (*e.g.* chloroform, hexane, and toluene). The QDs were transferred from the organic to the water phase by means of ligand exchange using penicillamine (**Pen**), starting from a procedure developed before in our laboratory.[75] The phase transfer protocol relies on the use of a biphasic mixture of QDs in chloroform and **Pen** in aqueous solution of precisely controlled pH of 9, in presence of the mild reducing agent TCEP (**Figure 2-4**). As mentioned in the introduction of this chapter, basic pH is of primary importance for achieving the deprotonation of the **Pen** thiol group, which results in stronger binding to the surface of the different ZnS-coated QDs. TCEP prevents **Pen** disulfide formation because this reaction does not only reduce the colloidal stability but also diminish the fluorescent quantum yield (QY).[75] The driving force of the phase transfer reaction is the higher binding energy of the thiolate functions with the ZnS surface of the QDs ($E_{binding}$ Zn-$S_{thiolate}$ = 194.7 kJ/mol, S-$S_{thiolate}$ = 105.1 kJ/mol)[85] in comparison with the initially coordinating carboxylic acids or TOPO ligands (no numerical data found).

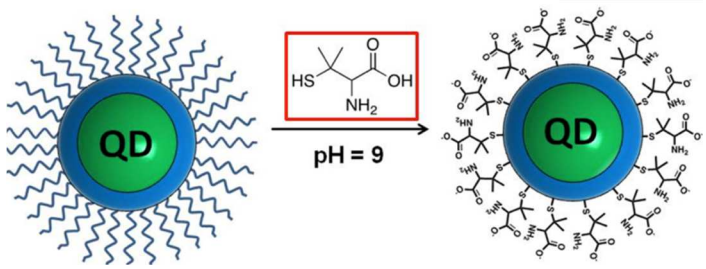

Figure 2-4. Schematic representation of the aqueous phase transfer of QDs using penicillamine (**Pen**)

An important factor to control is the purification step before the phase transfer, which assures the quantitative progress of the reaction. Any kind of side-product related to the synthesis, including excess of reagents or surfactants must be washed off to allow an efficient phase transfer. Therefore, pre-purified samples after synthesis were submitted to further purification steps. The initial purification comprises three cycles of precipitation through the addition of a methanol/chloroform mixture and excess acetone, centrifugation and redispersion in chloroform. This procedure is necessary to remove secondary products and ODE. The additional purification consists of three cycles of precipitation / redispersion using an ethanol/methanol mixture and chloroform, which assures the quantitative removal of excess shell precursors. This step is of particular importance when Zn stearate is used as the Zn precursor for shell growth instead of Zn oleate. In the case of the commercial CdSe/ZnS QDs the initial solvent decane was

changed to chloroform prior to phase transfer by precipitation with a methanol/isopropanol mixture followed by redispersion. All QDs are in 3-6 µM concentration in chloroform after the purification, as this solvent allows for solubilizing the ligands leaving the NC surface during the phase transfer reaction.

All the vials used are pre-autoclaved and the DI water solutions are filtered using a 0.2 µm filter and degassed. Phase transfer occurs within max. 2 hours upon vigorous mixing of the QD colloidal solution with a 0.2 M solution of **Pen** in MilliQ water containing 200 µL of a 0.5 M TCEP solution. After this step the samples are purified to remove excess **Pen** and TCEP by using size exclusion chromatography. Under optimized conditions, this phase transfer results in a very compact (around 1 nm thick) organic surface layer and very high colloidal stability for several years, as shown in the next section. The quantitative phase transfer was easily detected by the mutual colour change of both phases (***cf.* Figure 2-5**).

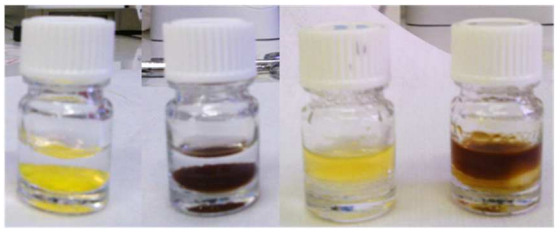

Figure 2-5. Mutual colour change of the chloroform phase (bottom) and aqueous phase (top) during phase transfer. Yellow sample: **QD530**; brown sample: **QD705**.

For the toxicity studies in **Chapter 4** also core InPZnS and CdSe QDs are used. For these samples, which are much more sensitive to surface modifications, different protocols have been tested to obtain a good phase transfer while preserving at least a minimum of fluorescence. First of all, the pre-purification step must be no aggressive, as repeated washing cycles with methanol remove surface ligands leading to unpassivated surface sites, which can act as PL quenching centers. For this reason purification was carried out using ethanol, and the phase transfer reaction has been stopped directly after completion (in this case after 60-90 min).

In conclusion, the chosen biphasic approach allows for solubilizing the different types of QDs investigated in this study (InPZnS and CdSe core, InPZnS@ZnSe/ZnS and CdSe@ZnS core@shell) with only minor variations of the protocol. In a subsequent post-functionalization step the maleimide containing bifunctional ligand **Mal1** is then introduced. This step is carried out under reduction of the disulfide group by means of TCEP (**Figure 2-6**).[36] Briefly, a solution of **Mal1** (1 mL, 10 mM) and TCEP (0.046 mL, 0.5 M) in degassed water are added to a suspension of **QD-Pen** (0.5 mL, 5.2 µM in degassed water) and the pH is adjusted to 7.0 by dropwise addition of 0.5 M tetramethylammonium hydroxide (TMAOH). The mixture is vortexed at *800* rpm overnight at room temperature. The resulting colloidal solution is purified by size exclusion

chromatography. The obtained **QD-Mal1** are then concentrated under vacuum to a final volume of 400 µL and stored at 4°C in the dark. The overall length of **Mal1** (around 3 nm) makes the maleimide functions stick out of the **Pen** corona and hence offer a better availability for subsequent antibody conjugation. According to our studies, the **Mal1** ligand does not affect the high colloidal stability of the **Pen**-capped QDs as both types of samples (QD-**Pen** and QD-**Mal1**) do not exhibit signs of aggregation even after storage for more than two years. Colloidal stability is assessed by using combined DLS and absorption spectroscopy measurements (see below).

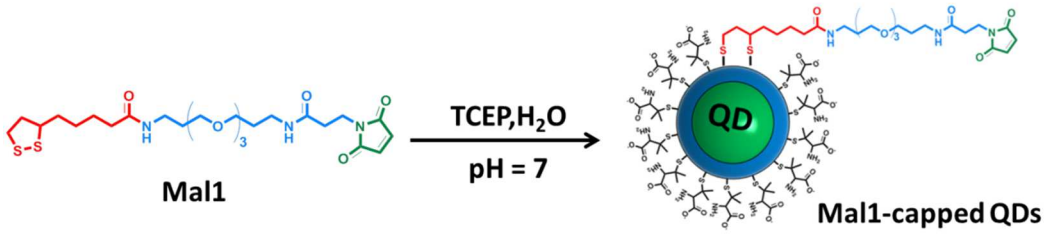

Figure 2-6. Scheme showing the post-functionalization of QDs with the heterobifunctional ligand **Mal1** after activation of the anchorage site by cleavage of the S-S bond using TCEP. An excess of **Mal1** is reacted at pH 7 with **Pen**-capped QDs in aqueous solution, followed by purification using size exclusion chromatography.

The control of the pH value is critical during the post-functionalization procedure. In particular, the pH of the reaction mixture should be < 8 as higher values increase the rate of hydrolysis of the maleimide group to non-reactive maleamic acids. In a series of control experiments we determined pH 7 to be optimal, leading to efficient post-functionalization with **Mal1** while preserving the reactivity of the maleimide function. For subsequent antibody conjugation the pH value should also be adjusted to around 7, because the maleimide group reacts specifically with the sulfhydryl group of proteins in a pH between 6.5 and 7.5, leading to the irreversible formation of a stable thioether linkage. Under more alkaline conditions (pH>8.5), the coupling with primary amines is favoured. We will discuss the antibody binding in more details in the next chapter (**Section 3.2**).

2.4 Characterization of the obtained QDs

2.4.1 Optical characterization

Once the functionalization and post-functionalization have been achieved, the optical and structural properties of the QDs were characterised by the means of various techniques. We start here with the main feature of the QDs, their optical characteristics.

For all types of QDs each functionalization step was firstly studied using absorption and photoluminescence spectroscopy. The absorption spectra exhibited the excitonic peak centred at 470, 590 and 620 nm for **QD530**, **QD605** and **QD655**, respectively, which is indicative of the lowest energy transition of the QD. For **QD705** this spectral feature is not visible, the absorption spectrum just presents a steady rise from the absorption onset on towards shorter wavelengths. The spectra shown in **Figure 2-7** demonstrate that no major changes were observed in the UV-Vis absorption spectra upon functionalization with **Pen** and **Mal1**. We attribute the decrease of absorbance in the UV/blue range visible in the spectra of **QD605** and **QD705** to the replacement of initial organic ligands eventually absorbing in this range by **Pen** and **Mal1**. Upon excitation at 400 nm (**QD530**) or 480 nm (all other QDs) in each case the bright emission of the QDs was observed as a narrow peak centred at 530, 615, 659, 715 for **QD530**, **QD605**, **QD655** and **QD705** respectively. Here also no major changes were observed in the shape and position of the emission spectra in comparison to those obtained for the hydrophobic samples. However, an important point to be addressed is the ubiquitously observed reduction of fluorescence upon phase transfer by ligand exchange. An average decrease of 20-30% has been observed during functionalization with **Pen**: the fluorescence emission efficiencies of the QDs in chloroform were very high with quantum yields of 0.50 (**QD530**), 0.80 (**QD605**), 0.60 (**QD655**) and 0.92 (**QD705**) (***cf.*** **Table 2-1**) and were decreased to 0.32, 0.60, 0.30 and 0.74, respectively. **QD655** is clearly less well performing compared to the other commercial QDs, with a loss of QY of 50%. On the other hand, these results confirm that our approach is suitable for the aimed application, as each one of the QDs exhibited QYs of at least 30% in the aqueous phase. It should be noted that in **Table 2-1** only the best performances were reported. In the case of some batches of **QD530**, upon phase transfer QYs below 15% were obtained whereas in the case of the Cd-based QD no significant difference were observed from one batch to another. As we tested various synthetic conditions for the InP-based QDs, the observed batch-to-batch variations were not unexpected. In contrast, due to the low batch-to-batch variation of the characteristics of the commercial Cd-based QDs can also be used as a control to optimize the functionalization and the post-functionalization.[90] The details of the PL QY measurements will be presented in the next section.

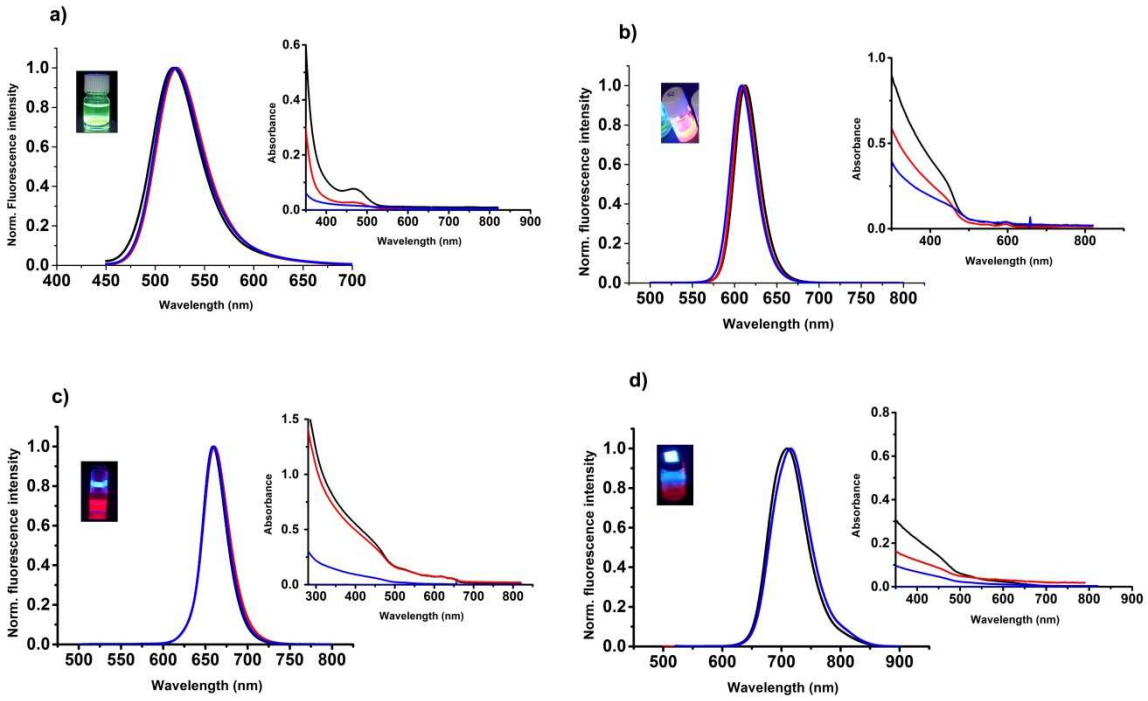

Figure 2-7. PL and UV-Vis spectra of **QD530** (**a**), **QD605** (**b**), **QD655** (**c**) and **QD705** (**d**) in chloroform (black), after functionalization with **Pen** (red) and with **Mal1** (blue) in 1X PBS buffer. Insets: photographs of the samples under UV light.

Table 2-1: Photophysical properties of the used QDs (emission wavelength for QD-**Pen**).

Sample	Excitation wavelength (nm)	Emission wavelength (nm)	QY in $CHCl_3$ (%)	QY with Pen (%)	QY with Mal1 (%)
QD530	400	530	50	32	14
QD605	480	615	80	60	23
QD655	480	659	60	30	13
QD705	480	715	92	74	54

Upon post-functionalization with **Mal1**, even if once again the shape of the emission spectra remained unchanged, the PL QY showed a further decrease by *ca.* 20-40% (**Table 2-1**). We do not have a detailed explanation for this behaviour but tentatively attribute it to the presence of the maleimide moiety in the close environment of the QDs, which could eventually act as a luminescence quencher. Furthermore, the bulkier dithiol-containing **Mal1** ligands may lead to a lower ligand density per QD surface area and induce unpassivated surface sites acting as trap states. However, since of the QYs of all final samples **QD-Mal1** are well above 10% they can still be used in the aimed application, albeit with an expected lower FRET efficiency for the samples of lower QY **QD530** and **QD655**.

Figure 2-8 shows the absorption (black) and fluorescence (red) spectra of the core-only InPZnS QDs after phase transfer with **Pen** in comparison with the InPZnS@ZnSe/ZnS core@shell NCs (**QD530**). The first absorption peak was at 410 nm for the core-only sample (*vs.* 470 nm for the core/shell system) and the PL emission peak at 510 nm (*vs.* 530 nm). It should be noted that the emission of the core-only sample after

phase transfer was still visible under UV light and detectable with the spectrometer but the PL QY was < 1%.

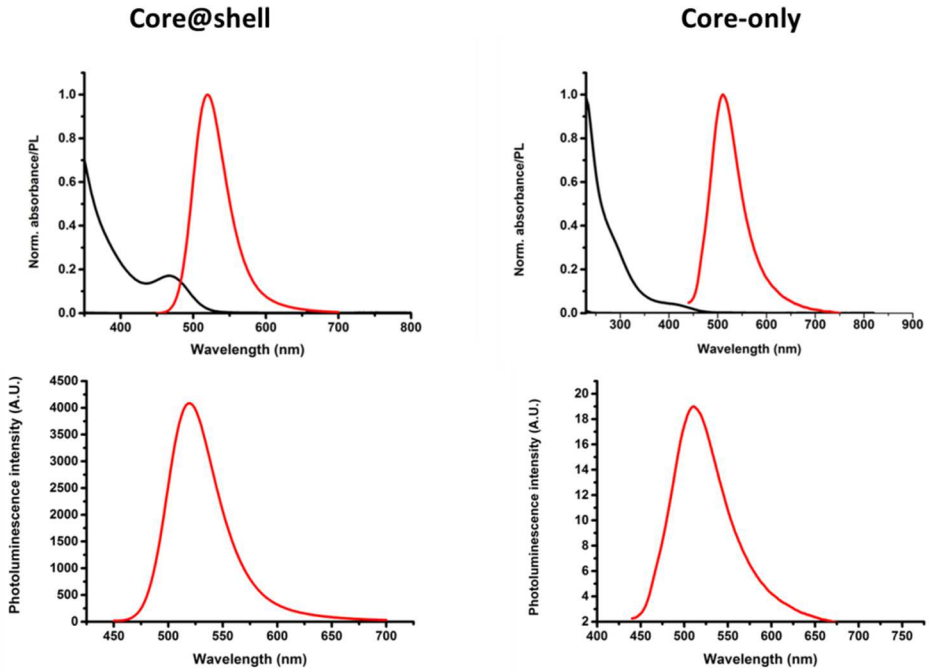

Figure 2-8. Upper panel: UV-Vis and PL spectra of **QD530** (left) core@shell and **QD510** (right) core-only after phase transfer. **Lower panel:** PL intensity

2.4.1.1 Fluorescence quantum yields

The absolute fluorescence QYs of each type of QDs were determined by comparison with a standard of known QY emitting in the same spectral range (freshly prepared solution of Fluorescein 27 in 0.1 M NaOH; QY = 93%, Rhodamine 6G in ethanol; QY = 95%[91] or **QD705** in chloroform; QY=92%[90]). The QY was calculated with the following formula:

$$\Phi_{NC} = \Phi_{Standard} \cdot (a_{NC}/a_{Standard}) \cdot (n^2_{NC}/n^2_{Standard})$$

where Φ is the QY, *a* the gradient (slope) of the plot of the integrated fluorescence intensity *vs.* absorbance (and *n* the refractive index of the solvent (1.375 for hexane, 1.446 for chloroform, 1.333 for water and buffer and 1.36 for ethanol[91]). All spectra were corrected for the instrumental response with calibration curves furnished by the supplier and the estimated errors on QY are ± 15% of the calculated values. Aliquots or purified samples of the QDs in hexane, chloroform or water were put into 1 cm quartz cuvettes and diluted until the absorbance at the excitation wavelength was under 0.1. At least four samples of different concentrations were prepared and measured for determining the slopes (***cf.* Figure 2-9**). Both the

sample and the reference were excited at 400 nm in the case of InP based QDs and at 480 nm for CdSe based QDs. We note that exciting fluorescein at 400 nm is of course far from optimal (480 nm), but unfortunately the large Stokes shift and broad excitonic peak of the InP-based QDs does not allow to excite this sample at longer wavelengths without losing part of its PL intensity. Therefore, in the future it will be better to use another standard (*e.g.* certified QDs emitting in the green range) or an integration sphere for a more precise determination of the QY of InP-based QDs.

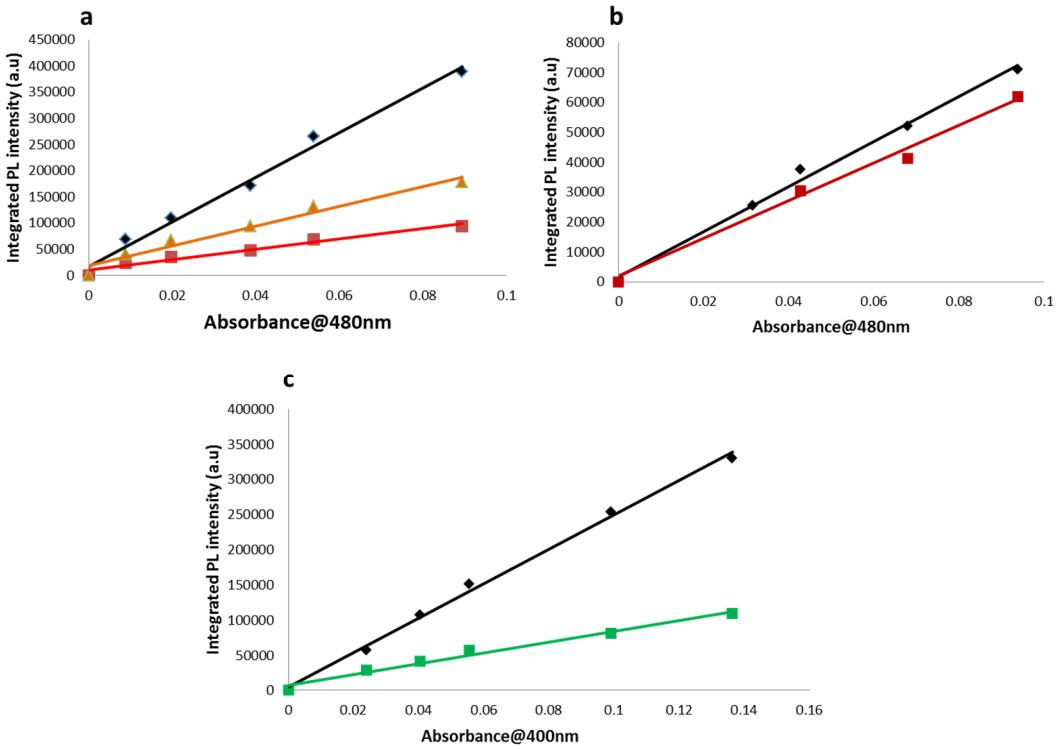

Figure 2-9. Integrated photoluminescence signal *vs.* absorbance plot for QD-**Pen**. **a)** Rhodamine (black), **QD655** (red), **QD605** (orange); **b) QD705** in $CHCl_3$ (black) and **QD705**-**Pen** (red); **c)** Fluorescein (black) and **QD530** (green).

2.4.2 Structural characterization

The size and morphology of the inorganic part of the QDs were characterized using transmission electron microscopy (TEM), revealing nearly monodisperse, spherical (**QD530**, **QD605** and **QD655**) or elongated (**QD705**) nanocrystals as depicted in **Figure 2-10.** The size distributions have also been calculated and are shown in the same Figure.

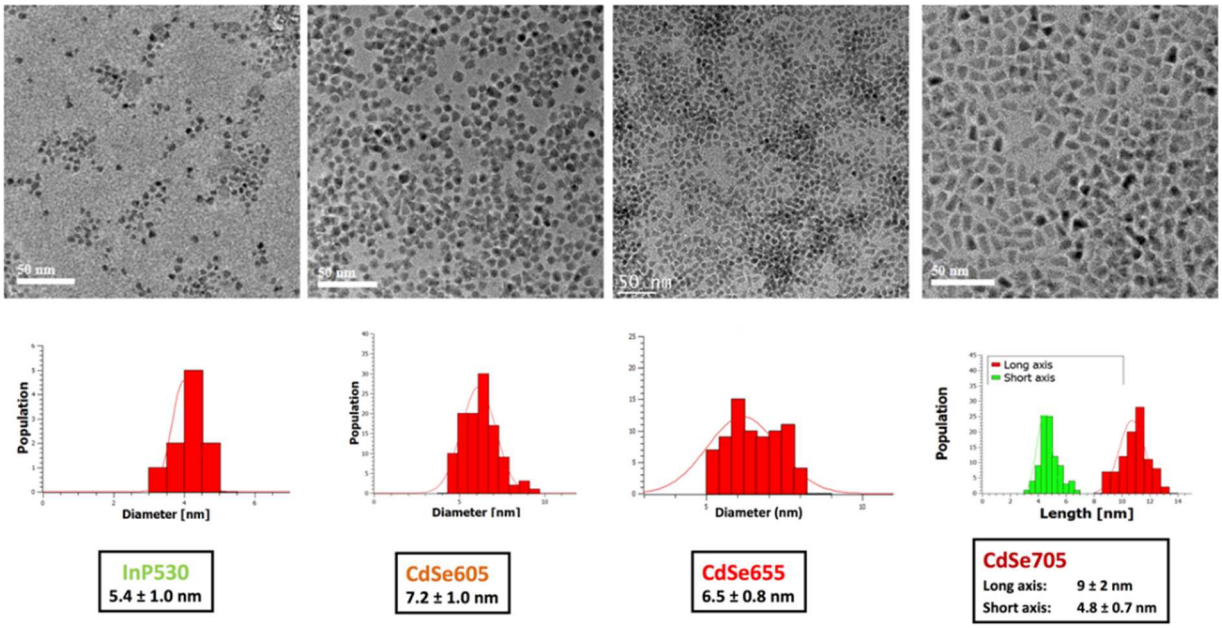

Figure 2-10. Transmission electron microscopy images of **QD-Pen**. Mean size from left to right **QD530**: 5.4 ± 1.0 nm; **QD605** 7.2 ± 1.0 nm; **QD655**: 6.5 ± 0.8 nm; **QD705**: long axis: 9 ± 2 nm, short axis: 4.8 ± 0.7 nm.

As shown in **Figure 2-11** in the case of the InP-based QDs a size increase was observed upon ZnSe/ZnS shell growth on the InPZnS core, from 3.5±0.5 nm to 5.4±1 nm. This increase in size of around 2 nm indicates that approximately 3 monolayers of the ZnSe/ZnS shell have been grown around the InPZnS core.

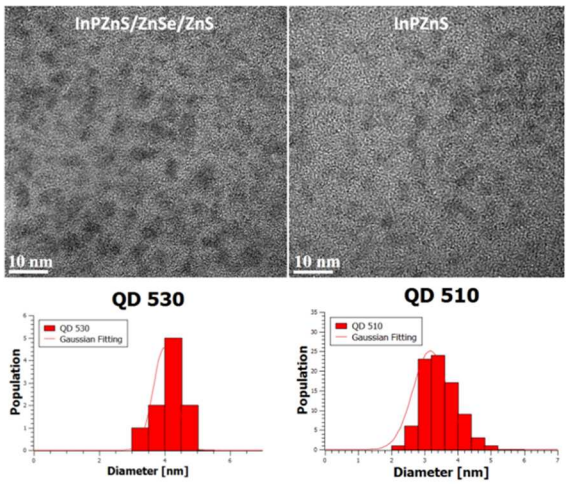

Figure 2-11. Transmission electron micrographs of InP-based QDs, the identical sample with (left) and without double shell (right) in water; *i.e.* core@shell and core-only respectively.

2.4.2.1 Hydrodynamic size and dispersibility of QDs

The hydrodynamic diameter and the dispersibility of the QDs are very important properties for their bio-applications and in our case to be used in FRET immunoassays. Hydrodynamic sizes of the QDs were evaluated by using dynamic light scattering (DLS). While TEM observations give information about the size of the inorganic core, DLS takes into account the surfactants and their interactions with solvents molecules. DLS thus allows determining the hydrodynamic diameter of the QDs. In the case of anisotropic nanoparticles (**QD705**), the size of the particle is approximated by a sphere having the same volume. These measurements confirmed the narrow size distributions observed with TEM and revealed small hydrodynamic diameters, which slightly increased with each functionalization step. **QD-Pen** exhibits a hydrodynamic diameter, which is 1.5 nm larger than the TEM diameter, corresponding to a 0,75 nm thick ligand shell in accordance with the compact size of the **Pen** molecule. Upon post-functionalization, an increase of the hydrodynamic diameter has also been detected. As shown in **Figure 2-12**, an increase of the hydrodynamic diameter from **QD-Pen** to **QD-Mal1** of *ca.* 3-4 nm has been observed. This increase is consistent with the successful grafting of the ligand **Mal1** at the QD surface, which has a stretched length of approximately 3 nm. Even the largest sized QDs (**QD705**) exhibit a small hydrodynamic diameter and narrow size distribution after each step of functionalization.

The zeta potential is another important parameter for the characterization of the QDs allowing the estimation of the magnitude of the electrostatic charge / repulsion of the QDs, which is one of the fundamental parameters affecting their stability. Both the **Pen**-capped and **Mal1**-capped QDs exhibited negative zeta potential values between –22 and –36 mV and low polydispersity indices (PDI) confirming good colloidal stability (**Table 2-2**). The good colloidal stability in the aqueous phase is assured by the electrostatic repulsion between the QDs, caused by negative charge on the carboxylate group of the Pen ligands. Upon post-functionalization the zeta potential changes from a mean value of –33 mV to –24 mV due to the reduction of the fraction of the negatively charged **Pen** ligands at the QD surface in favour of the neutral **Mal1** ligands. However, we expect that the short PEG moieties of **Mal1** also contribute to the colloidal stability of **QD-Mal1** in aqueous media.

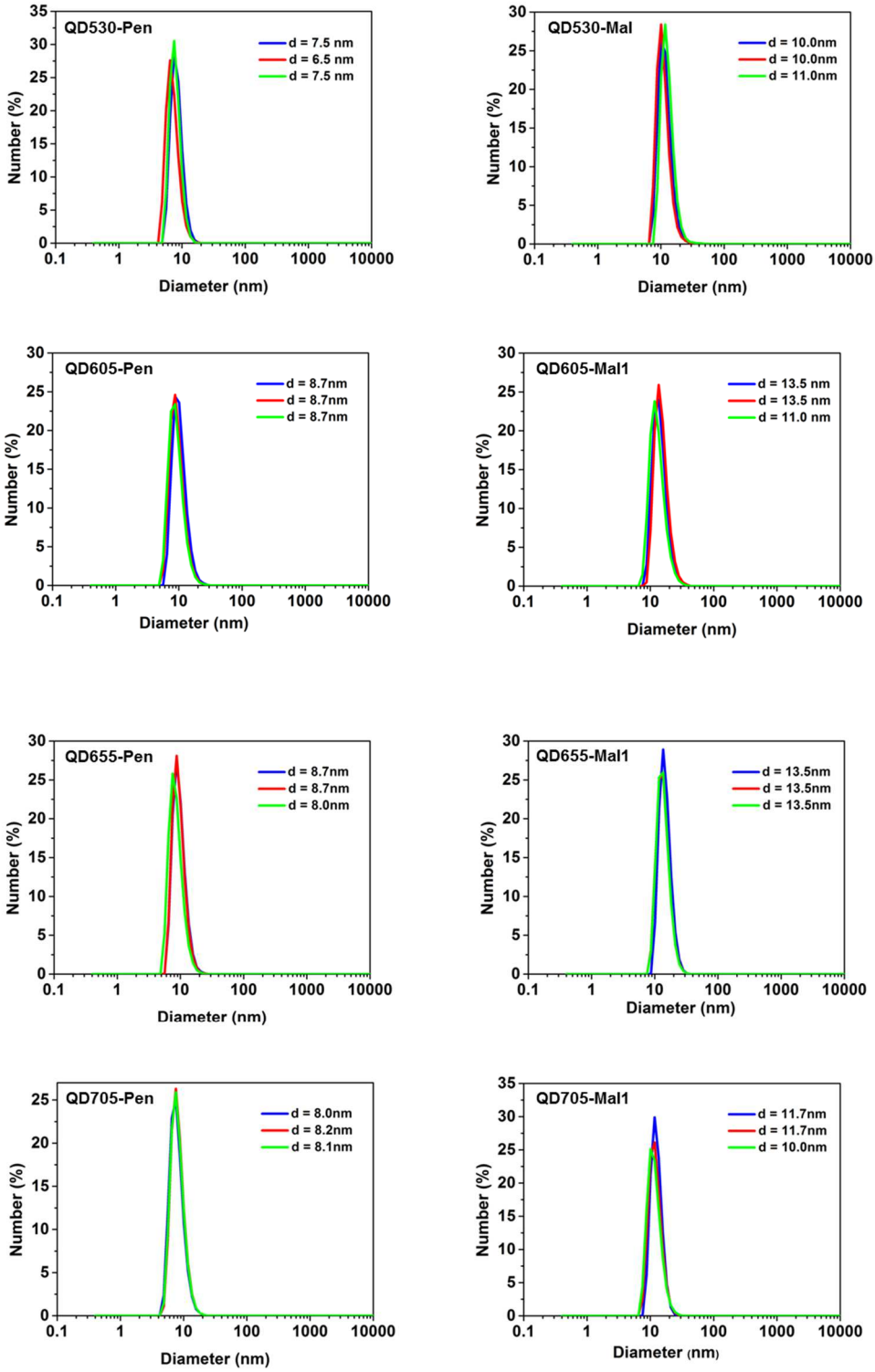

Figure 2-12. DLS measurements of the different types of QDs before and after post-functionalization with Mal1. The average hydrodynamic diameter *d* (nm) of each measurement, repeated 3 times, is given in the legend.

Table 2-2. Polydispersity indices (PDI) and zeta potentials of the **Pen**- and **Mal1**-capped QDs.

Sample	PDI-Pen	PDI-Mal1	Zeta-Pen (mV)	Zeta-Mal1 (mV)
QD530	0.33	0.58	-31	-24
QD605	0.15	0.23	-33	-27.5
QD655	0.12	0.57	-34	-22
QD705	0.08	0.23	-36	-24

In each case, the system was controlled over a period of more than two years, showing no aggregation and very good colloidal stability. The absence of aggregation was verified by DLS, after checking that the concentration had not changed using UV-vis spectroscopy. As an example the long-term study of **QD705-Pen** is depicted in **Figure 2-13.** Even after 2 years the zeta potential values remained quasi-unchanged and were evaluated at -30 mV confirming still good colloidal stability. In between 12 months and 2 years of observation, a slight increase of the hydrodynamic diameter from around 10.0 to 12.0 nm has been observed, which could be the result of a modification of the solvation sphere around the QD rather than a sign of aggregation, which should lead to a larger diameter increase. However, a decrease in the QY from 74% to 23% for **QD705** was observed, as depicted in **Figure 2-14**. This could be due to the desorption of a small fraction of **Pen** ligands from the NC surface, which does not affect the hydrodynamic diameter or the colloidal stability of the QD, but may generate surface trap states. Desorbed Pen ligands may also undergo dimerization under disulfide formation generating additional quenching centers.

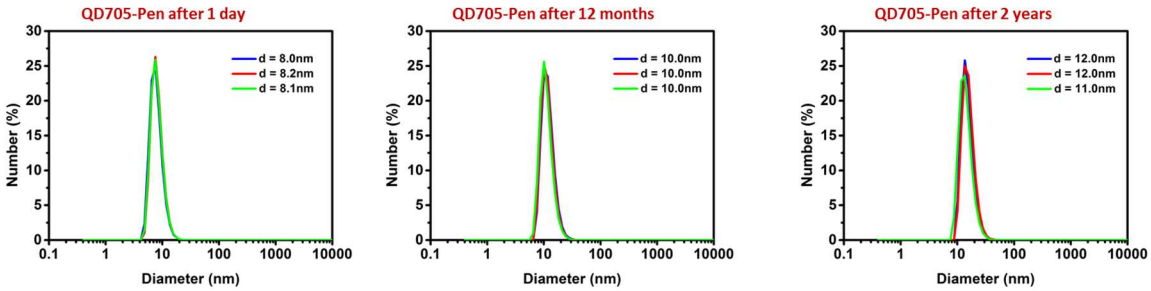

Figure 2-13. DLS measurements of **QD705-Pen** after 1 day, 12 months and 2 years.

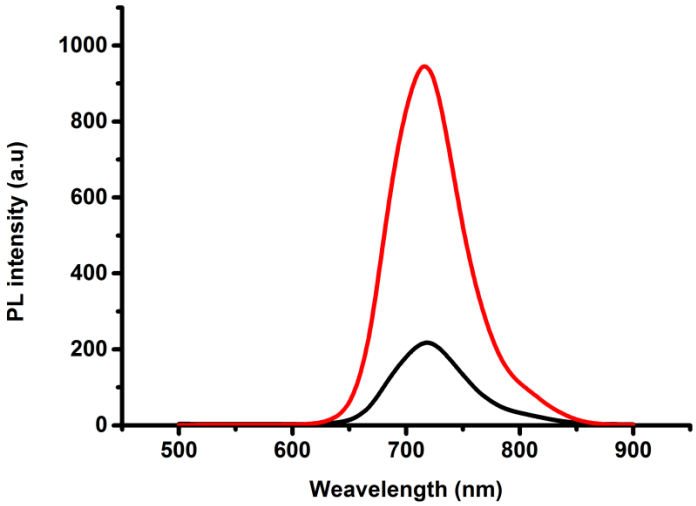

Figure 2-14. PL spectra of **QD705-Pen** 1 day (red) and 2 years (black) after aqueous phase transfer.

The colloidal stability and high PL QY in the aqueous phase is evident even by checking with the bare eyes when looking at the different samples under UV-illumination (**Figure 2-15**).

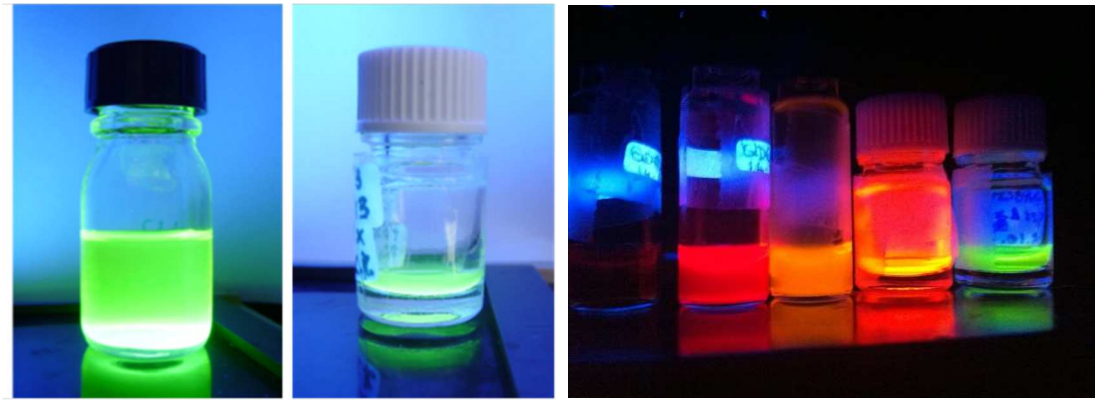

Figure 2-15. Left two images: photographs **QD530** dispersed in chloroform (left) and of **QD530-Pen** in water (right). Right: Photographs of Pen-functionalized **QD705**, **QD655**, **QD605** (2x) and **QD530** taken two years after aqueous phase transfer with **Pen** (all samples under UV illumination).

2.4.2.2 FTIR spectroscopy and gel electrophoresis

With the goal to put into evidence the successful surface functionalization, FTIR spectra of QDs capped with **Pen** and **Mal1** were measured and compared with the spectra of **Pen** and **Mal1** alone. We emphasize that all types of QDs behave similarly; therefore we just name them QD without further specification in the FTIR studies. As shown in **Figure 2-16** (left) the characteristic S-H stretching vibration band of **Pen** at 2500-2600 cm^{-1} has completely disappeared in the FTIR spectrum of **QD-Pen**, reflecting the binding of the thiolate groups to the ZnS surface of the QDs. In addition, FTIR also clearly revealed the peaks corresponding to the carbonyl stretch vibrations of the maleimide function centred at 1000 cm^{-1} in QD-Mal1 (**Figure 2-16** right). This showed that the maleimide function is intact, and that it points out of the QD surface as its vibrations remained unchanged with respect to the free molecule.

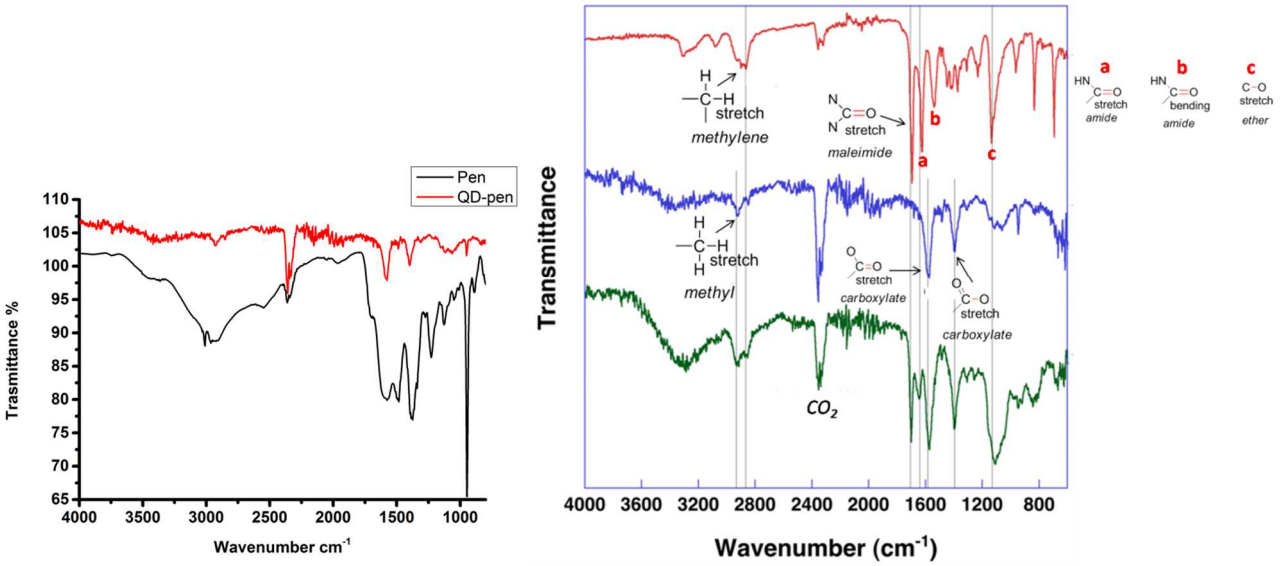

Figure 2-16. Left: FTIR spectra of **Pen** and QD-**Pen**. Right: FTIR spectra of **Mal1** (red), QD-**Pen** (blue) and QD-**Mal1** (green) and indication of the characteristic vibrations.

In addition, **QD-Pen** post-functionalized with **Mal1** was monitored using agarose gel electrophoresis, a technique normally used for DNA, RNA and protein separation. Based on the charges present on the molecules, loaded DNA, RNA and proteins will move toward the positive side at different speeds. The movement speed is based on the molecular weights of segments; the smaller the molecule weight, the faster the movement speed. Gel electrophoresis has also been proven to be useful in the analysis of nanoparticles, as for example in the separation of QD-DNA conjugates.[92] More generally it has been shown that gel electrophoresis can be used for the separation both of QDs and QD-biomolecule conjugates.[93] Furthermore, by comparing the size of different conjugates, samples showing complete conjugation can be separated from samples with incomplete conjugation. As depicted in **Figure 2-17**, nanoparticles at the first

and second step of functionalization (**QD-Pen** and **QD-Mal1**) were loaded on the gel. For each type of the QDs a delay in the migration pattern was observed in the case of **QD-Mal1**. This retardation is indicative of the successful post-functionalization with **Mal1**, remains however a qualitative signature. In order to quantify the number of **Mal1** we tried different techniques, unfortunately without success. First we attempted to use NMR spectroscopy but, due to the high concentrations required, we were not able to quantify the Mal1/Pen ratio. Next we tried to exploit colorimetric approaches based on the differences in the absorption spectra of the different ligands. However, as the absorbance of the QDs is extremely high in the UV range where **Pen** and **Mal1** absorb, their quantification by this method is not possible without large error bars. Then again we tried to quantify using a DNA ladder (DirectLoad™ 50 bp DNA Step Ladder, from Sigma Aldrich) which required 2% agarose gel concentration; however at this concentration it was not possible to observe the QDs band.

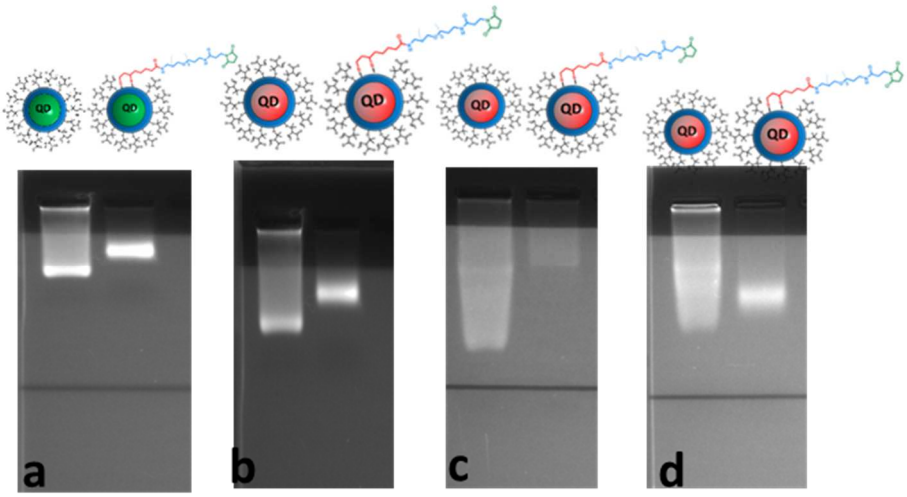

Figure 2-17 Gel electrophoresis characterization of the samples **QD530** (**a**), **QD705** (**b**), **QD605** (**c**) and **QD655** (**d**) capped with Pen (left bands) or **Mal1** (right bands), carried out on 1% agarose gel in 25 mM Hepes buffer at 100 V on a RunOne System. Prior to gel electrophoresis, to each sample a solution corresponding to 20% of the sample volume and containing Orange G and 30% glycerol in 6% loading buffer was added. For visualization, the gel was placed on a UV transilluminator, and an image was captured with a Gel Doc XR system (Bio-Rad, Hercules, CA). In (**a**) the image shown here was acquired after 10 min while in **b**, **c** and **d** it was taken after 20 min.

2.5 Conclusion

In this chapter we developed a versatile phase transfer and post-functionalization approach, applicable to QDs of various compositions, sizes and shapes. In the first step, the aqueous phase transfer of InPZnS@ZnSe/ZnS NCs core@shell NCs emitting at 530 nm, InPZnS core-only QDs emitting at 510 nm and of commercial hydrophobic CdSe-based QDs emitting at 605, 655 and 705 nm was achieved by surface ligand exchange with penicillamine (**Pen**). In the second step, we introduced maleimide functional groups on the NC surface, which can bind to sulfhydryl groups, for example, in the hinge regions of antibodies.[94] This coupling between maleimide and sulfhydryl groups is known to be highly efficient and to provide a stable linkage.[36, 86] The post-functionalization has been achieved by applying the heterobifunctional crosslinker **Mal1** containing a lipoic acid anchoring function and a maleimide group, separated by three poly(ethylene) glycol moieties. The bidentate (reduced) lipoic acid function is able to substitute **Pen** molecules and provides excellent stability of the **Mal1** ligand on the NC surface. Successful grafting of the **Mal1** ligand has been evidenced by dynamic light scattering (DLS), FTIR and agarose gel electrophoresis, even though the exact number of **Mal1** ligands per NC could not be quantified. One challenge was to identify appropriate conditions in terms of ligand concentration and pH value, which allowed preventing from undesired crosslinking reactions this ligand is prone to. This method yielded very compact (hydrodynamic diameter < 10 nm) and strongly fluorescent probes (QYs up to 54%), with excellent long-term stability (> 2 years) in various buffers and water. Due to the dynamic binding interactions between the thiol and ZnS, QDs coated with monothiol ligands normally tend to have shorter shelf lives.[95] In the literature the stability of QDs after ligand exchange has been evaluated to be less than one year.[96] We attribute the improved stability in first place to the optimized aqueous phase transfer with **Pen**, in particular to the precise pH control enabling deprotonation of the thiol function and enabling strong thiolate binding to the QD surface, while preventing from disulphide formation due to the addition of TCEP. Efficient electrostatic repulsion of the QDs is assured by the negatively charged carboxylate groups of the **Pen** ligand, as demonstrated by zeta potential measurements. Although post-functionalization with the (neutral) **Mal1** ligand leads to a smaller absolute value of zeta potential, the colloidal stability is not affected, presumably due to the presence of the short PEG chains. Importantly, FTIR indicates the integrity of the maleimide functions, which are expected to stick out of the **Pen** ligand shell of the QDs. The application of these functions for the conjugation of antibodies will be explored in the next chapter.

2.6 Experimental section

Chemicals. D-Penicillamine, tetramethylammonium hydroxide (TMAOH), phosphate-buffered saline solution (10X PBS), tris(2-carboxyethyl) phosphine hydrochloride solution 0.5 M (TCEP), tris(hydroxylmethyl)aminomethane (TRIS/Cl), agarose powder, indium acetate (99.99%), myristic acid (>99%), tris(trimethylsilyl)phosphine (95%), 1-dodecanethiol (97%), 1-octadecene (90%), were purchased from Sigma-Aldrich. Zinc stearate (90%) was acquired from Riedel de Haën. MAL-dPEG3-Lipoic acid (**Mal1**) was purchased from Quanta Biodesign. QD CdSe 605, 655 and 705 were purchased from Life Technologies/Thermo Fisher.[27] Solvents were purchased from Aldrich, Fluka, and Acros, and used without further purification. All water solutions were prepared from ultrapure laboratory grade water (resistivity 18 MΩ cm) that was filtered and purified using a Millipore MilliQ cartridge system and autoclaved.

Instruments. Absorption and emission spectra were recorded on the following spectrometers: HP 8452A and Perkin Elmer Lambda 35 for UV-Vis absorption; Hitachi F-4500 fluorescence spectrophotometer equipped with a 150 W xenon lamp and excitation monochromator. The hydrodynamic diameter (by dynamic light scattering) and zeta potential of the NCs dispersed in water were measured using a Malvern Zeta Sizer (NanoZS). Fourier transform infrared (FTIR) spectra were taken on a Perkin Elmer Paragon 500 spectrometer equipped with an attenuated total reflection (ATR) setup. Gel images were acquired using a Gel Doc XR system (Bio-Rad, Hercules, CA).

Transmission Electron Microscopy

Conventional and high resolution transmission electron microscopy (HRTEM) images were recorded on a JEOL 3010 working at 300 kV, equipped with a LaB_6 gun and a GatanOrius SC 200 2k x 2k CCD camera. Size distributions were determined manually on some hundred NCs using Fiji software; the low contrast of the QDs on the amorphous carbon film supported by a copper grid did not allow reliable binarization of the images and automatic determination of the mean size and its standard deviation.

InPZnS@ZnSe/ZnS QD Synthesis.

The synthesis of InPZnS@ZnSe/ZnS alloy core / gradient shell nanocrystals is based on reported procedures.[23, 97] All steps except for nanocrystal purification have been carried out under inert atmosphere.

Preparation of precursor solutions.

For the preparation of the indium myristate ($In(MA)_3$) stock solution (0.1 M), 1 mmol of anhydrous indium acetate was mixed with 3 mmol of myristic acid (MA) and 10 mL of 1-octadecene (ODE) in a 50 mL three-neck flask equipped with a condenser. The mixture was heated to 100-120 °C for 1 h under vacuum until an optically clear solution was obtained. After backfilling the flask with Ar and cooling to room temperature, the turbid solution of indium myristate was stored in a glovebox. For the zinc oleate ($Zn(OA)_2$) stock solution (0.4 M), 5 mmol of zinc acetate, 10 mmol of oleic acid (OA) and 9.35 mL of ODE were loaded into a 50 mL three-neck flask and the same procedure as for the preparation of $In(MA)_3$ was followed. The zinc stearate ($Zn(St)_2$) stock solution (0.1 M) was prepared by heating 1 mmol of $Zn(St)_2$ with 10 mL of ODE at 120°C for 1 h. A 0.4 M TOPSe stock solution was prepared by the dissolution of 2 mmol Se powder in 5 mL of trioctylphosphine (TOP) under stirring for 24 h. A TOP-S stock solution was prepared with the same procedure using elemental sulphur.

Synthesis of InPZnS alloy nanocrystals.

In a glovebox, 1 mL of the $In(MA)_3$ stock solution (0.1 mmol $In(MA)_3$), 1 mL of the $Zn(St)_2$ stock solution (0.1 mmol), 0.1 mmol of 1-dodecanethiol (DDT) and 7.5 mL of ODE were added to a 50 mL three-neck flask. Afterwards the flask was equipped with a condenser and connected to a Schlenk line. Next, the mixture was heated under vigorous stirring to 300°C with a ramp of around 60°C/min using a molten salt bath. When the temperature inside the flask reached 100°C, 0.1 mmol of tris(trimethylsilyl)phosphine ($P(TMS)_3$), diluted with 1 mL of ODE, were injected. During the heating, NC formation is visible by the color change of the reaction mixture to dark yellow/orange. After 30 min, the reaction mixture was cooled to below 220 °C to stop growth.

Growth of a ZnSe/ZnS gradient shell.

For the ZnSe/ZnS gradient shell growth, a 10 fold excess of precursors was used with respect to the core synthesis, and a Se:S ratio of 0.2. Briefly, $Zn(OA)_2$ (1 mmol, 2.5 mL of the 0.4 M stock solution) was added dropwise to the reactive mixture at 220°C. This was followed by the successive injection of TOP-Se (0.2 mmol, 0.5 mL of the 0.4 M solution) and TOP-S (0.8 mmol, 2 mL of the 0.4 M solution). The resulting mixture was heated to 300°C within 10 minutes and then kept at this temperature for 20 min. After cooling down to room temperature, purification of the QDs was performed via three cycles of precipitation/redispersion. First, 10 mL of a 1:1 (v/v) mixture of chloroform/methanol and 100 mL of acetone was added. Then the resulting suspension was centrifuged (*8000* rpm for 5 minutes), the supernatant discarded and the obtained solid dispersed in 5 mL of chloroform. Finally, the QDs can be dispersed and stored in a variety of organic solvents, like hexane, toluene or chloroform.

Determination of the molar extinction coefficient and of the concentration of InP-based QDs.

While literature data can be found on InP core nanocrystals,[98, 99] the molar extinction coefficient and size/excitonic peak correlations for InPZnS alloy or InPZnS/ZnSe/ZnS core/shell QDs are unknown. Therefore we determined the molar extinction coefficient of our **QD530** NCs in order to be able to conveniently estimate their concentration in divers colloidal solutions by simply taking a UV-vis absorption spectrum. First, with a known amount of the parent **QD530** sample thermogravimetric analysis (TGA) was carried out; by this way the total fraction of the organics (surface ligands) was obtained. The inorganic diameter of the NCs has been estimated from TEM (depending on the batch between 4.8 and 5.4 nm) and for the calculations a mean density value of 4710 kg/m^3 has been taken, the values of InP, ZnSe and ZnS being 4810 5650 and 3980 kg/m^3, respectively. Assuming spherical shape a 4.9 nm sample results for example in a molar weight of 174 kg/mol, based on which the molar quantity of NCs in the sample used for TGA can be calculated. Finally, the knowledge of the molar concentration enables us to calculate the molar absorptivity of the given sample at the wavelength λ by measuring its absorption spectrum and using Lambert-Beer's law (***cf.*** **Figure 2-18**):

$$A = \varepsilon * c * l$$

where A, ε, c and l are the absorbance at λ (dimensionless), molar absorptivity ($M^{-1}\cdot cm^{-1}$), molar NC concentration (M), and path length of the cuvette in which the sample is contained (cm), respectively. For our InPZnS/ZnSe/ZnS QDs we determined ε at 450 nm as 4.15×10^5 $M^{-1}\cdot cm^{-1}$, which is in good agreement with the literature on InP QDs.[39] As a consequence, the concentration of InP NCs can easily be estimated from the absorption spectrum using Lambert- Beer's law. One of the major advantages of the described method is that it is entirely based on the properties of the inorganic core of the NCs and not on the organic surfactant layer, giving therefore more accurate results.[13]

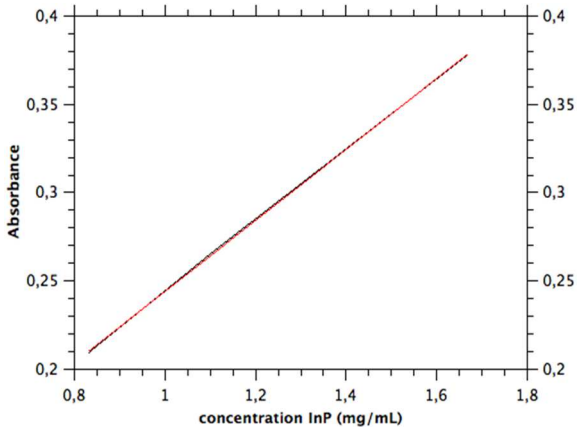

Figure 2-18. Concentration versus absorbance plot (at 450 nm) for **QD530** (path length of the cuvette: 1 cm). The slope of the graph equals the molar absorptivity.

Purification prior to phase transfer.

Thorough purification of the initial QDs, enabling the complete removal of excess surface ligands or side products is crucial for successful phase transfer. 1 mL of the InPZnS@ZnSe/ZnS QDs in chloroform were mixed with 1 mL of anhydrous ethanol (in some case the QDs in chloroform were purified with a 4 mL of ethanol/methanol (3:1 v:v) mixture) and centrifuged at *10 000* rpm for 2 minutes. The clear solution of supernatant was discarded and the precipitate was dispersed in 1 mL of chloroform. This cycle was repeated three times. For the commercial CdSe/ZnS-based QDs in decane the solvent was changed to chloroform prior to phase transfer. 4 mL of a methanol/isopropanol (3:1 v:v) mixture were added to 1mL of the QD colloidal solution and centrifuged for 2 min at *10 000* rpm. The supernatant was discarded and the resulting pellet dispersed in 1mL of chloroform.

Surface Modification of QDs with Pen and Mal1:

- ***Phase transfer***. A 0.2 M solution of penicillamine (containing 200 µL of 0.5 M TCEP) was prepared in 1 mL of degassed MilliQ water (18 MΩ). The pH was adjusted to 9 by drop-wise addition of 0.5 M TMAOH. 500 µL of the phase transfer solution was mixed with 1 mL of a 3-5 µM colloidal solution of QDs in chloroform. The biphasic mixture was stirred vigorously at ~*1400* rpm for 2 h at room temperature. At the end of the transfer, affording QD-pen, the biphasic mixture results either in a clear separation of two phases or in an emulsion. Finally, the mixture is centrifuged at *5000* rpm for 1 min to obtain a clear phase separation. The QDs in the (upper) aqueous phase are separated from the (lower) organic phase.
- ***Purification and storage*.** A NAP™-5 -10, -25 size exclusion column (Sephadex™ G-25 DNA Grade from GE Healthcare) was vertically clamped and equilibrated according to the manufacturer's protocol. QDs in water were added and after being adsorbed on the gel bed, they were eluted using 1X PBS buffer and kept at 4°C in the dark for storage.
- ***Post-functionalization***

The steps for dissolving and conjugating the **Mal1** linker to the quantum dots are described below:

1. In a round bottom glass vial, to 3 mL ultrapure DI H_2O 0.0165 g of **Mal1** are added (final concentration ~ 10 mM).
2. The vial wrapped with Al-foil is placed on a stirrer: *300* rpm, 12 hours at room temperature.
3. The solution of **Mal1** and a solution of TCEP (0.046ml, 0.5M) in degassed DI water are added to the dispersion of QD-**Pen** (0.5ml 5.0 x 10^{-6} M).
4. The pH of the solution is adjusted to approx. 6.5-7.0 with TMAOH.

5. The solution is flushed with argon for 10 minutes and mixed at room temperature at *800* rpm for 8 hours.

6. Samples are purified using PD-10 column from GE-Healthcare according to manufacturer's protocol (the column is backlit with UV light to collect effectively QDs).

7. The purified samples are then concentrated using 30 K 4 mL Amicon spin columns at 4000g for 4 min affording a final volume of 400 µL. Alternatively concentration can be achieved under vacuum. The samples are kept at 4°C in the dark for storage.

Characterization of the QDs

Hydrodynamic size and dispersibility of QDs

The hydrodynamic diameter of the water-soluble NCs dispersed in water was measured by dynamic light scattering, using a Malvern Zeta Sizer (NanoZS). Given the sensitivity of the instrument, multiple runs (>3) were performed to avoid erroneous results. The spectra have been corrected by the instrument software for viscosity (0.882 mPa 3s at 25 °C), absorption (0.01), solvent (water) refractive index (1.33) and material (InPZnS/ZnSe/ZnS and CdSe/ZnS) refractive index (2.7 and 2.45). The data are collected in automatic mode and expressed in number %. The zeta potential is measured in the same instrument but under zeta potential settings. The used **Pen**-capped NCs were passed through Nap5 size exclusion columns from GE-Healthcare, dispersed in 1x PBS buffer and filtered (0.22 µm) prior to the measurements.

Gel electrophoresis

Preparation: For a 1 % gel, 0.4 g agarose powder were mixed in a 100 mL Erlenmeyer flask with 40 mL of 25 mM Hepes buffer, and heated in a microwave oven for some minutes until the solution started to boil. The flask was panned to help the agarose powder to dissolve totally, the flask was then again heated to the boiling point.

The hot and clear agarose was poured in a 10.7 x 5.2 cm gel tray levelled in a gel caster (RunOne System). A comb (12 wells) was placed into the gel. The gel was allowed to cool down to room temperature and to solidify within at least 1 hour. The comb was removed, the gel was taken out of the casting device and placed into the electrophoresis device which was filled with 25 mM Hepes buffer until the whole gel was covered.

Loading and running: The samples were mixed with about 20 % of their volume with the loading buffer (30 % glycerol in 25mM Hepes) and carefully filled into the wells. The electrophoresis devices were run at a constant voltage of 100 V.

Imaging: After 5, 10, 20, 30 minutes the gels were taken out and a digital picture was taken (BioRad Gel Doc) showing the gel under visible or UV light. The resulting images were saved on the computer connected to the camera.

3 Application of QDs in biological detection and imaging

3.1 Introduction

This chapter is devoted to the investigation of the applications and unique properties of quantum dots (QDs) and lanthanide (Ln) complexes for biological detection and imaging. Ln ions and QDs provide exceptional photophysical properties that cannot be found in any other luminescent material.[100]

In the first section we focus on FRET immuno-assays based on terbium complexes acting as the donor and QDs acting as the acceptor in a sandwich complex Tb-AB1-AG-AB2-QD (AB1, AB2: antibodies, AG: antigen/biomarker). In the second part of this chapter, we discuss the bio-applications of Ln-QD conjugates obtained by direct grafting of Ln complexes on the QD surface.

As mentioned in the introduction **Chapter 1**, FRET-immuno-assays are based on biomolecular recognition events that occur between a biomarker and two specific antibodies labeled with different fluorophores. Upon the immune interaction, the spatial proximity of the two dyes can enable Förster resonance energy transfer, which can be used to quantify the biomarker concentration.

However, while the development of monoclonal antibodies provides very specific interactions with biomarkers, the use of conventional fluorescent labels shows limited detection sensitivity and no possibility of multiplexed analysis on a single sample.[28] Indeed, fluorescent proteins and organic fluorophores are extensively used in many bioimaging and in biosensing investigations.[101] However, their fluorescence is relatively weak and unstable, which precludes the use of high excitation densities and limits the possibility of long-term studies.[102] Additionally, their PL lifetimes are in the same range (few nanoseconds) as the biological autofluorescence, which does not allow time-gated (TG) detection for increasing the signal-to-noise ratio (SNR) and for better differentiation between different target molecules.[103, 104] As already mentioned, QDs possess unique optical properties, which make them interesting alternatives over traditionally used organic dyes or fluorescent proteins, namely: size-dependent, narrow, tunable emission spectra and broad excitation spectra, large absorption cross-sections, high fluorescent quantum yields and long-term resistance against photobleaching.[32, 105] In particular in combination with luminescent lanthanide complexes (LLCs) and time-resolved FRET (TR-FRET) spectroscopy these nanoprobes provide significant sensitivity, distance, and multiplexed detection advantages compared to other donor-acceptor pairs.[106-108]

Within the plethora of QD-FRET biosensing applications for the analysis of biomolecular interactions, homogeneous sandwich immunoassays, which quantify biomarkers via two different antibodies that engage in FRET upon biomarker recognition, are highly selective and sensitive but also range among the most challenging systems. This is because the relatively large sizes of ABs (*ca.* 10 nm in length) and QDs (depending on their emission wavelength and surface coatings) plus the connection of the ABs via a

biomarker (often proteins with sizes of up to several nm) lead to long distances between the QDs and their FRET partners. FRET-immunoassay have been developed using QDs as donors[9, 79, 109-115] as well as acceptors.[11, 49, 116-119] These Tb-to-QD FRET immunoassays could provide multiplexing capability and clinically relevant limits of detection (LODs) in serum samples.[11, 49]

Although QDs are theoretically very well suited as FRET acceptors due to their strong absorbance over a broad wavelength range yielding large overlap integrals, the unavailability of stable, reproducible, biocompatible QDs has restricted their use in real applications. Nonetheless, several commercial suppliers of biocompatible QDs exist.[120] However, if QDs are used as FRET acceptors there is an efficient direct excitation of the QD at almost any wavelength used for donor excitation (due to the broad absorption spectrum of the QD). This will hamper the selective excitation of the respective FRET donor and therefore results in inefficient FRET.

The solution for this problem is the use of donors with long excited-state lifetimes such as LLCs (lifetimes up to several milliseconds) in combination with pulsed excitation. This offers the possibility of delayed or time-gated acquisition of the emitted light. By this way, autofluorescence of the sample, fluorescence of other labels and light scattering are largely suppressed, and the signal to background ratio is improved. Additionally, the combination of LLCs donors and QD acceptors for FRET enables energy transfers over large distances exceeding 10 nm and in exceptional cases up to 20 nm, due to the large spectral overlap.

As mentioned in the **Chapter 2** (**section 2.3**), the aqueous phase transfer process– for which QDs have to be chemically modified to be stable in aqueous solutions and tagged with the recognition molecules or drugs for biomedical applications-is a critical process. These steps can cause significant alterations in brightness, stability and size of the QDs.[121]

Normally, the relatively large surface of QDs gives rise to multiple interactions with the biological environment, which can cause further changes in their physical and chemical properties. Many literature protocols and commercial products rely on the encapsulation of the QDs with bulky amphiphilic polymers, which leads to hydrodynamic diameters in the range of 15-20 nm or more resulting in long FRET donor-acceptor distances and unfavorable binding conditions. This leads to lower sensitivities compared to conventional time-resolved (TR)-FRET immunoassays that use lanthanide donor and organic dye acceptor AB conjugates.[101, 122] These assays are frequently used in diagnostics and are commercially available under the brand name HTRF (homogeneous time-resolved fluorescence), TRACE (time-resolved amplified cryptate emission) or LANCE (lanthanide chelate excitation).[123-125] The development of QD-AB conjugates with compact surface functionalization for aqueous phase transfer and high-performance photophysical properties for efficient FRET immunoassays would therefore present a milestone of utmost importance for the integration of QDs into clinical *in-vitro* diagnostics (IVD). Further improvement of the sensitivity and selectivity of these assays can be achieved thanks to 1) the multiplexing possibilities offered by the QDs as

well as 2) by the development of efficient NIR emitting QDs, maximizing the spectral overlap integral with Ln complexes.

As presented in the **Chapter 2**, we focus on direct ligand exchange, which yields a much more compact surface coating beneficial for FRET applications. In fact, our approach represents a novel QD functionalization and bioconjugation approach, which yields stable and highly luminescent QD-antibody conjugates for improved TR-FRET immunoassays.

Aqueous phase transfer of lab-synthesized InPZnS@ZnSe/ZnS QDs emitting at 530 nm and commercial CdSe@ZnS QDs (Life Technologies) emitting at 605, 655 and 705 nm was achieved by surface ligand exchange with penicillamine (**Pen**). These QD emission wavelengths have been selected as they give minimal interference with the emission of Tb-complexes, used as FRET donor (**Figure 3-1**). Under optimized conditions, this functionalization results in a very compact, around 1 nm thick, organic surface layer while preserving high PL quantum yields. The zwitterionic **Pen** also results in low non-specific binding and very high colloidal stability of several years in aqueous buffers, as shown in **section 2.4**.

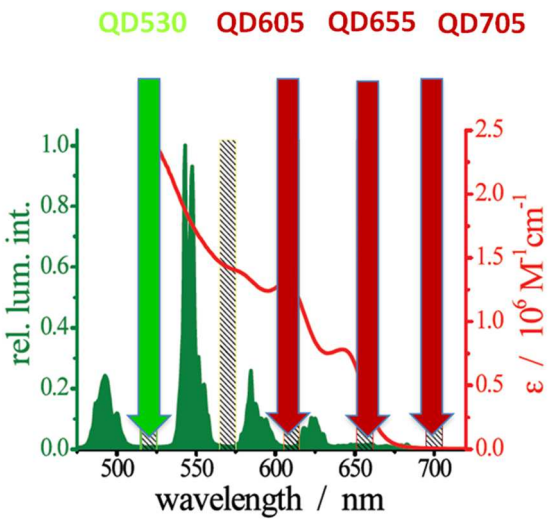

Figure 3-1. Typical narrow and well separated emission bands of Tb^{3+} allowing for a large choice of possible FRET acceptors, whose emission bands should be selected such as to avoid overlap allowing for the suppression of Tb background emission. The absorption spectrum of **QD705** is also indicated (red line).

Routine fluorescence-based immunelabeling strategies depend on four main parameters, which impose limitations on their practical use: the affinity of ABs, the optical properties of the fluorescent probes, the labeling method, and the size of the resultant conjugate composed of the AB, fluorescent probe, and optional linker molecules. The use of luminescent terbium complexes as FRET donors for QD acceptors is a great possibility to overcome the large distances in homogeneous FRET immunoassays and to provide at the same time high sensitivity and multiplexing capability.[107, 108, 126, 127]

Figure 3-2 presents the absorption and PL spectra of the different types of QDs used in this study in comparison with the PL of the Tb donor (Lumiphore™). The extremely long excited-state lifetimes of up to few ms of the Tb complex can be used for time-gated PL detection, which leads, as stated before, to a very efficient reduction of background fluorescence.[107, 126-129]

The conjugation of a fluorescent probe with an antibody (AB)[130] allows both specific recognition of the target and quantitative detection of the associated fluorescent signal.

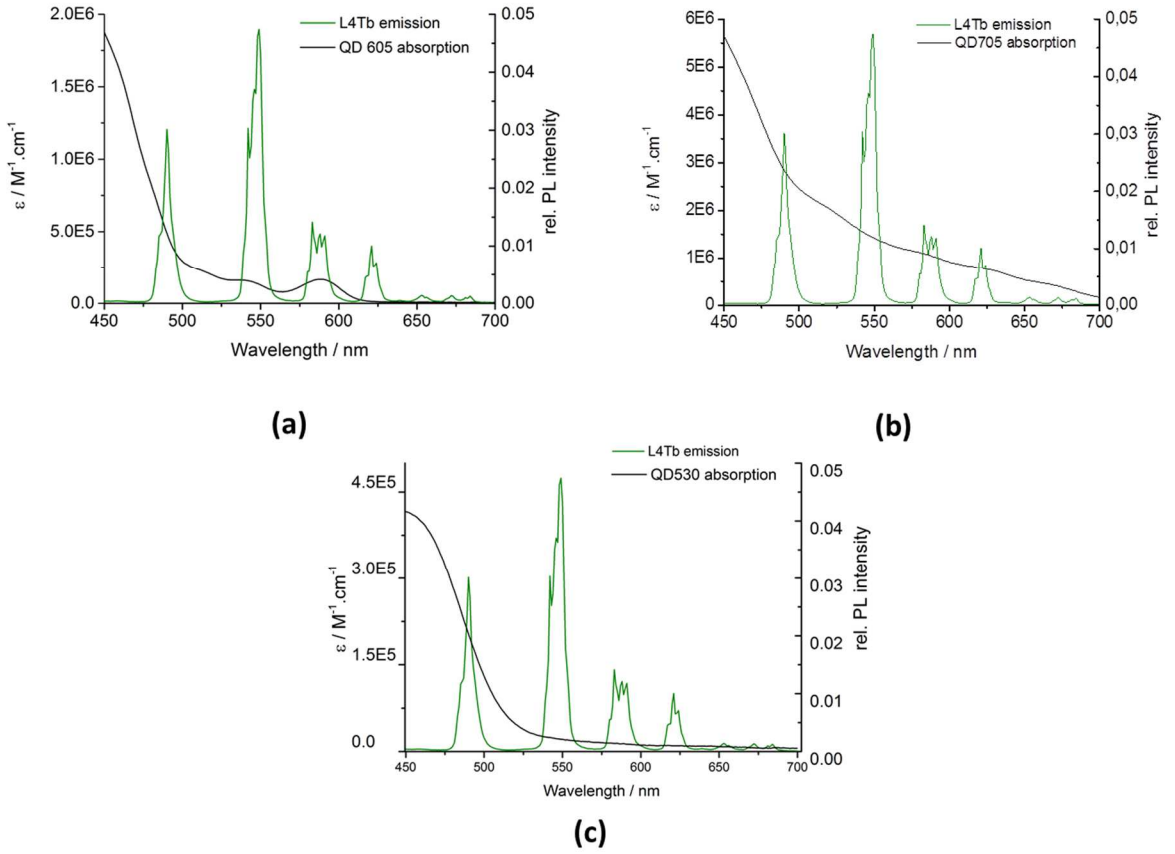

Figure 3-2. Spectral overlap of the different types of QD used in this study, **a) QD605**, **b) QD705** and **c) QD530** absorption spectra (black line) and area-normalized Tb-complex emission spectra (green line).

In the following paragraphs we will give a brief overview about antibodies, the procedure to obtain the immune-probe (QD-antibody bioconjugates) and their application as FRET acceptors in homogeneous time-gated immunoassay using Tb-ABs as FRET donors, both coupled by an immunological sandwich complex between the two ABs and a prostate specific antigen (PSA).

3.1.1 Antibodies and fragments of antibodies- structure and function

Antibodies defend vertebrates against infection by inactivating viruses and microbial toxins and by recruiting the complement system and various types of white blood cells to kill invading pathogens.[45]

The simplest antibodies are Y-shaped molecules with two identical antigen binding sites, one at the tip of each arm of the Y (**Figure 3-3**).[45] They are composed of four polypeptide chains, two identical heavy and two identical light chains. Parts of both the heavy and light chains usually combine to form the antigen-binding sites. There are five classes of antibodies (IgA, IgD, IgE, IgG, and IgM), each with a distinctive heavy chain (a, d, e, g, and m, respectively).[131]

The heavy chains also form the tail (Fc region) of the antibody, which determines the biological properties of the antibody class. Either type of light chain (k or l) can be associated with any class of heavy chain; this choice has no effect on the properties of the antibody, except for its specificity for antigens. Each light and heavy chain is composed of a number of Ig domains—βsheet structures constructed from about 110 amino acids. A light chain has one variable (VL) and one constant (CL) domain, while a heavy chain has one variable (VH) and either three or four constant (CH) domains (**Figure 3-4**). The amino acid sequence variation in the variable domains of both light and heavy chains is concentrated in several small hypervariable regions, which protrude as loops at one end of these domains to form the antigen-binding site.

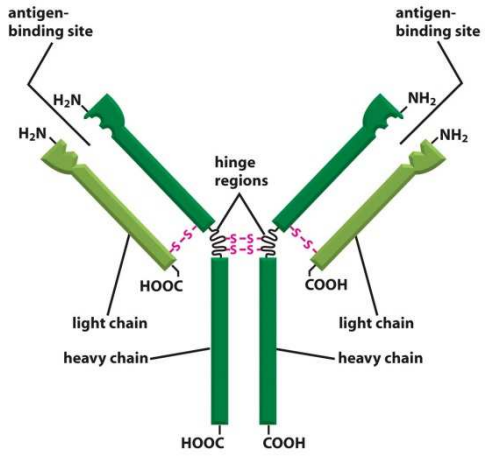

Figure 3-3. Schematic representation of an immunoglobulin (IgG). It should be distinguish the heavy chains (dark green), the light chains (light green), the disulfide bridges and the amino groups in the terminal portion, which also represents the binding site for the antigen.[45] Image taken from *Molecular Biology of the Cell (©Garland Science 2008)*

The conjugation of nanoparticles with antibodies combines the properties of the nanoparticles themselves with the specific and selective recognition ability of the antibodies to antigens.[132]

To achieve this reaction, the antibodies do not only need to be conjugated to the QDs, they also need to preserve their binding efficiency for their antigen, to allow another primary antibody (labeled with LLCs) to bind to the same antigen and to offer a donor-acceptor distance short enough for efficient FRET. With this

in mind, we investigated the QDs-antibody (QD-AB) conjugation and purification efficiency using entire IgG ABs and Fab fragments ABs. Fragmentation is performed using standard fragmentation kit, working with papain and pepsin cleavage as shown in **Figure 3-4**.

One method of introducing sulfhydryl residues into antibody molecules for conjugation with maleimide-actived QDs is to reduce indigenous disulfide group in the hinge region of the immunoglobulin structure. In the following sections, we will investigate this bio-conjugation.[36]

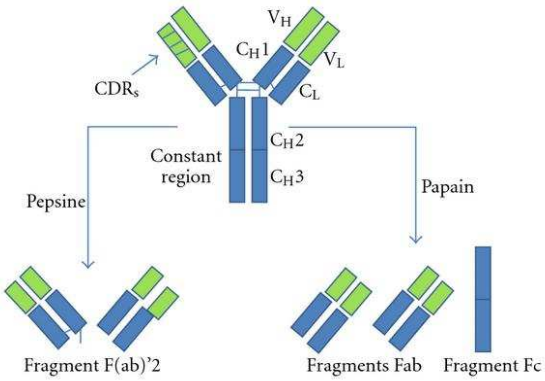

Figure 3-4. Structure of an IgG molecule and relative fragments antibody obtain from the action of enzymes papain and pepsin. Image taken from [132]

3.1.2 Flexible antibody conjugation and purification

Initial attempts for the conjugation of full IgG antibodies with the QDs did not yield satisfying results in terms of FRET efficiency. The complex in this scenario is composed of a QD (*ca.* 8 nm diameter), a first AB (*ca.* 150 kDa corresponding to a length of approximately 10 nm for the Y-shaped IgG), a biomarker (different sizes, *e.g.*, 32 kDa or *ca.* 2 nm for prostate specific antigen, PSA), and finally a second AB with the Tb complex. In order to have a more compact system with lower separation distance between the donor and acceptor, monoclonal fragmented antibodies (F(ab), *ca.* 50 kDa) and full-size IgG against PSA were conjugated to QDs and Tb complex, respectively.[11] These probes enabled the realization of homogeneous Tb-to-QD FRET immunoassays.

The Tb complexes (Lumi4-Tb-NHS) were labelled directly to available primary amines of the IgGs while the coupling of F(ab) to the QDs employs sulfhydryl chemistry[94] where the reactive maleimide functionalities introduced on the QD surface target free biomolecular thiols, such as those in the hinge region of Ab or F(ab). Such bioconjugation allows the formation of a nanocrystal (NC) retaining its optical properties with the specific and selective recognition ability of the antibodies to antigens.[132] As depicted in **Figure 3-5c** the F(ab) were first activated through reduction of the S–S bond by TCEP and the maleimide group was coupled with the free thiol group of the reduced F(ab) to form a covalent thioether bond.[36] The same

functionalization and post-functionalization approach was implemented to allow the linkage of F(ab) to all types of QDs studied, namely InPZnS@ZnSe/ZnS emitting at 530 nm (**QD530**) and CdSe@ZnS emitting at 605 and 705 nm (**QD605** and **QD705**). As mentioned before, these wavelengths have been selected, as they give minimal interference with the emission of Tb-complexes, used as FRET donor (**Figure 3-1).** Another important aspect of our investigation was the performance evaluation of QDs with different PL emission wavelengths and composition (**QD530**, **QD605**, and **QD705**). This evaluation is very important for their application as acceptors in FRET assays with Tb donors because the variations in shapes, sizes, spectral overlap (QD absorption with Tb emission), and PL wavelength range lead to differences in FRET and detection efficiencies, which can result in significant differences in sensitivity. Therefore a careful photophysical characterization and sensitivity evaluation within comparable immunoassays for the same antigen are indispensable for designing and optimizing such homogeneous FRET immunoassays, in particular for multiplexed detection with different QD colors. In the following paragraphs, we will discuss the photophysical properties of the assay constituents (Tb and QD AB-conjugates) and we will show their performances in Tb-QD FRET immunoassays for the detection of PSA in low volume serum samples. We would like to point out that these results have been obtained in the frame of an ongoing collaboration with the NanoBioPhotonic group of IEF Orsay.

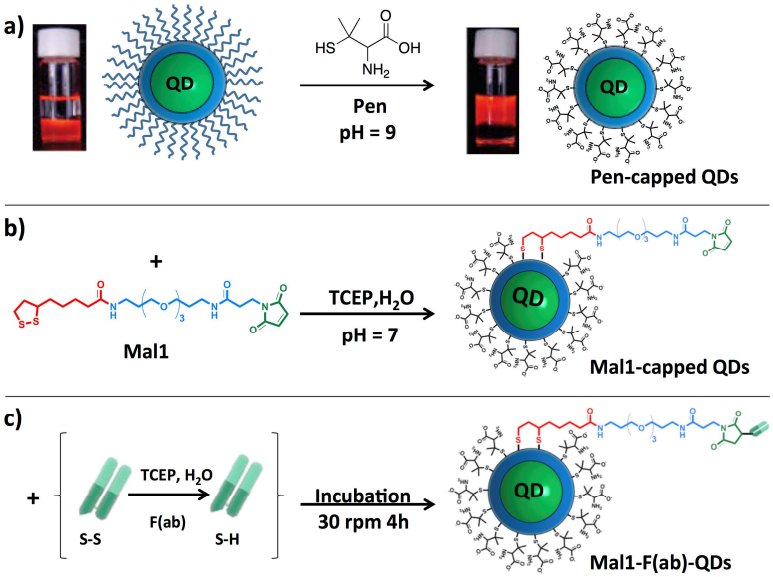

Figure 3-5. Schematic representation of the aqueous phase transfer of QDs with penicillamine (**Pen**) and post-functionalization with **Mal1** for subsequent conjugation to sulfhydryl groups of fragmented F(ab) antibodies.

3.1.3 Photophysical characterization of the Tb-QD-AB conjugates

As already described in the **Chapter 2**, surface functionalization of the QDs with **Pen** and post-functionalization with **Mal1** did not lead to significant modifications of their UV-Vis and PL spectra (***cf.* section 2.4**). The absorption and PL spectra of the three QD-AB conjugates are shown in **Figure 3-6**. QDs concentrations were determined using the molar attenuation coefficients of ε_{450nm}(**QD530**) = 4.2 x 10^5 M^{-1} cm^{-1} (experimentally determined), ε_{405nm}(**QD605**) = 2.8 x 10^6 M^{-1} cm^{-1} and ε_{405nm}(**QD705**) = 8.3 x 10^6 M^{-1} cm^{-1} (provided by the supplier).[27] The photophysical properties of the QDs were slightly altered by the F(ab) conjugation, as summarized in **Table 3-1**, compared to the **Pen**-capped QDs.

A PL red shift of 4 nm could be detected for the CdSe-based **QD605** and **QD705**, while a blue shift of 3 nm was found for the InP-based **QD530**. Further experiments are needed to unequivocally elucidate the origin of these shifts; we tentatively ascribe them to the quantum confined Stark effect, induced by the change of the dielectric environment of the QDs upon conjugation with F(ab).[39] AB-conjugation also led to changes in the PL lifetimes (**Table 3-1**) from 24 to 18 ns for **QD530**, from 4.6 to 10 ns for **QD605**, and from 79 to 41 ns for **QD705**. These changes are attributed to the generation (lifetime shortening) or filling (lifetime increase) of electronic trap states acting as competing de-excitation channels upon F(ab) attachment.

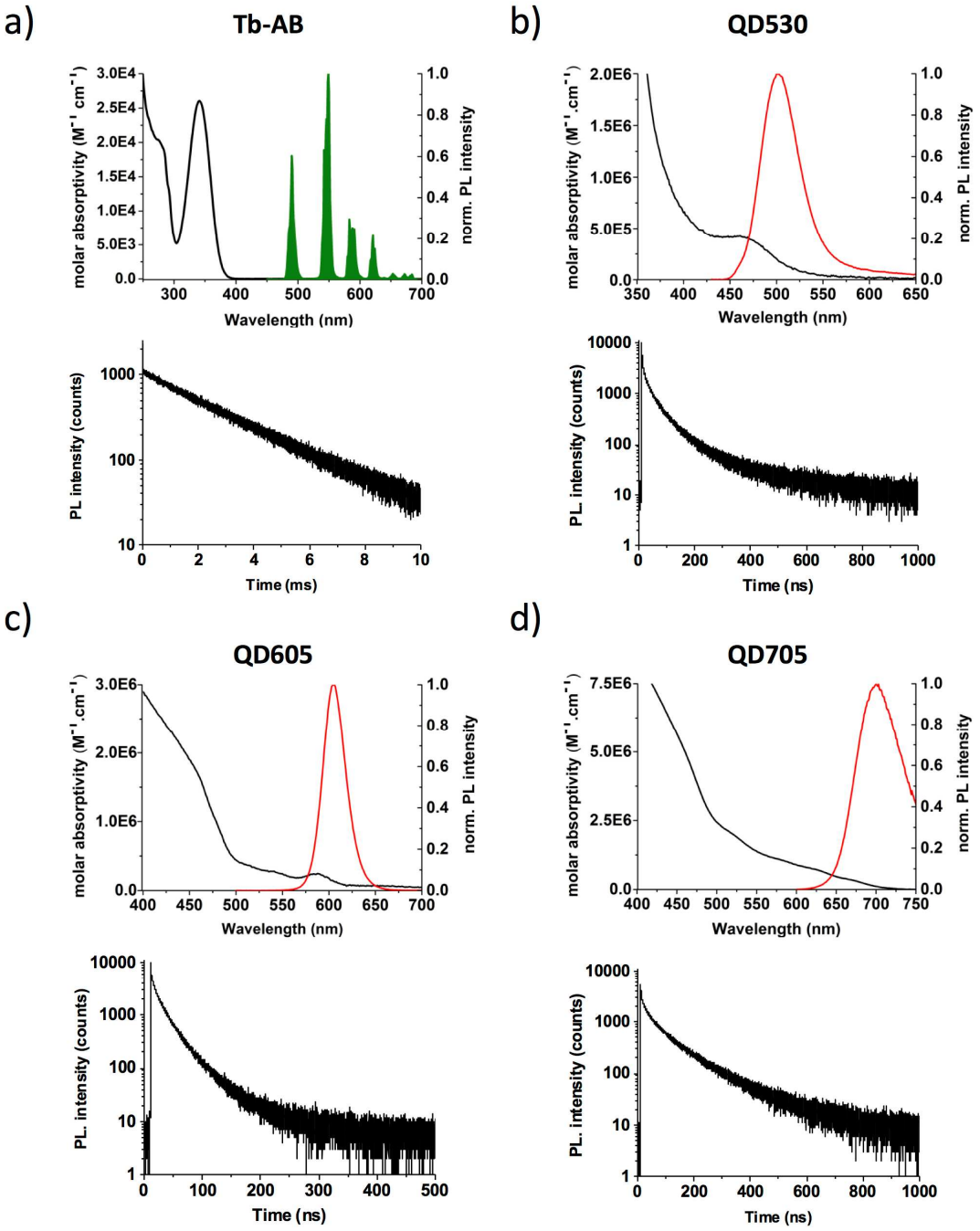

Figure 3-6. **a)** Top: absorption (black line) and PL (green, excitation wavelength 365nm) spectra of Tb-AB conjugate. Bottom: Tb-AB PL decay curve (490±0.5nm) upon pulsed excitation at 365nm with a repetition rate of 100 Hz. Amplitude-averaged decay time: τ(Tb) = (2.6±0.7) ms. **b-d)** Top: absorption (black) and PL (red) spectra; bottom: PL decay curves of F(ab)-conjugated InPZnS@ZnSe/ZnS (**QD530**), CdSe@ZnS (**QD605**), and CdSe@ZnS (**QD705**) QDs in 1X PBS buffer. Amplitude-averaged PL lifetimes: τQD530 = (17.7 ± 2.8)ns, τQD605 = (10.4 ± 1.1)ns, and τQD705 = (40.7 ± 6.4)ns.

Table 3-1. Optical characterization of QD-F(ab) conjugates, performed by excitation at 405 nm using as excitation sources a continuous-wave Xe lamp and a pulsed laser diode from Edinburgh Instruments for steady-state and time-resolved measurements, respectively.

Sample	**InPZnS/ZnSe/ZnS 530**		**CdSe/ZnS 605**		**CdSe/ZnS 705**	
	-Pen	**-F(ab)**	**-Pen**	**-F(ab)**	**-Pen**	**-F(ab)**
$\lambda_{emission}$ (nm)	**505 ± 1**	**502±1**	**602±2**	**606±0.5**	**699±2.5**	**703±0.5**
Average lifetime (ns)	**24.3±6.1**	**17.7±2.8**	**4.6±0.4**	**10.4±1.1**	**79.4±20.8**	**40.7±6.4**

Sizes and morphologies of the inorganic parts of the QDs were characterized using transmission electron microscopy (TEM), which revealed nearly monodisperse spherical (**QD530** and **QD605**) and elongated (**QD705**) nanocrystals (***cf.* section 2.4**). The hydrodynamic diameters of the QDs were evaluated by dynamic light scattering (DLS). As shows in **Figure 3-7**, these measurements confirmed the narrow size distribution observed with TEM and revealed small hydrodynamic diameters, which increase with each functionalization step. As exemplified by **QD705** (***cf.* Figure 3-7b)**, introduction of the **Mal1** ligand led to a size increase from 8 to 10 nm with respect to **QD705**-**Pen**, which is expected for a ligand with an approximate length of 3.0 nm. Conjugation with F(ab) led to a further increase to 13 nm as total hydrodynamic diameter, which makes this AB-QD conjugate one of the smallest AB-functionalized NIR emitting nanoprobes ever reported. Colloidal stability of the QDs in water or relevant buffer solutions is of crucial importance for biological detection. The obtained **Pen**- and **Mal1**-functionalized QDs showed no sign of aggregation after storage of more than two years at 4°C in the dark in 1xPBS buffer (pH = 7.4), as confirmed by combined periodical DLS and UV-Vis absorption measurements (**Section 2.4**). After F(ab) conjugation, the colloidal stability was determined to be at least 3 months, which is the current limit of our measurements. The photophysical and morphological characterization results have confirmed that our approach of using an optimized ligand exchange with **Pen**, followed by post-functionalization with **Mal1**, is an efficient and simple way of obtaining highly luminescent, stable, and compact QDs ready for further functionalization with small F(ab) ABs to yield very small fluorescent AB-nanoprobes.

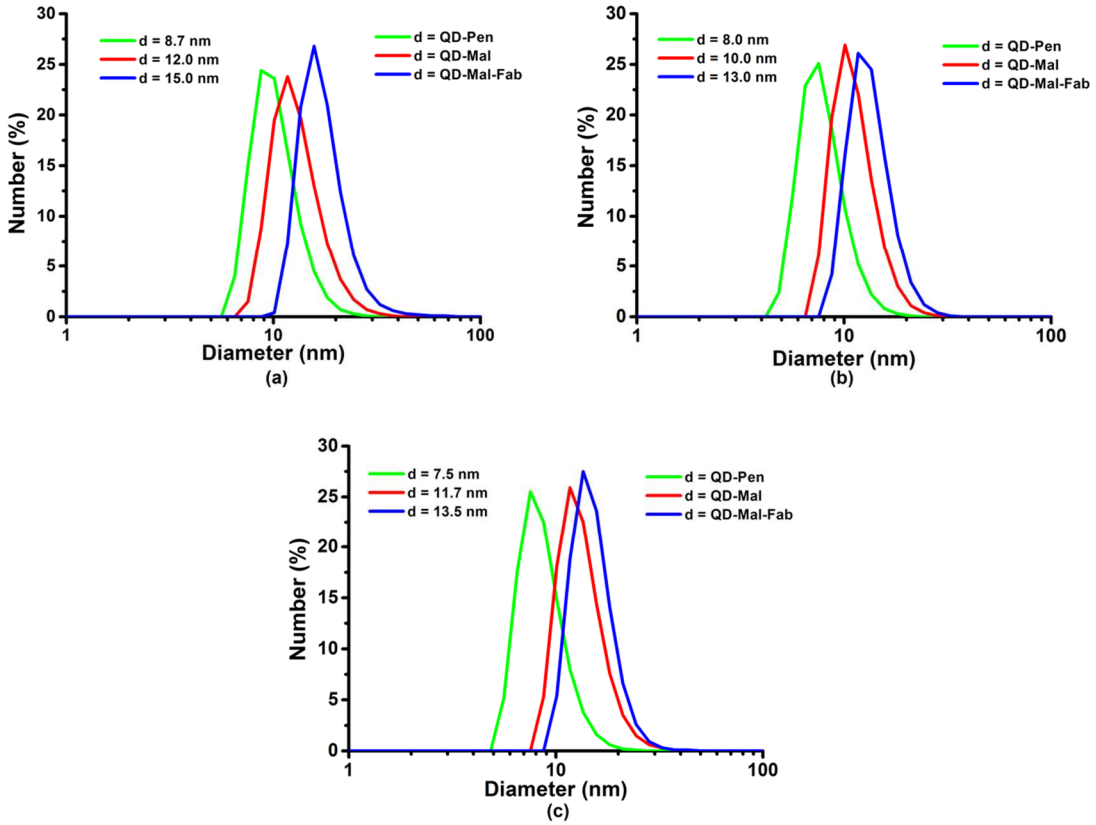

Figure 3-7. Size distribution of **a) QD605**, **b) QD705** and **c) QD530** after each functionalization step (**Pen**-capping: green; **Mal1**-functionalization: red; F(ab)-conjugation: blue) obtained by DLS measurements. The average hydrodynamic diameter d (nm) of each measurement is given in the legend.

Gel electrophoresis and FTIR (**Figure 3-8**) measurements further confirmed successful post-functionalization with **Mal1** and F(ab) conjugation of the QDs. For all QDs, the bands on the agarose gel corresponding to the QD-F(ab) conjugates were the most retarded due to the larger sizes of the AB-QD conjugates. FTIR revealed, by comparison to the free, *i.e.* not QD-bound, molecules, peaks corresponding to the carbonyl stretching vibrations of the maleimide function in QD-**Mal1** as well as the characteristic band of the N-H stretching vibration of F(ab) in QD-**Mal1**-F(ab). In these characterizations all three types of QDs (*i.e*. InP and CdSe-based QDs), which was expected as they mainly differ in the inorganic core composition but all possess an identical ZnS outer shell and the same first ligand exchange procedure with **Pen** has been used.

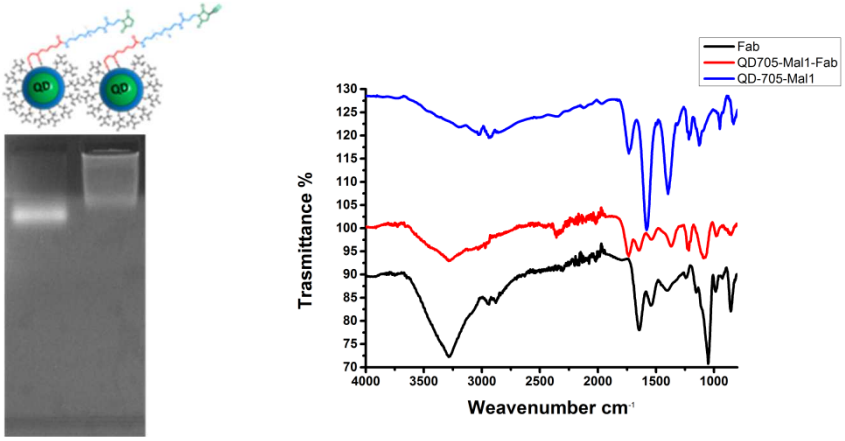

Figure 3-8. Left: Gel electrophoresis of the sample **QD530**; the image shown were acquired after 10 min. The left band refers to the sample functionalized with **Mal1** and the right to that bioconjugated with F(ab). **Right:** FTIR spectra of F(ab) and of CdSe/ZnS **QD705**-**Mal1** and **QD705**-**Mal1** after F(ab) conjugation.

3.1.4 Homogeneous FRET immunoassays for PSA.

To demonstrate the functionality of the compact QD-AB conjugates, we performed homogeneous Tb-to-QD FRET immunoassays against PSA on a KRYPTOR compact plus clinical fluorescence plate reader (Cezanne/Thermo Fisher) **(*cf*. Figure 3-9)**. PL intensities of Tb (I_{Tb}) and QDs (I_{QD}) were acquired simultaneously in a time-gated detection window between 100 µs to 900 µs after pulsed excitation at 337 nm using a nitrogen laser operating at 20 Hz.

Due to the extremely long PL lifetimes of Tb (ms) compared to QDs (ns), the time-gating allows efficient suppression of short-lived sample autofluorescence and direct excitation of the QDs. This allows obtaining solely the pure FRET signals (FRET-quenched Tb PL and FRET-sensitized QD PL). Optical band pass filters for the Tb donor and QD acceptor detection channels were (494±10) nm for Tb and (522±6) nm, (607±4) nm, and (707±8) nm for **QD530**, **QD605** and **QD705**, respectively. The FRET-ratio was defined as:

$$\mathrm{FRET-ratio} = \frac{\mathrm{I_{QD}}(100-900\ \mu\mathrm{s})}{\mathrm{I_{Tb}}(100-900\ \mu\mathrm{s})}$$

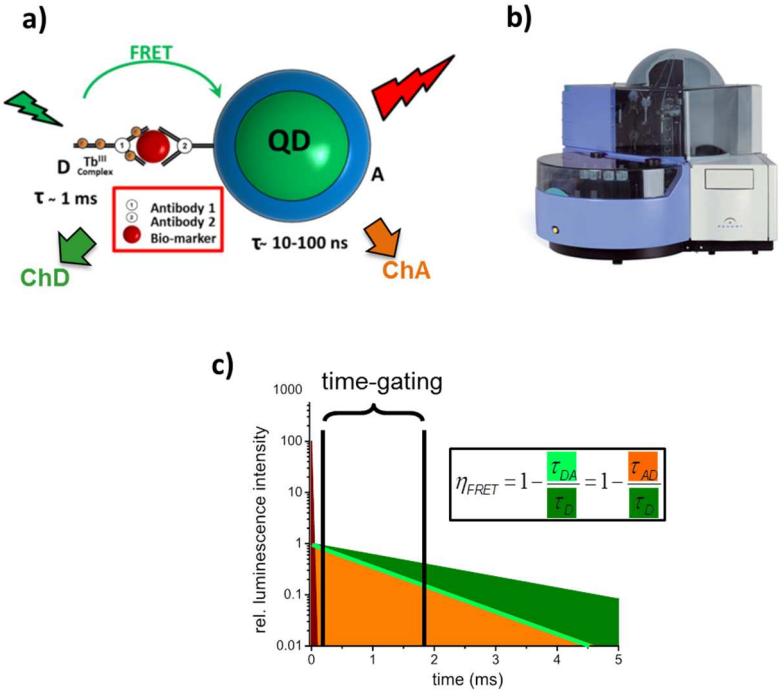

Figure 3-9. a) Scheme of the immunoassay relying on FRET from the donor D (terbium complex) to the acceptor A (InP or CdSe based QD). **b)** KRYPTOR compact plus fluorescent plate reader used for our measurements. The samples are excited with a nitrogen laser (337 nm) and the emission from the sample is separated via dichroic mirrors and bandpass filters into two channels, which were measured simultaneously. In one channel the donor (Terbium emission) is collected, named ChD, and in the other channel the emission of the acceptor (QDs) named ChA. **c)**The intensity of the two channels are measured in a time window from 100 µs to 900 µs after the excitation pulse (time-gating). The ratiometric measurement allows correcting errors like fluctuation in laser intensity.

Within all the FRET-assays the Tb-AB and QD-AB concentrations were kept constant (3 nM Tb-AB with 3 nM QD605-AB or QD705-AB, and 9 nM Tb-AB with 9 nM QD530-AB) while PSA concentrations, prepared in serum, ranged from 0.05 nM (for **QD605** and **QD705**) or 0.1 nM (for **QD530**) to 9 nM. 50 µL of each AB-conjugate (Tb-AB and QD-AB) were mixed with 50 µL of serum for a total working volume of 150 µL. The three immunoassay calibration curves (FRET-ratio over total PSA concentration) are presented in **Figure 3-10**.

All three assays showed a steep FRET-ratio increase with increasing PSA concentration up to *ca.* 2 to 4 nM, which was expected due to a saturation of Tb-QD FRET complexes (in the concentration range of Tb-AB or QD-AB). It should be noted that the FRET-ratio increase was very small (only *ca*. 5 % at the maximum) for the Tb-QD530 assay, which was most probably related to the lower Förster distance of Tb-QD530 (R_0 = 6.6 nm) compared to the values of Tb-QD605 (R_0= 8.3nm) and Tb-QD705 (R_0 = 11 nm). These findings can be understood by analyzing the overlap integrals of the different D-A pairs (***cf.*** **Figure 3-2**).

As described in the introduction **Chapter 1**, one of the most important parameters in order to achieve efficient FRET is the overlap spectra between D and A (the emission spectra of the donor has to overlap with the absorption spectrum of the acceptor), is evident that for the probe **QD605** and **QD705** they have a large spectral overlap in comparison to the probe **QD530**. Therefore, only the latter two FRET systems (for which the FRET-ratio increases were *ca.* 45 % and 100 % at maximum) could be used for a quantitative evaluation of PSA immunoassays (**Figure 3-10b and c**).

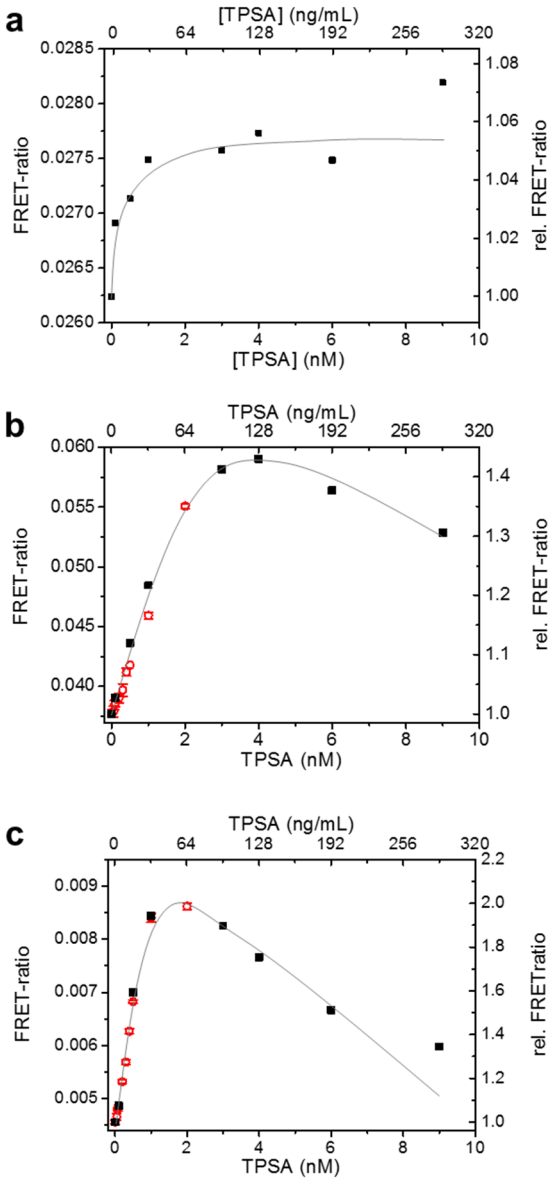

Figure 3-10. Calibration curves for total PSA (TPSA) homogeneous FRET immunoassays using Tb-QD530 (**a**), Tb-QD605 (**b**), and Tb-QD705 (**c**) FRET pairs. The assays **b** and **c** could be used for quantitative analysis. Black data points (squares) were from a first set of experiments using PSA concentrations between 0 and 9 nM. Red data points (circles) were taken in a second set of experiments for a statistical analysis of LODs in the linearly increasing parts of the assay curves. Grey lines in the graphs are added to guide the eye.

A first assay calibration curve over a concentration range of 0 to 9 nM (black squares) revealed a linear FRET-ratio increase, followed by a saturation and a FRET-ratio decrease. This decrease is due to the so-called Hook-effect, describing the increase of the fraction of single fluorophore (Tb-AB-PSA and QD-AB-PSA) binding complexes compared to sandwich FRET (Tb-AB-PSA-AB-QD) binding complexes. A second calibration curve, with many more PSA concentrations in the linearly increasing parts of the assay curves (red circles), was used to determine the LODs. This is done by dividing three times the standard deviation of the FRET-ratio from PSA-free samples by the slope of the linearly increasing part of the calibration curve in the 0 to 1 nM concentration range. All samples for the statistical analysis were prepared and measured in triplicates (n=9) apart from the PSA-free samples which were prepared 10 times and measured in triplicates (n=30).

Förster distances (donor-acceptor distance of 50 % FRET efficiency) were calculated as:

$$R_0 = 0.02108\ (\kappa^{2\Phi_{Tb}n^{-4}}J)^{\frac{1}{6}}\ \text{nm}$$

Where:

κ^2 (orientation factor) = 2/3

Φ_{Tb} (Tb luminescence quantum yield) = 0.67

η (refractive index) = 1.35

J (overlap integral) = $\int_{450}^{700} F_{Tb}\varepsilon_{QD}\lambda^4 d\lambda$

With F_{Tb}: area-normalized Tb emission spectrum and ε_{QD}: QD molar absorptivity spectra (***cf.*** **Figure 3-2**).

In **Table 3-2** the Förster distances for all FRET-pairs and LODs obtained for the Tb-QD605 and Tb-QD705 FRET pairs are summarized. We also added the LOD values obtained for the same Tb-to-QD FRET immunoassays against PSA using the readily surface-coated (thick PEG/polymer coating) hydrophylic **QD605** and **QD705** from the same supplier (Life Technologies).[49] It should be noted that the only difference from our **QD605** and **QD705** samples is therefore the surface functionalization. Both Tb-QD assays with compact QDs provide LODs below the clinical cut-off value for PSA (4 ng/mL),[26] and these LODs are also 6.2 and 2.5 fold lower compared to the same assays using the larger commercial QDs.[49] These results confirm the superior performance of the compact QD-AB conjugates for homogeneous FRET immunoassays.

Table 3-2. Förster distances R_0 and LODs of Tb-QD FRET immunoassays against PSA.

Donor-AB	**Acceptor-AB**	**R_0 (nm)**	**LOD (nM)**	**LOD (ng/mL)** ***compact QDs (this study)***	LOD (ng/mL) * *Qdot ITK™ amino PEG*	Clinical cut-off level of PSA
Tb-IgG	**QD605-F(ab)**	**8.3**	**0.12**	**3.7**	23	4 ng/mL
Tb-IgG	**QD705-F(ab)**	**11.0**	**0.02**	**0.8**	2.0	
Tb-IgG	**QD530-F(ab)**	**6.6**	**-**	**-**		

*Taken from reference.[49] Same Tb-QD FRET immunoassays against PSA, which used the same commercial QDs but with a thick PEG/polymer coating (as provided by the supplier).

In conclusion, the advantages of the compact (hydrodynamic diameter < 13 nm), stable, and strongly fluorescent QD-AB conjugates for clinical diagnostics has been demonstrated in Tb-to-QD FRET immunoassays for the detection of prostate specific antigen (PSA) in 50µL serum samples on a commercially available clinical fluorescence plate reader (KRYPTOR). While the spectral overlap integral of the 530 nm emitting probe with the Tb donor is too low for practical use, the limit of detection (LOD) determined for the 705 nm probe is significantly lower (0.8 ng/mL) than the clinical cut-off level (4 ng/mL); the LOD of the 605 emitting probe is 3.7 ng/mL.

The achieved LODs down to 0.8 ng/mL are 2.5 fold lower than the best Tb-to-QD PSA FRET immunoassays reported so far that used commercial QDs with thick organic surface coatings. Another important aspect of this investigation was the performance evaluation of QDs with different PL emission wavelengths and composition (**QD530**, **QD605**, and **QD705**).

This evaluation is very important for their application as acceptors in FRET assays with Tb donors because the variations in shapes, sizes, spectral overlap (QD absorption with Tb emission), and PL wavelength range lead to differences in FRET and detection efficiencies, which can result in significant differences in sensitivity.

3.2 Dual modality probes by grafting of lanthanide complexes on the QD surface

In this section the development of a dual modality probes for Magnetic Resonance Imaging (MRI) and fluorescence imaging will be presented. The InP-based QDs (**QD530**) have been used for these studies as they have a high potential as less toxic nanocrystals in biological imaging application. Part of these results have been recently published.[133]

MRI is an imaging technique based on Nuclear Magnetic Resonance (NMR) where a map of ^{1}H NMR signals from a given sample is generated.[134] It is a widely applied imaging technique, which allows the non-invasive acquisition of anatomical images with high spatial resolution, using the body's natural magnetic properties to produce detailed images from any part of the body. For imaging purposes, the hydrogen nucleus is used because of its abundance in water and fat. However, MRI is also a low sensitive technique. Indeed, most diseases manifest themselves by an increase in water content, so MRI is a sensitive test for the detection of disease. The exact nature of the pathology can be more difficult to ascertain: for example, infection and tumor can in some cases look similar. This drawback can be overcome by the introduction of external agents, named contrast agents, which increase the signal intensity. Among the most commonly employed molecules to induce an improvement in signal intensity, the lanthanide complexes, mainly Gd^{3+} complexes are the most efficient.[135] A further strategy to improve the image quality is the combination of different imaging modalities, in order to create a multimodal agent. Bimodal Optical Imaging (OI)/MRI, is of particular interest due to the great gain in sensitivity by OI.[136] Indeed, a bimodal probe allows combining the high resolution of MRI with the high sensitivity of optical imaging.

This section is devoted to the study of grafting lanthanide complexes on QDs to be used as probes for MRI and for OI. One way of preparation of these probes is to graft Gd complexes on quantum dots (**Figure 3-11**). The replacement of gadolinium by another lanthanide (*i.e.* Eu, Tb, Yb) allows us studying the mechanisms of charge or energy transfer. In these systems, the QDs can act as antenna for sensitizing the emission of the grafted Ln ions.

3.2.1 Grafting of Gd complexes on InPZnS@ZnSe/ZnS nanocrystals and MRI studies

Lanthanide ions have attracted broad attention for a wide range of applications spanning from material science to bioanalysis due to their specific intrinsic photophysical properties, narrow emission lines, large effective Stokes shifts, high resistance to photobleaching.[137-139] In this study, we carried out the preparation of bimodal probes by grafting gadolinium picolinate complexes (Gdebpatcn) with three different spacers (lipoic acid, mercaptobenzoique and methylenemercaptobenzoique) on the In-based QDs (**QD530**). Gd(DO3ApropSH) has been tested as well to compare with a system already reported in literature. The molecular structures of the Ln complexes are presented in **Figure 3-11,** they have been prepared by Maria Moula-Karimdjy during her PhD thesis at CEA/INAC/SCIB Grenoble. The grafting of the Gd complexes on the InPZnS@ZnSe/ZnS-**Pen** QDs (**QD530**) was achieved following a procedure reported earlier in our laboratory.[140] Briefly, it relies on adding 200 equivalents of Gd-complexes to one equivalent of QDs in presence of 9000 equivalents of tris(carboxyethyl)phosphine (TCEP) as a reducing agent and followed by vortexing (*800* rpm) for 12hs at 20°C. TCEP is used to cleave and to avoid the formation of the disulfide bonds, *in situ* facilitating the grafting of thiols on the ZnS shell. As the reducing ability of TCEP is compromised at higher pHs, only slightly basic pH (9) was maintained to facilitate thiolate formation and drive the ligand exchange process. After purification the spectroscopic properties of the QDs did not change. The fluorescence quantum yield is 8% in 1xPBS (**Table 3-3**).

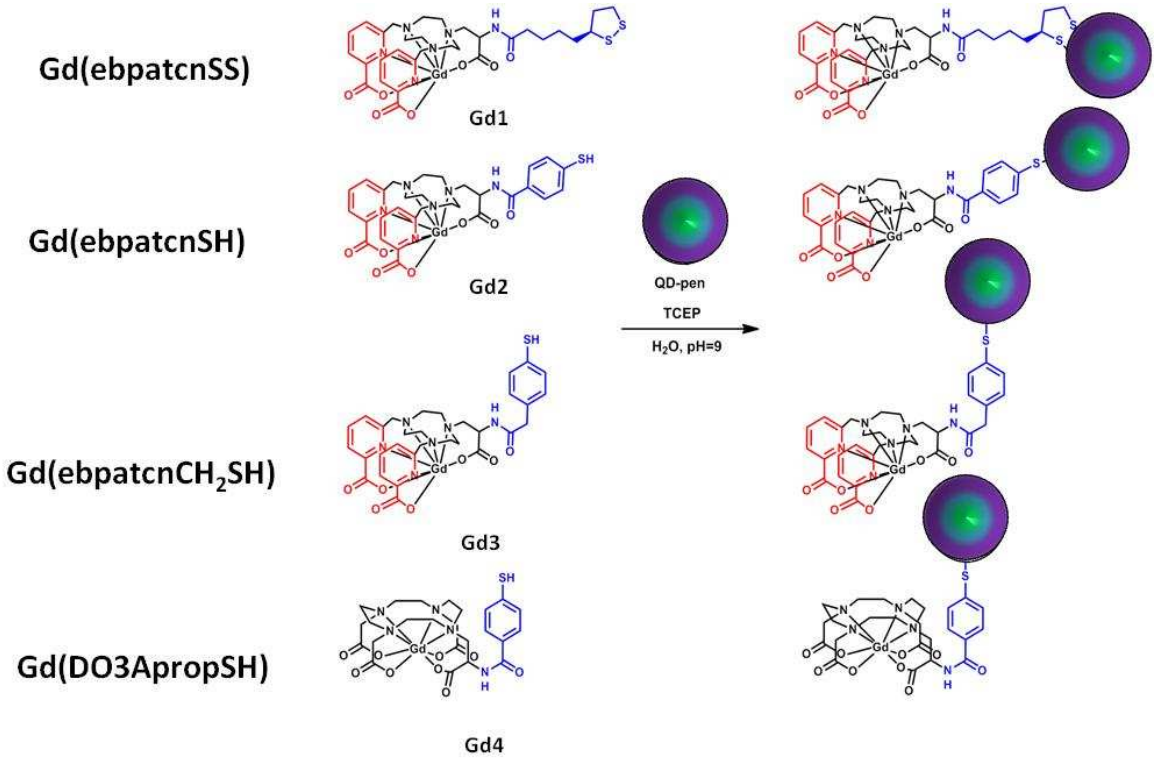

Figure 3-11. Diagram showing the grafting of the Gd complexes on penicillamine capped In-based QDs. **Gd1** [Gd(ebpatcnSS)]; **Gd2**[Gd(ebpatcnSH]; **Gd3**[Gd(ebpatcnCh$_2$SH)]; **Gd4**[Gd(DO3ApropSH)].

These **Gd** complexes have been selected due to their good performances and characteristics obtained before in our laboratory:

- the lipoic acid spacer (**Gd1**), offers the possibility to grafting a great number of complexes, due to their long chain;
- the mercaptobenzoique spacer (**Gd2**), gives a high relaxivity for Gd thanks to their rigidity;
- the methylenemercaptobenzoique (**Gd3**), for combining the rigidity with the steric distance.
- The [Gd(DO3ApropSH)(H_2O)] (**Gd4**) has also been selected to have a comparison with this standard contrast agents

The first evidence of successful grafting comes from the increase of the mean hydrodynamic diameters from around 6nm for the penicillamine (**Pen**) capped QDs to 8-10 nm depending on the different Gd complexes grafted as shown in **Figure 3-12A.**

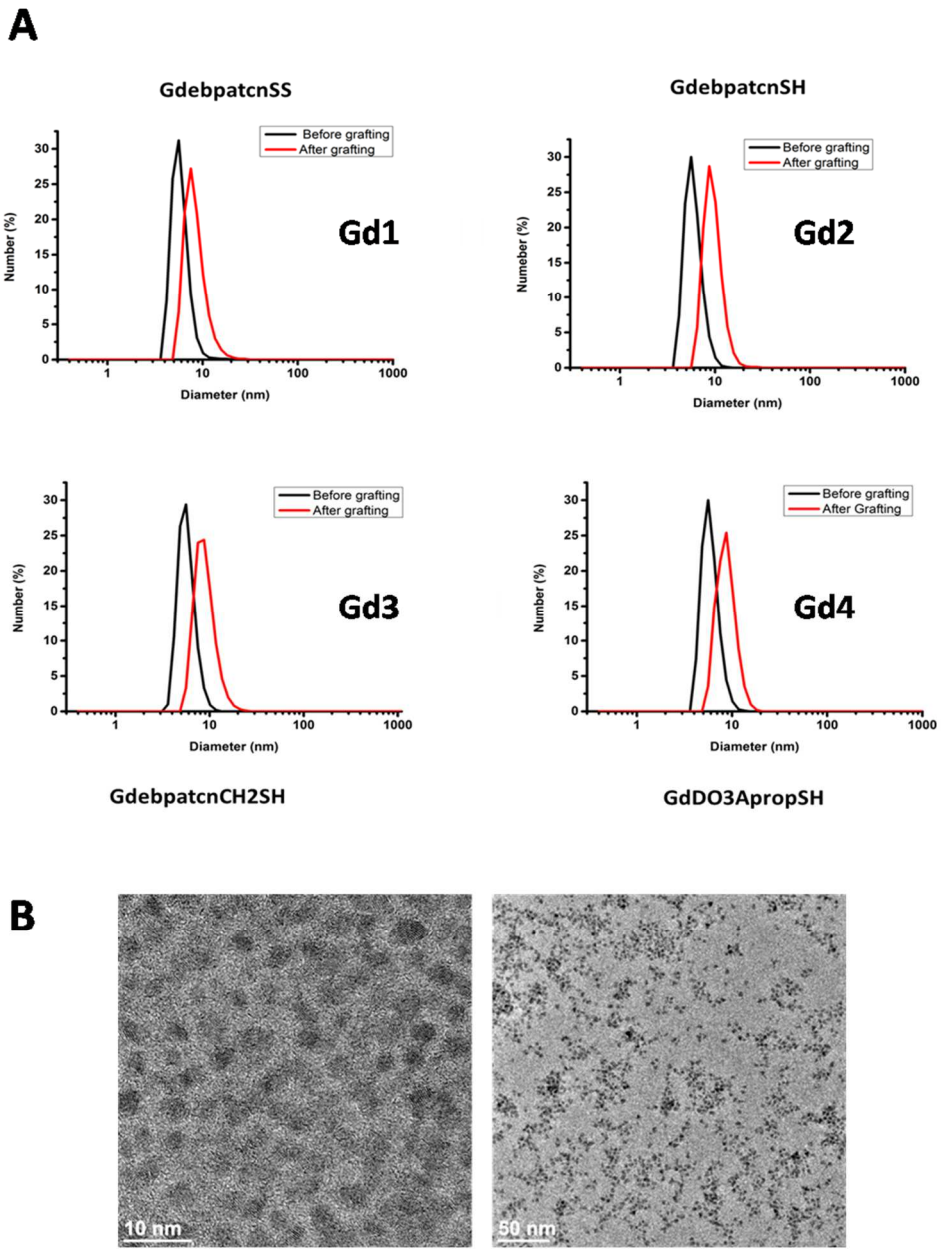

Figure 3-12. A) DLS spectra of QD-**Pen** before (black) and after (red) grafting Ln-complexes: **a) Gd1** [Gd(ebpatcnSS)]; **b) Gd2** Gd(ebpatcnSH; **c) Gd3 [**Gd(ebpatcnCh$_2$SH)]; **d) Gd4 [**Gd(DO3ApropSH)].**B)** Transmission electron micrographs of **QD530** and QD-**Gd1** at two different magnifications.

In addition, we investigated the fluorescence properties of **QD530** grafted with the different Gd complexes. **Figure 3-13** shows the absorption and photoluminescence spectra of the samples. The absorption spectra show the excitonic peak around 450 nm. As described in the **chapter 2** (experimental section), we experimentally determined the molar absorptivity of ε_{450nm}(**QD530**) = 4.2 x 10^5 M^{-1} cm^{-1} in relation to the first excitonic peak and the diameter following the equation described in the experimental section. These data allow us calculating the concentration of the QDs. The intensity of excitonic peak is not the same and a

slight spectral shift is observed. The former is likely caused by concentration differences, while the latter arises from small differences in the batches of the used QDs.

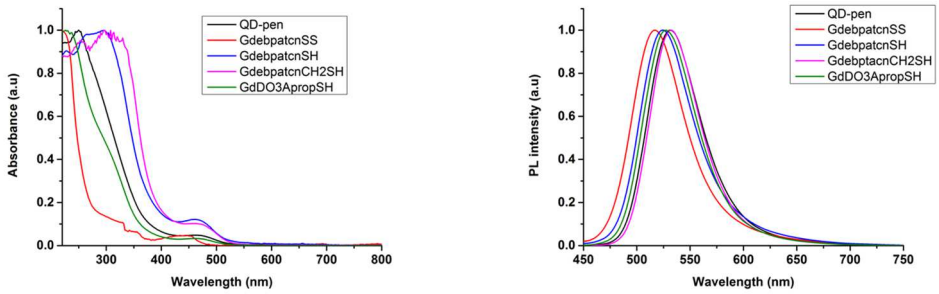

Figure 3-13. Absorbance (left) and luminescence spectra (right) of QD-**Pen** (**QD530)** after grafting with Gd complexes

The emission efficiency of QDs is expressed in terms of the fluorescence quantum yield (QY), which is the ratio between the number of absorbed photons and the number of emitted photons (described in the experimental part). We observed a slight diminution of the QY after grafting Gd complexes, but in general the presence of Gd complexes did not change significantly the optical properties of **QD530** (**Table 3-3).**

Table 3-3. Fluorescence QY before and after grafting of the Gd complexes

	QY before grafting (%)	QY after grafting (%)
GdebpatcnSSQD (Gd1)	8	7
GdebpatcnSQD (Gd2)	7	6
GdebpatcnCH$_2$SQD(Gd3)	8	6
GdDO3ApropSQD (Gd4)	7	6

The zeta potential values are between -40 and -30 mV confirming sufficient electrostatic repulsion for good colloidal stability and moreover no significant change was observed after the grafting. Second, the nuclear magnetic resonance dispersion (NMRD) profile of the purified sample showed a marked increase in relaxivity, r_1 at around 20 MHz as compared to the free Gd complexes (**Figure 3-14**). The relaxivity – the increase of $1/T_1$ per mM of added Gd complexes – is the efficiency of contrast agents.

It should be noted that the complex properties that affect relaxivity of water protons are (a) the hydration number, *q* (b) the distance between the water proton and the unpaired electron spin of the Gd ions, r (c) the rotational correlation time, τ_R (d) the water exchange rate, τ_m *i.e.* the rate of water exchange between the water molecule directly coordinated to the Gd ions and the water present in the bulk solvent and (e)

the electronic relaxation time, *T*. The intensity of the MRI signal depends on the relaxivity of water protons; with increase in r_1 the MRI signal increases.[141] The presence of Gd complexes improves the MRI signal by increasing the relaxivity (r_1) of the surrounding water molecules. The increase in r_1 depends on both the properties of the complex as well as the applied magnetic field. In NMRD experiments the dependency of the relaxivity on the magnetic field and the profile is also affected by the change in the properties of the complex in the presence of QDs. The NMRD profiles of the different samples are shown in **Figure 3-14**, which plots the variation of the relaxivity as a function of the applied magnetic field.

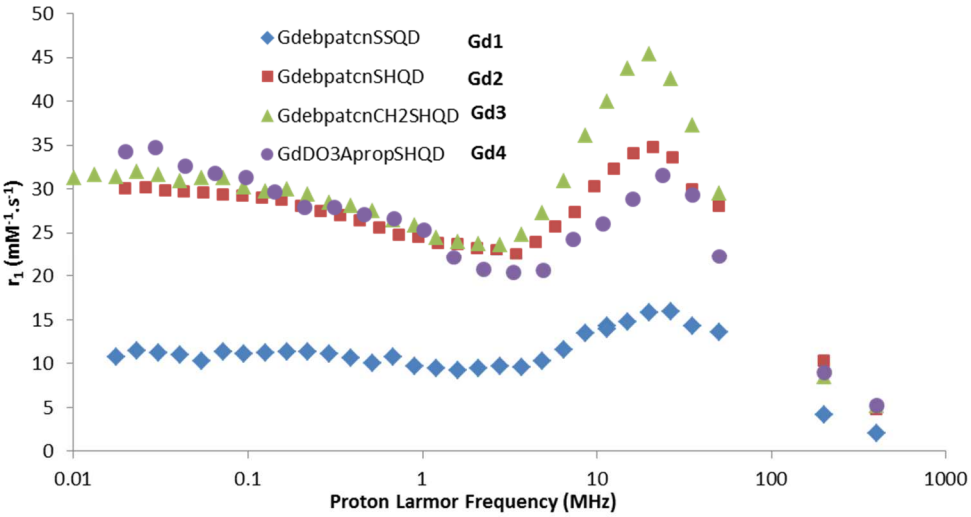

Figure 3-14. NMRD profiles for the different Gd complexes grafted on the QD surface indicating the relaxivity per Gd ion.

The increase of relaxivity depends on the number of complexes grafted per QD and on the spacer used. The number of complexes per QD was determined by combining two techniques, absorption spectroscopy to determine the concentration of QDs and Gd complexes in solution and magnetic susceptibility measurements to know the global complex concentration. This allows us measuring the number of Gd complexes per QD: 110, 30, 80, and 50 for **Gd1=[**Gd(ebpatcnSS)**]**; **Gd2=[**Gd(ebpatcnSH**]**; **Gd3=[**Gd(ebpatcnCh$_2$SH)**]**; **Gd4=[**Gd(DO3ApropSH)**],** respectively (***cf.*** **Table 3-4**).

The flexible lipoic acid spacer (**Gd1**), allows for grafting the largest number of complexes on the QD surface (110), due to the decrease in the steric interactions between the complexes and QDs. The phenyl spacer (**Gd2**), on the other hand, shows the smallest number for complexes par QD, but by adding methylene group (**Gd3**) between the aromatic group and the amide bond, the steric interaction decreases and this feature offer the possibility to grafting a larger number of complexes on QD surface. Due to their rigidity, the phenyl spacers result in a stronger increase of relaxivity per Gd, up to 37 $mM^{-1}s^{-1}$ per Gd at 35 MHz and

25°C, which represents an almost tenfold increase with respect to the standard commercial contrast agent (GdDOTA: 4.3 $mM^{-1}s^{-1}$).

Table 3-4 summarizes the number of complexes per QD as well as r_1 of the free and grafted complexes.

Table 3-4. Relaxivity r_1 in $mM^{-1}s^{-1}$ at 35 MHz and 25° C for gadolinium complexes in solution and after grafting on QD surface. For comparison r_1 (GdDOTA) = 4.3 $mM^{-1}s^{-1}$ at 35 MHz and 25°C.

	r_1	r_1 per Gd	Number of complexes per QD	r_1 per QD
	Free complexes	Grafted complexes		
Gd1	4.18±0.05	14±1	~ 110	~ 1500
Gd2	1.76±0.05	30±2	~ 30	~ 900
Gd3	4.31±0.05	37±2	~ 80	~ 3000
Gd4	1.23±0.05	29±2	~ 50	~ 1500

Summarizing, we have demonstrated the preparation of a well MRI/optical probes based on less toxic InP QDs, which show high relaxivity obtained by the direct covalent attachment of Gd complexes to the nanocrystal surface. In particular, the use of a flexible and long spacer results in a small effect on the relaxivity (**Gd1**), while using a more rigid spacer such as mercaptobenzoic (**Gd2**) and methylenmercaptobenzoic (**Gd3**), induces a significant increase of *r1* per Gd. Moreover, in **Gd3** the presence of a methylene group in vicinity of the thiol anchoring function allows reducing the steric interactions and results in a larger number of complexes, grafted on QDs surface. This system results in the highest *r1* per Gd among the systems used in this study and is a promising progress towards bimodal probes.

3.3 Grafting of Eu, Tb and Yb complexes on InPZnS@ZnSe/ZnS nanocrystals and optical studies: energy transfer *vs.* dual emission probes

The versatile synthetic strategy used herein allows the introduction of additional modalities on the QDs. Indeed we also demonstrate the covalent attachment of the chemically equivalent visible and NIR emitting Tb, Eu and Yb complexes that will be presented in the following paragraphs.

Biluminescent Ln-QD conjugates with energy transfer from the QD to a Ln can also find applications as light sources in white LEDs.[142] Moreover, the size-tunable absorption and emission wavelengths and the large absorption cross sections make QDs appealing chromophores for the sensitization of various Ln^{III} ions. The sensitization of Ln^{III} emission by QDs has not been achieved so far in QD-Ln conjugates. In fact, to date only the luminescence sensitization of Tb^{III} in doped CdSe and of Eu^{III} in doped InPZnS nanocrystals have been reported.[143, 144]

In the first section of this chapter the energy transfer from the lanthanide to the QD has been applied to develop highly sensitive in time-resolved fluoroimmunoassay. Here the energy transfer from the QD to lanthanides is investigated.

The same batch of **core@shell** InPZnS@ZnSe/ZnS QDs (**QD530**) functionalized with **Pen** has been used to graft the Eu, Tb and Yb complexes and the ligand **Gd1-**[Ln (ebpatcnSS)] (***cf.*** **Figure 3-11**) was chosen, which provides strong grafting via its dithiol function. **Figure 3-15** shows the grafting of the Ln complexes on the **QD530** surface that was achieved following the same procedure as described before for the Gd complexes.[140]

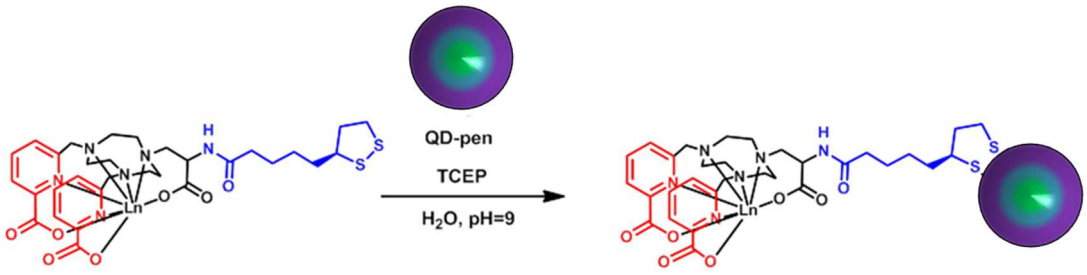

Figure 3-15. Scheme showing the grafting of Ln complexes (Ln= Eu, Tb and Yb) on **QD530.**

As for the Gd complexes, DLS measurements revealed that the QD-Ln conjugates show an increase of the hydrodynamic diameter (from 6 nm to 9-10 nm) and a narrow size distribution (**Figure 3-16**).

The zeta potential values are again between -40 and -30 mV. The UV-Vis and PL spectra were not affected by the grafting (***cf.*** **Figure 3-17**). However, we noted a difference in the PL quantum yield and lifetime. The QY of the used **QD530** was 15%, after grafting of the complexes on the QD surface, values in the range of 1-10% have been measured, depending on the grafted Ln complex (**Table 3-5**).

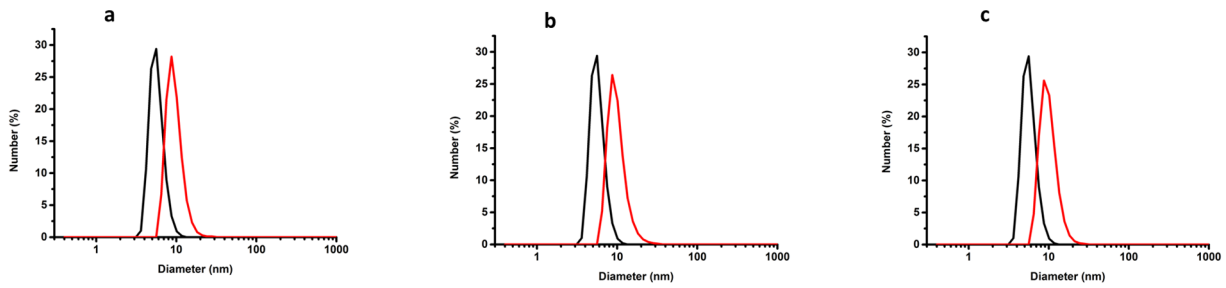

Figure 3-16. DLS spectra of QD-Pen before (black) and after (red) grafting, of the Ln complexes [Ln(ebpatcnSS)] with **a)** Ln=Eu, **b)** Ln=Tb and **c)** Ln=Yb.

The PL lifetimes have been fitted with 3 exponentials using the following Formula:[145]

$$I(t) = \sum_{i=3}^{3} \alpha_i e^{\tau/\tau_i}$$

With t_i: Life time

α: weighing factor

The shortest decay lifetime is typically associated with surface related traps of shallow nature, the two longer ones with excitonic recombination and defects on the core/shell interface.

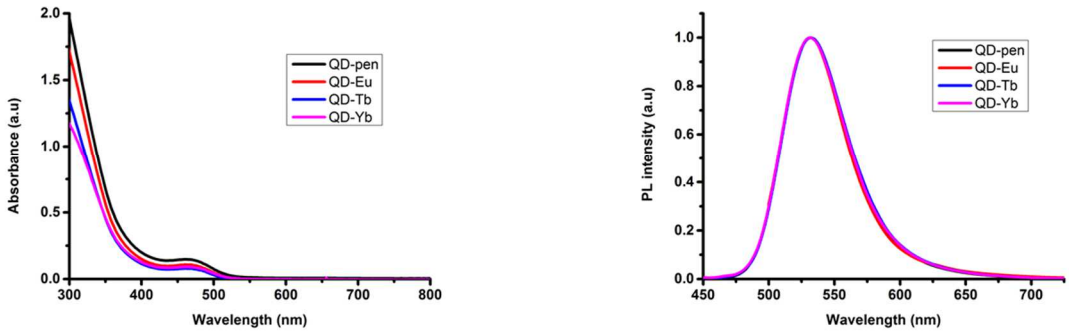

Figure 3-17. UV-Vis absorption (left) and photoluminescence spectra (right), excitation wavelength: 400 nm, of QD-**Pen** (**QD530)** after grafting with Ln complexes.

Table 3-5. Quantum yield (Φ) and lifetimes (τ) before and after grafting

	QD530	QD-Eu	QD-Tb	QD-Yb
Φ	15	1	10	5
τ_1 (QD)	3.9	0.9	3.3	3.2
τ_2 (QD)	22.9	5.6	18.9	16.4
τ_3 (QD)	83.6	55.6	71.8	61.8

The decrease of PL QY and concomitant decrease of the lifetimes suggest an energy transfer from QDs to Ln complexes providing an additional deexcitation path to radiative recombination. This drop is the most pronounced for QD-Eu and the least one for QD-Yb. The values of the lifetime follow the same trend. To confirm the Ln sensitization via the QDs, PL measurements were performed using 273 nm and 370 nm as excitation wavelengths (**Figure 3-19**). The former excites both the piconilate ligand and the QDs, the latter excites exclusively the QDs.

Direct excitation at the absorbance band of the picolinate ligand (273 nm) resulted in the characteristic Eu($^5D_0 \rightarrow {}^7F_j$) and Tb($^5D_4 \rightarrow {}^7F_j$) luminescence emission of the Eu^{III} and Tb^{III} complexes (**Figure 3-18**). In addition, the emission spectra show a band centered at 525 nm resulting from the photoluminescence of the QDs. In QD-Yb, the excitation at 273 nm in the absorption band of the ligand did not result in the luminescence emission of the Yb^{III} in the near infrared region. In this case the sensitization of Yb^{III} through the ligand is not possible. Indeed, for QD-Yb, excitation at 273 nm results in the absence of emission, probably due to a weaker efficiency of both the Xenon lamp (low power) and the gratings (tail) in this region compared to 370 nm. The combination of these two factors makes the Yb^{III} NIR luminescence too weak to be detected at 273 nm as observed for QD-Eu.

Moreover, the presence of a coordinated water molecule leads to deactivation of the Yb^{III} luminescence emission. On the other hand, excitation at 370 nm results in a weak emission of the Eu^{III} at 618 nm (**Figure 3-18**, left) and of Yb^{III} at 978 nm assigned to the $^2F_{5/2} \rightarrow {}^2F_{7/2}$ transition (**Figure 3-18**, right and **Figure 3-20**). The presence of QD-sensitized Eu^{III} and Yb^{III} emission was confirmed by the absence of luminescence when the free complexes were excited at 370 nm. For QD-Eu, the decrease of the QD lifetimes is most pronounced, while the Eu^{III} emission lifetime measured in QD-Eu is similar to the one measured in the free complex in water (0.49 and 0.48 ms, respectively). These data indicate that an energy transfer occurs in QD-Eu from the QD to Eu^{III} but is quenched by probable non-radiative deactivation pathways, the emission of the QD and the first accepting electronic level of the Eu^{III} ($^5D_0$) being very close in energy and in resonance.

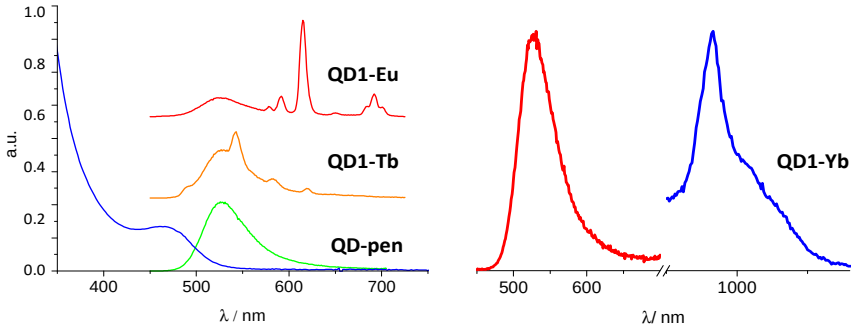

Figure 3-18. (Left) Normalized absorption spectra of **QD530** (blue) and emission (Ex at 273 nm) spectra of QD (green), QD-Ln (Tb: orange, Eu: red); (right) normalized emission spectra (Ex at 370nm) of QD-Yb in the Vis (red) and NIR range (blue).[133]

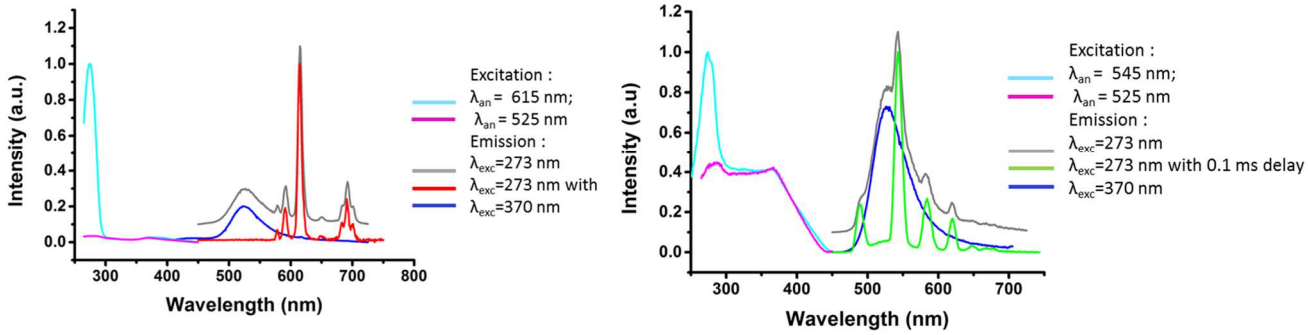

Figure 3-19. Excitation (at 273 nm and 370 nm) and emission spectra of QD-Eu (**left**) and QD-Tb (**right**) in 1X PBS buffer.

For QD-Tb, the decrease of the QD lifetime is less significant compared to QD-Eu and QD-Yb. Moreover, in that case, the emission of QD overlaps the Tb ($^5D_4$) level, suggesting no (or little) energy transfer in this case.

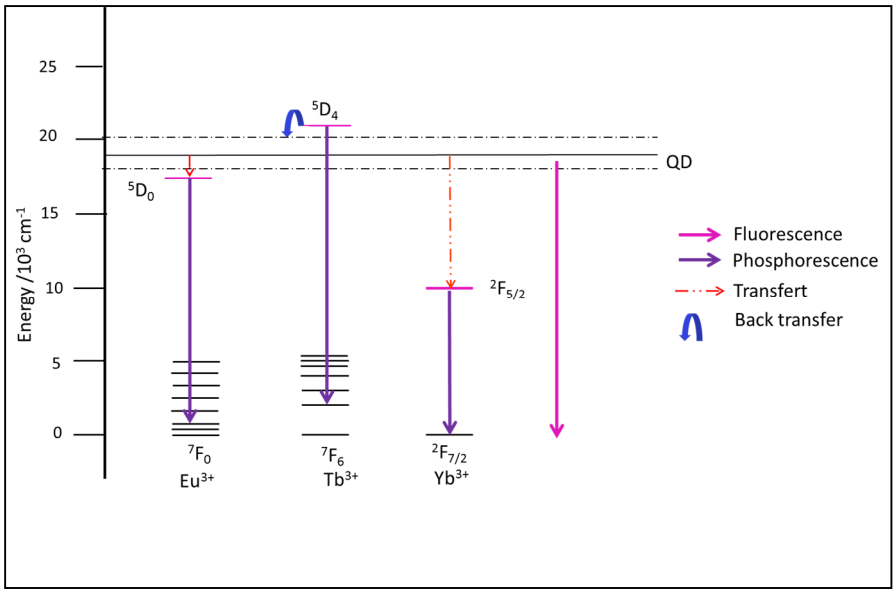

Figure 3-20. Energy levels and transitions of Eu^{3+}, Tb^{3+}, Yb^{3+} and **QD530**.

3.4 Conclusion

In this chapter the interaction and specific optical properties of QDs and Ln complexes have been explored for creating novel probes for biological detection and imaging. In the first section we used a terbium complex as a FRET donor and InP- or CdSe-based QDs as FRET acceptor in homogeneous immunoassays for detection of PSA. In this type of immunoassays the relatively large dimensions of the biological recognition system that contains antibodies, biomarkers, and a nanoparticle have limited the application of QDs.[146]
While, Tb-to-dye FRET immunoassays have been demonstrated for the multiplexed detection of up to five different tumor markers,[47] the application of Tb-to-QD FRET has so far been limited to the detection of single antigens. Lab-synthesized QDs have been used for the detection of alpha-fetoprotein (AFP) and carcinoembryonic antigen (CEA) in buffered solution[116, 117] and commercial QD-antibody conjugation kits for the detection of prostate specific antigens (PSA) or the epidermal growth factor receptor (EGFR).[11, 119]
In this study we presented a two-step procedure for the preparation of compact, highly luminescent, and colloidal stable QDs that were further used for the simple and functional conjugation with fragmented F(ab) ABs, to yield the smallest fluorescent AB-nanoparticle conjugates reported to date. This compact size is an efficient means to maximize the FRET efficiency and hence the sensitivity of the assays. In the first step aqueous phase transfer was achieved by ligand exchange with zwitterionic penicillamine. The second post-

functionalization step introduced a bifunctional ligand, which contained reactive maleimide functions. The latter could be used for the selective and stable conjugation to sulfhydryl groups on ABs. Although this bioconjugation strategy was demonstrated only with InPZnS@ZnSe/ZnS, and CdSe@ZnS core/shell QDs and F(ab) antibodies, we expect that it is applicable to a wide variety semiconductor nanocrystals and metal nanoparticles containing surface atoms with binding affinity for thiolate ligands and biomolecules containing sulfhydryl groups (*e.g.*, on available cysteines).

The immediate applicability of the compact QD-AB conjugates to biosensing was demonstrated in homogeneous FRET immunoassays against PSA, using Tb-ABs as FRET donors and the QD-ABs as FRET acceptors, both coupled by an immunological sandwich complex between the two ABs and the PSA biomarker. Detection of PSA in 50 µL serum samples with subnanomolar (20 pM = 0.8 ng/mL) detection limits showed the clinically relevant concentration range, in which these FRET immunoassays can be applied for. Not only were the LODs of two Tb-QD FRET immunoassays (using 605 nm and 705 nm emitting QDs) well below the clinical cutoff value of PSA (4 ng/mL), the utilization of the compact QD-AB conjugates also provided a 6.2 and 2.5 fold sensitivity improvement compared to the same commercially available QDs that were purchased with a standard PEG/polymer-based coating. These highly sensitive and homogeneous Tb-to-QD FRET immunoassays are suitable for any other biomarker against which two specific ABs exist. Our results show that the compact QD-AB conjugates have a large potential for improving diagnostic applications, and given the multiplexing capability of Tb-QD FRET, and demonstrated that these small nanoparticle-AB fluorescent probes will become important players in clinical *in-vitro* diagnostics.

In the second part of this chapter QDs and Ln^{III} complexes have been chosen to promote either the generation of dual modality (MRI/PL) or dual emission (QD and Ln) probes. Here we focused on InP-based QDs, due to their lower toxicity compared to CdSe-based QDs. The obtained results show that an efficient grafting of various Ln complexes on the QDs surface has been obtained.

The incorporation of Gd complexes with a more rigid spacer such as mercaptobenzoic and methylenmercaptobenzoic, induced a significant increase of the relaxivity. Moreover the presence of methylene groups allowed reducing the steric interactions and linking a larger number of complexes on the QDs surface. This system is promising for future application *in vivo* as bimodal probes combining MRI and fluorescence imaging capabilities.

Finally, the synthesis of stable hybrid nanoparticles combining InPZnS@ZnSe/ZnS QDs and grafted Luminescent Ln Complexes has been performed. The obtained QD-Ln conjugates demonstrate the potential of using QDs to sensitize both the visible and NIR emission of lanthanide ions incorporated into QD grafted complexes. One exception are QD-Tb conjugates for which the photophysical properties only slightly change. In this case, the emission of the QDs overlaps the Tb ($^5D_4$), first accepting level with the presence of a back transfer from Tb to the QDs. When the energy level of the excited state of the Ln ion is lower than the QDs ones, the QDs can populate the energy levels of the excited state of Ln and the Ln reemits this

energy. On the other hand, when the energy level of the Ln is higher than the QDs one, there is a possibility that a back transfer occurs. And, we clearly demonstrated an energy transfer for QD-Eu and QD-Yb.

The exact mechanism of this energy transfer is unclear and future studies will be directed towards the optimization of the transfer through an appropriate matching of the Ln and QD energy levels and the thorough investigation of the transfer mechanism.[147]

Finally I would like to conclude this chapter by citing Wegner and Hildebrandt: ”Although QD-based bioimaging is a relatively young research field and although applications as imaging agents in humans are a rather long-term perspective, the future of QDs for more *in vitro* and *in vivo* investigations are brilliant just as the QD fluorescence”.[28] Indeed, despite several advantages of QDs over fluorescent proteins and other organic dyes they have still not become standard fluorophores for diagnostic applications or bioimaging tools on humans. The main reasons come from reproducibility and stability problems of QD-bioconjugates.[34] The assessment of biocompatibility and biosafety of QDs and related toxicity issues, which will be addressed in the next chapter, are a critical issue for further applications as well. Although toxicity issues have been largely resolved by the application of appropriate surface coatings so their application in IVD is not so much hampered by that issues, the main problem is still limiting QD application in living system. We will investigate the toxicity of these promising NCs in the next chapter.

3.5 Experimental section

Chemicals. D-Penicillamine, tetramethylammonium hydroxide (TMAOH), phosphate-buffered saline solution (10X PBS), tris(2-carboxyethyl) phosphine hydrochloride solution 0.5 M (TCEP), tris(hydroxylmethyl)aminomethane (TRIS/Cl), bovine serum albumin (BSA), agarose powder, indium acetate (99.99%), myristic acid (>99%), tris(trimethylsilyl)phosphine (95%), 1-dodecanethiol (97%), 1-octadecene (90%), were purchased from Sigma-Aldrich. Zinc stearate (90%) was acquired from Riedel de Haën. MAL-dPEG3-Lipoic acid (Mal1) was purchased from Quanta Biodesign. QD CdSe 605 and 705 were purchased from Life Technologies/Thermo Fisher[27] while the NHS-activated terbium complex (Lumi4-Tb) was provided by Lumiphore in lyophilized form. Prostate specific antigen (PSA) and monoclonal primary antibodies against PSA (IgGs: "PSR222" and "PSS233") were provided by Cezanne/ThermoFisher. Solvents were purchased from Aldrich, Fluka, and Acros, and used without further purification. All water solutions were prepared from ultrapure laboratory grade water (resistivity 18 MΩ cm) that was filtered and purified using a Millipore MilliQ cartridge system and autoclaved.

Instruments. Absorption and emission spectra were recorded on the following spectrometers: HP 8452A and Perkin Elmer Lambda 35 for UV-Vis absorption; Hitachi F-4500 fluorescence spectrophotometer equipped with a 150 W xenon lamp and excitation monochromator as well as PicoQuant Fluotime 300 for photoluminescence (PL). Decay curves were acquired on the Fluotime 300 and fitted using EasyTau (PicoQuant). The hydrodynamic diameter (by dynamic light scattering) and zeta potential of the NCs dispersed in water were measured using a Malvern Zeta Sizer (NanoZS). Fourier transform infrared (FTIR) spectra were taken on a Perkin Elmer Paragon 500 spectrometer equipped with an attenuated total reflection (ATR) setup. Gel images were acquired using a Gel Doc XR system (Bio-Rad, Hercules, CA). HRTEM analyses were performed on a JEOL 3010 working at 300 kV, equipped with a LaB_6 gun and a Gatan Orius SC 200 2k x 2k CCD camera.

InPZnS@ZnSe/ZnS QD Synthesis. The synthesis of InPZnS@ZnSe/ZnS alloy core gradient shell nanocrystals is based on reported procedures.[23, 97] All procedures except for nanocrystal purification have been carried out under inert atmosphere.

Preparation of precursor solutions. For the preparation of the indium myristate ($In(MA)_3$) stock solution (0.1 M), 1 mmol of anhydrous indium acetate was mixed with 3 mmol of myristic acid (MA) and 10 mL of 1-octadecene (ODE) in a 50 mL three-neck flask equipped with a condenser.

The mixture was heated to 100-120 °C for 1 h under vacuum until an optically clear solution was obtained. After backfilling the flask with Ar and cooling to room temperature, the turbid solution of indium myristate was stored in a glovebox. For the zinc oleate ($Zn(OA)_2$) stock solution (0.4 M), 5 mmol of zinc acetate, 10 mmol of oleic acid (OA) and 9.35 mL of ODE were loaded into a 50 mL three-neck flask and the same procedure as for the preparation of $In(MA)_3$ was followed. The zinc stearate ($Zn(St)_2$) stock solution (0.1 M) was prepared by heating 1 mmol of $Zn(St)_2$ with 10 mL of ODE at 120°C for 1 h. A 0.4 M TOPSe stock solution was prepared by dissolution of 2 mmol of Se powder in 5 mL of trioctylphosphine (TOP) under stirring for 24 h. A TOPS stock solution was prepared with the same procedure using elemental sulfur.

Synthesis of InPZnS alloy nanocrystals. In a glovebox, 1 mL of the $In(MA)_3$ stock solution (0.1 mmol $In(MA)_3$), 1 mL of the $Zn(St)_2$ stock solution (0.1 mmol), 0.1 mmol of 1-dodecanethiol (DDT) and 7.5 mL of ODE were added to a 50 mL three-neck flask. Afterwards the flask was equipped with a condenser and connected to a Schlenk line. Next, the mixture was heated under vigorous stirring to 300°C with a ramp of around 60°C/min using a molten salt bath. When the temperature inside the flask reached 100°C, 0.1 mmol of tris(trimethylsilyl)phosphine ($P(TMS)_3$), diluted with 1 mL of ODE, were injected. During the heating, NC formation is visible by the color change of the reaction mixture to dark yellow/orange. After 30 min, the reaction mixture was cooled to below 220 °C to stop growth.

Growth of a ZnSe/ZnS gradient shell. For the ZnSe/ZnS gradient shell growth, a 10 fold excess of precursors was used with respect to the core synthesis, and a Se:S ratio of 0.2. Briefly, $Zn(OA)_2$ (1 mmol, 2.5 mL of the 0.4 M stock solution) was added dropwise to the reactive mixture at 220°C. This was followed by the successive injection of TOP-Se (0.2 mmol, 0.5 mL of the 0.4 M solution) and TOP-S (0.8 mmol, 2 mL of the 0.4 M solution). The resulting mixture was heated to 300°C within 10 minutes and then kept at this temperature for 20 min. After cooling down to room temperature, purification of the QDs was performed via three cycles of precipitation/redispersion. First, 10 mL of a 1:1 (v/v) mixture of chloroform/methanol and 100 mL of acetone were added. Then the resulting suspension was centrifuged (*8000* rpm for 5 minutes), the supernatant discarded and the obtained solid dispersed in 5 mL of chloroform. Finally, the QDs can be dispersed and stored in a variety of organic solvents, like hexane, toluene or chloroform.

Purificationbefore phase transfer. Thorough purification of the initial QDs, enabling the complete removal of excess surface ligands or side-products is crucial for successful phase transfer. 1 mL of the InPZnS/ZnSe/ZnS QDs in chloroform were mixed with anhydrous ethanol (1mL) and centrifuged at *10 000* rpm for 2 minutes.

The clear solution of supernatant was discarded and the precipitate was dispersed in 1 mL of chloroform. This cycle was repeated three times. For the commercial CdSe/ZnS-based QDs in decane the solvent was changed to chloroform prior to phase transfer. 4 mL of a methanol/isopropanol (3:1 v:v) mixture were added to 1mL of the QD colloidal solution and centrifuged for 2 min at *10 000* rpm. The supernatant was discarded and the resulting pellet dispersed in 1mL of chloroform.

Phase transfer. A 0.2 M solution of penicillamine (containing 200 µL of 0.5 M TCEP) was prepared in 1 mL of degassed MilliQ water (18 MΩ). The pH was adjusted to 9 by drop-wise addition of 0.5 M TMAOH. 500 µL of the phase transfer solution was mixed with 1 mL of a 3-5 µM colloidal solution of QDs in chloroform. The biphasic mixture was stirred vigorously at *~1400* rpm for 2 h at room temperature. At the end of the transfer, affording QD-pen, the biphasic mixture results either in a clear separation of two phases or in an emulsion. In the latter case, the mixture is centrifuged at *5000* rpm for 1 min to obtain a clear phase separation. The QDs in the (upper) aqueous phase are separated from the (lower) organic phase.

***Purification and storage*.** A NAP™-5 -10, -25 size exclusion column (Sephadex™ G-25 DNA Grade from GE Healthcare) was vertically clamped and equilibrated according to the manufacturer's protocol. QDs in water were added and after being adsorbed on the gel bed, they were eluted using 1x PBS buffer and kept at 4°C in the dark for storage.

***Post-functionalization*.** Solutions of Mal1 (1 mL, 10 mM) and TCEP (0.046 mL, 0.5 M) in degassed water were added to a suspension of QD-**Pen** (0.5 mL, 5.2 µM in degassed water) and the pH was adjusted to 7.0 by drop wise addition of 0.5 M TMAOH. The mixture was vortexed at *800* rpm overnight at room temperature. The resulting fine suspension was purified by size exclusion chromatography with a NAP™-10, -25 columns (Sephadex™ G-25 DNA Grade from GE Healthcare). The obtained QD-**Mal1** were then concentrated under vacuum or by using a 30 kDa molecular weight cut-off (MWCO) spin column from Millipore, centrifuging at *4000g* for 4 min with a final volume of 400 µL. Storage at 4°C as above.

***Preparation of QD-F(ab) conjugates*.** IgGs were fragmented to F(ab) using Pierce™ Mouse IgG F(ab') $F(ab')_2$ preparation kit following the instructions provided by the supplier. Prior to conjugation of the QDs to the F(ab)s in a molar ratio of 1:20, disulfide bonds of the latter were reduced to sulfhydryls with 5 mM of TCEP in 1X PBS by mixing for 30 minutes at *30* rpm at room temperature. Purification from excess TCEP was performed using Zeba 7K spin columns (Thermo Fisher) according to the manufacturer's protocol. The resulting purified F(ab) was then mixed with the QDs in 1X PBS and incubated for 4 hours while rotating at *30* rpm at RT.

Conjugates were washed from unbound F(ab)s 4 times with 1 mL 1X PBS pH 7.5 using a 100 kDa MWCO spin column from Millipore at *1000g*. Supernatants were taken after a final centrifugation at *4000g* for 5 minutes.

QD PL quantum yields. The absolute fluorescence QYs of the QDs were determined by comparison with a standard of known QY (freshly prepared solution of Fluorescein 27 in 0.1 M NaOH; QY = 93%, Rhodamine 6G in ethanol; QY = 95%[91] or **QD705** in chloroform; QY=92%[90]). The QY was calculated with the following formula:

$$\Phi_{NC} = \Phi_{Standard} \cdot (a_{NC}/a_{Standard}) \cdot (n^2_{NC}/n^2_{Standard})$$

Where Φ is the QY, *a* the gradient (slope) of the plot of the integrated fluorescence intensity *vs.* absorbance and *n* the refractive index of the solvent (1.375 for hexane, 1.446 for chloroform, 1.333 for water and buffer and 1.36 for ethanol[30]). All spectra were corrected for the instrumental response with calibration curves furnished by the supplier and the estimated errors on QY are ± 15% of the calculated values. Aliquots or purified samples of the QDs in hexane, chloroform or water were put into 1 cm quartz cuvettes and diluted until the absorbance at the excitation wavelength was around 0.1. At least four samples of different concentration were prepared and measured for determining the slopes. Both the sample and the reference were excited at 460 nm for InP based QDs and at 480 mn for CdSe based QDs.

Hydrodynamic size and dispersibility of QDs. The hydrodynamic diameter of the water-soluble QDs was measured by dynamic light scattering (Malvern Zeta Sizer NanoZS). Multiple runs (>3) were performed and averaged, and the QDs in 1X PBS buffer were filtered (0.22 µm) prior to the measurements. The spectra have been corrected by the instrument software for viscosity (0.882 mPa *s* at 25 °C), absorption (0.01), solvent (water) refractive index (1.33) and material refractive index (assumed as 2.7 and 2.45 for In- and Cd-based QDs, respectively[31]). The data were collected in automatic mode and expressed in number %. The zeta potential was measured using the same instrument under zeta potential settings.

Gel electrophoresis. A 1% gel was prepared in 25 mM Hepes buffer (pH 7.4) and poured in a 10.7 x 5.2 cm gel tray leveled in a gel caster (RunOne System). A comb (12 wells) was placed into the gel. The gel was allowed to cool down to room temperature and to solidify within at least 1 hour. The comb was removed and the gel was taken out of the casting device and placed into the electrophoresis device which was filled with 25 mM Hepes buffer pH 7.4 until the whole gel was covered.

The samples were mixed with about 20 % of their volume with the loading buffer (30 % glycerol in 25mM Hepes buffer with 0.3% Orange G) and carefully filled into the wells. The electrophoresis devices were run at a constant voltage of 100 V. After 5, 10, 15 and 30 min an image was taken placing the gel on a UV transilluminator (Gel Doc XR system, Bio-Rad).

FRET immunoassays. All FRET assays contained 50 µL of each AB-Tb and QD-AB conjugate (in 10 mM TRIS/Cl; 0.5% BSA pH 7.4) at constant concentrations, to which 50 µL of serum with increasing concentrations of TPSA was added. The homogeneous FRET immunoassays were measured on a modified "KRYPTOR compact plus" clinical fluorescence plate reader from Cezanne/Thermo Fisher. The reader simultaneously detects the time-gated PL intensities, in a time window from 100 µs to 900 µs, in the Tb donor and the QD acceptor channels.

Preparation QD-Ln. Solutions of lanthanide complexes (0.25 mL, 2.1 mM, 200 eq) and TCEP (0.046 mL, 0.5 M, 9000 eq) in degassed water were added to the suspension of **QD-Pen** (0.5 mL, 5.2 µM, 1 eq) in degassed water, and the pH of the resulting suspension was adjusted to 9 with 0.5 M tetramethylammonium hydroxide solution (TMAOH). The mixture was shaken at *800* rpm overnight at 20°C. The resulting colloidal solution was purified by size exclusion chromatography with a NAP^{TM}-25 columns (Sephadex^{TM} G-25 DNA Grade from GE Healthcare) eluted in 1x PBS buffer.

The number of Ln^{III} complexes per QD was determined for independent syntheses by combined magnetic susceptibility measurements (on the Gd complex) and UV-visible spectroscopy.

4 Nanotoxicology studies on QDs

4.1 Introduction

In this chapter we will focus on nanotoxicology studies on QDs providing firstly a brief literature overview and secondly the results obtained in the framework of two collaborations with specialists in this interdisciplinary field, which have been initiated during my thesis.

As already mentioned in the first chapter, it is extremely important to address these issues. While a huge body of work exists on inorganic nanoparticles (*e.g.* TiO_2, ZnO, Au, Ag, etc.), nanotoxicological studies on QDs focus mainly on Cd-based materials. Moreover, the comparability of the data suffers from variations in the sample preparation and used methodology. In the case of InP QDs, only very scarce literature data exists.[18, 19] Indeed, new bio/non-bio interactions have to be taken in consideration as soon as a biological molecule is linked to a nanoscale support. Nanosized functional objects present chemical and physical characteristics at the same size scale (or even smaller) as that of cell surface receptors and they may interfere with cellular processes, eliciting undesired responses, such as cell uptake, sequestration in endosomal/lysosomal compartments, and activation of signaling cascade pathways or affecting the epigenetic program.[148]

Moreover, the widespread use and the fast-growing advances in the synthesis and engineering of colloidal NCs for manifold applications, spanning from biology, optics, electronics to medicine,[5] has promoted the need to investigate potential toxic effects due to unintentional release or contamination of the environment through powder/water waste-streams[65-68] and even an urgent evaluation of their toxicity on human beings is strongly needed. In fact, the employment of nanoparticles in biomedical research and clinical practices for diagnosis and therapy need adequate toxicological evaluation, so that this technology can be used in a responsible and sustainable manner and with minimal risks for human health.[149, 150] The elicitation of several pathways concerning the internalization, the activation of genetic cascades, and biochemical networks[151] have been found upon NPs exposure. However, the whole processes provoked in a cell/living organism upon NP exposure are complex and dependent on the NP and the biological target. Recent literature suggests manifold pathways possibly involved, from oxidative stress to pro-inflammatory gene activation[151-153] but still remain separate pieces of a complex puzzle.[154]

The exposure routes of nanomaterials envisaged in humans are inhalation (principal channel for the worker), ingestion (predominant pathway for the general population) and skin contact. While the pulmonary route has been subject of numerous research projects, the toxicity in the other two channels is much less explored. In the case of high tech products containing QDs, the manufacturing phase does not appear to be a critical phase from the point of view of health and environmental risk. Indeed, most often, these QDs are synthesized in organic phase and the steps of the manufacturing process (*e.g.* use in

optoelectronics, like displays and screens) involve inclusion in polymer matrices in the early stages of manufacture. This embedding and also the fact that QDs are colloids with surfactants which tend to stick to surfaces very strongly decrease the risk of exposure via inhalation as the volatility of these NCs is extremely low as compared to other types of surfactant-free nanoparticles obtained for example by grinding of ball-milling of bulk materials.

However, an accidental dermal exposure of the worker must be considered. The skin is the most likely body surface to come into contact with the nanomaterials; QDs can be absorbed through the skin into the blood. Moreover the skin is the largest organ of the human body and fulfills many different functions: it acts as the first barrier to xenobiotics, it prevents dehydration and allows the metabolism of several compounds and moreover it also plays an important role in the temperature regulation and in the immunological response. Skin absorption of nanoparticles is a wide issue, which needs to be better understood and there are conflicting results in the literature about QDs skin penetration. Tang and coworkers demonstrated penetration and permeation of QDs through rat skin, since cadmium was found inside the liver and kidney after skin exposure, raising concerns on QDs systemic toxicity.[155]

Wang and coworkers demonstrated QD penetration into the skin only after 8 h of skin exposure but not after 24 h.[156] In summary, QDs can permeate the skin, mostly when it is damaged or exposed to UVB light, and Cd leached out of the QDs can diffuse into internal organs. Accordingly, the aim of our study was to investigate the impact of InP-based QDs – with and without shell and using also Cd-based QDs for comparison –*in vitro* on cells extracted from human skin. In the quest of identifying QDs less toxic to human health we used InP as alternative material for safer and advanced biological applications. These studies have been carried out in collaboration with Dr. Adeline Tarantini and Dr. Marie Carrière from our Institute. As mentioned above, in the literature most of the studies focus on the toxicity related to Cd-based QDs and there are only very few reports on InP-based QDs. Moreover, working with primary keratinocytes from human skin biopsies is difficult due to the differences found for samples from different donators; therefore our approach is for the moment still in its preliminary phase.

In a complementary study, we decided to investigate the *in vivo* toxicity using *Hydra vulgaris*– a primitive organism at the basis of metazoan evolution– as a model in collaboration with Dr. Claudia Tortiglione from the Nanobiomolecular Group at National Research Council (CNR), Pozzuoli, Italy. *Hydra* assays are fast, reliable and less expensive than cell culture assays, and yet provide an extraordinary wide repertoire of responses, and determination of toxicity endpoints, both *in vivo* and *in vitro*. The decision to combine and investigate *in vivo* systems was motivated by the fact that, although cultured cells represent valid models to describe basic interactions with nanomaterials, they do not fulfill the *in vivo* response complexity. *Hydra* is mainly used by biologists to study developmental and regeneration processes and has been shown to have

great potential, inspiring both chemists and toxicologists as a new model to decipher the molecular basis of the bio/non-bio interaction and to assess nanoparticle toxicity.[157] Since 2007 the Nanobiomolecular Group at CNR pioneered the use of cnidaria species for nano-eco-toxicology study. In the following paragraph we will first describe the effect of QDs on *Hydra vulgaris*, and then the effects on primary keratinocytes from human skin biopsies, cultured *in vitro*. Finally, we will try to correlate the observed behavior of the same NCs in these two systems and to assess similarities and differences.

4.2 Toxicity studies of InPZnS@ZnSe/ZnS-and CdSe@ZnS nanocrystals

4.2.1 Quantum dot preparation

InP-based QDs, namely InPZnS@ZnSe/ZnS core/shell NCs emitting at 530 nm (**QD530**) and alloyed InPZnS core-only NCs emitting at 510nm (**QD510**), are synthesized in our laboratory and transferred from the organic to the water phase by means of ligand exchange using penicillamine (**Pen**), following the procedure described in **Chapter 2**. Under optimized conditions this functionalization results in a very compact, around 1 nm thick organic surface layer while preserving high fluorescence quantum yields.

Moreover, zwitterionic **Pen** results in low non-specific binding and a very high colloidal stability of more than two years. In parallel, the same functionalization chemistry was applied on hydrophobic commercial QDs based on CdSe/ZnS: **QD605**/**QD655**/**QD705** from Life Technologies (Thermo Fisher), emitting at 605, 655 and 705 nm.

The present study deals with the toxicity of InP-based **QD530** whose optical properties are shown in **Figure 4-1a**, in comparison with CdSe-based **QD605** and **QD655** (**Figure 4-1c-d**) used as references considering that their degradation and toxic effects are much better documented. In all cases the QDs are coated with an outer ZnS shell and present the same surface chemistry (**Pen** capping). In parallel the core-only InPZnS NCs **QD510 (Figure 4-1b)** are evaluated as well. For the Cd-based QDs (**QD605** and **QD655**), the study of the core-only systems was not possible, because on the one hand the corresponding QDs were not commercially available and on the other hand CdSe core QDs prepared in our lab lost all fluorescence upon aqueous phase transfer with **Pen**.

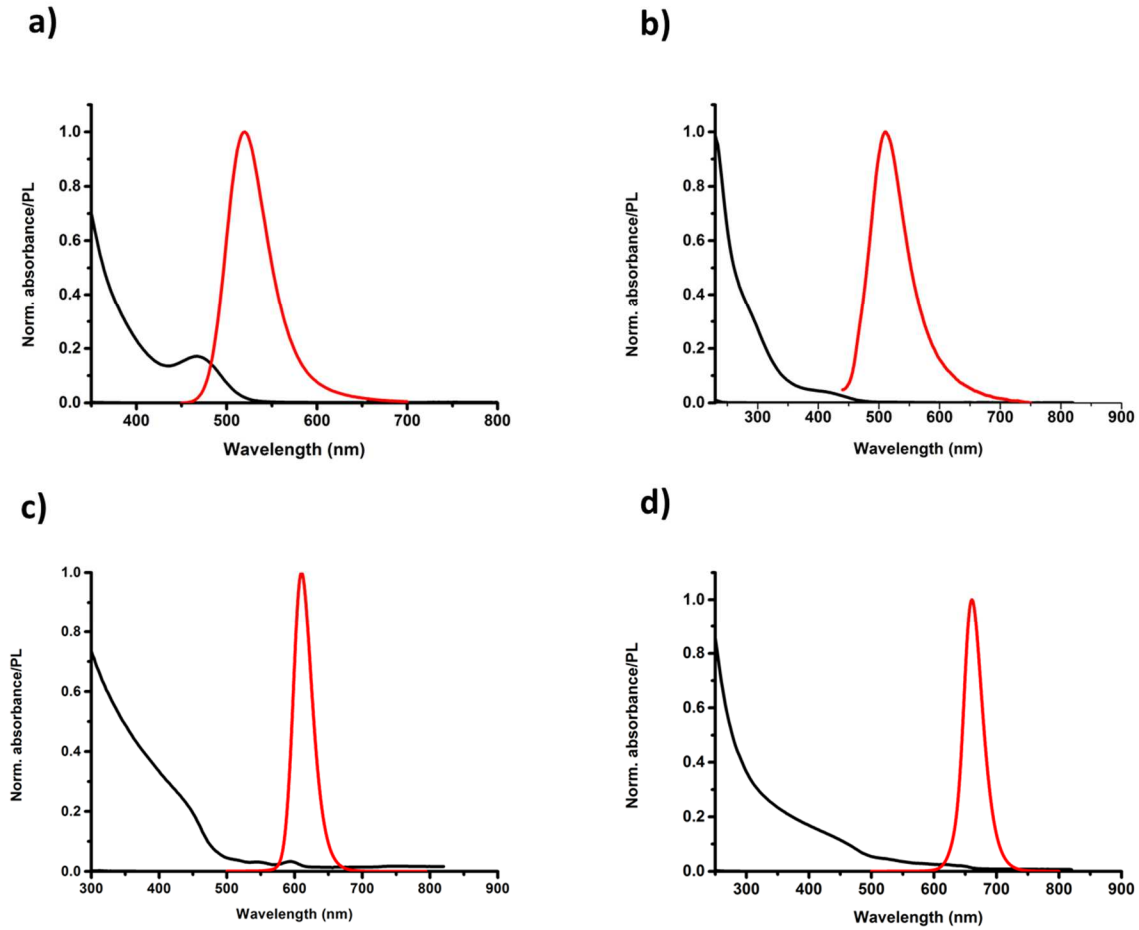

Figure 4-1. UV-Vis (black line) and PL (red line) spectra of the QDs used for *in vivo* nanotoxicological studies in *Hydra vulgaris* after aqueous phase transfer with penicillamine (**Pen**): InPZnS/ZnSe/ZnS core/shell **QD530** (**a**), InPZnS alloy core **QD510** (**b**), CdSe/ZnS **QD605** (**c**) and CdSe/ZnS **QD655** (**d**).

4.2.2 *Hydra Vulgaris* as a model system for nanotoxicology studies

In this small section we will briefly describe the structural anatomy and physiology of *Hydra* to facilitate the understanding of the mechanisms of tissue dynamics, reproduction, and regeneration, on which the subsequent toxicity tests rely, highlighting at the same time the advantages of using this model organism.[158]

The freshwater coelenterate *Hydra vulgaris* belongs to the animal phylum Cnidaria that arose almost 600 million years ago[159] **(Figure 4-2**).

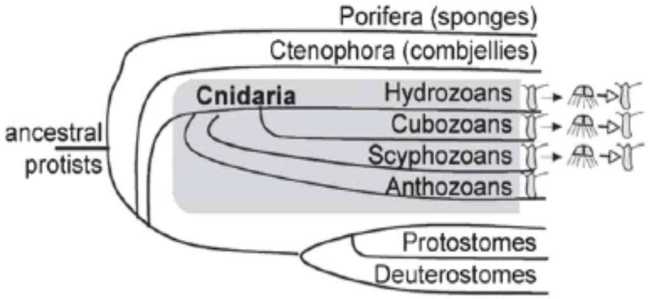

Figure 4-2. Cnidaria position in Metazoan phylogeny.

Its body plan is very simple, consisting of a single oral–aboral axis with radial symmetry. The structures along the axis are a head, a body column and a foot to anchor to a substrate. It is shaped as a tube, about 5-20 mm long and 0.3-1.0 mm wide. The head is divided in two structures, the hypostome (mouth) at the apex; below comes the tentacle zone from which a ring of six to eight tentacles emerges (**Figure 4-3**).

Figure 4-3. Photograph of living *Hydra vulgaris* showing an adult animal with a bud emerging from the gastric region.

The body has a bilayer structure, made of two unicellular sheets (ectoderm and endoderm) continuously dividing and migrating towards the animal oral and aboral extremities to be sloughed off. A third cell lineage, the interstitial stem cells lineage, is located in the interstices, among the epithelial cells of both layers and absent in the regions of the head and foot (**Figure 4-4**). These interstitial cells are multipotent stem cells that differentiate into nematocytes, secretory cells, gland cells, neurons and gametes.

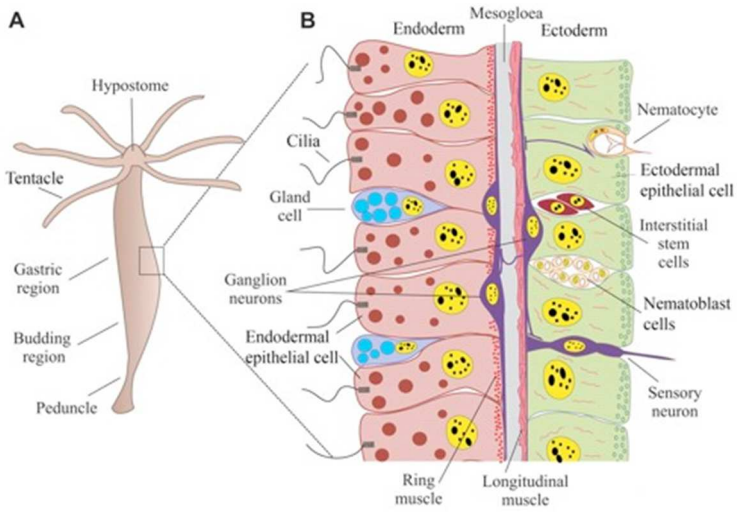

Figure 4-4. Anatomical structure of *Hydra vulgaris*. A) The animal is shaped as a hollow tube with a head at the apical end, and a foot, or basal disc at the other. The head is in two parts, the hypostome (mouth) at the apex, and below the tentacle zone from which a ring of six to eight tentacles emerges. **B) Schematic representation of the bilayered structure of the animal:** the body wall is composed of two self-renewing cell layers, an outer ectoderm and an inner endoderm, separated by mesoglea. Along the body the two epithelial layers are composed by epithelia muscular cells, while the interstitial cells and their differentiated products (neurons, nematocytes and secretory cells) are interspersed among the two layers.

Most of the *Hydra* body is occupied by the gastric region, where the digestion takes place. In the lower part of the body the budding of new animals occurs, and this process accounts for the rapid asexual reproduction, which enables massive culturing of the animal in laboratory conditions. In fact the epithelial cells structuring the body continuously divide and contribute to the formation of new individuals, budding from the gastric region, and detaching from the mother in about 3 days.[160] The biological cycle of *Hydra*, unlike other cnidarians, includes only one stage of polyp that can reproduce by both asexual and sexual means. *Hydra* in their natural habitat typically reproduces by budding during the regular feeding regime, but they produce male gametes and / or female in autumn **(Figure 4-5).**

In laboratory condition, the main method of reproduction is budding. Massive culturing is achieved thanks to fast mitotic reproduction, warranting a large number of identical clones.[161]

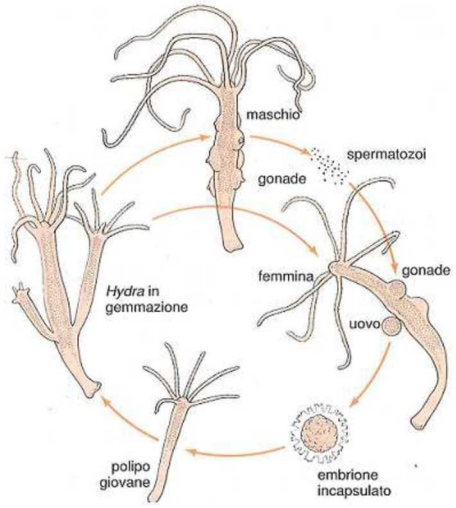

Figure 4-5. Biological cycle of *Hydra*. *Hydra* polyps reproduce both sexually and asexually.

The growth rate of *Hydra* tissue is normally regulated by a balance between the epithelial cell cycle length, phagocytosis of ectodermal cells in "excess", and bud formation.[162] Environmental factors, such as the presence of pollutants or the feeding regime, can affect this balance. Thus, the population growth rate is an indirect measure of the *Hydra* tissue growth rate and cell viability. Another peculiar feature of *Hydra* physiology is the remarkable capacity to regenerate amputated body parts (see **Figure 4-6**). In fact, following amputation at mid-gastric level, the two polyp halves immediately initiate an asymmetric process at the wound site: the upper half undergoes foot regeneration in about two days, whereas the lower half initiates the head regeneration process, which is completed in three days (**Figure 4-6**). Morphogenetic processes take place during the first 48 h post amputation, followed by cell proliferation to restore the adult size.[163, 164] This ability of self-regeneration is due to the continuous production of adult tissue cells and signaling factors. The tissue regeneration shows a directional property called polarity, which confer the capability to regenerate a head in the apical part, and a foot in the basal extremity. The polarity depends on a gradient of molecules, which provide positional information.[165] In contrast to vertebrates, in which the morphogenetic signal is active only during embryogenesis, in *Hydra* it is continuously active, which makes *Hydra* a source of stem cells.[164]

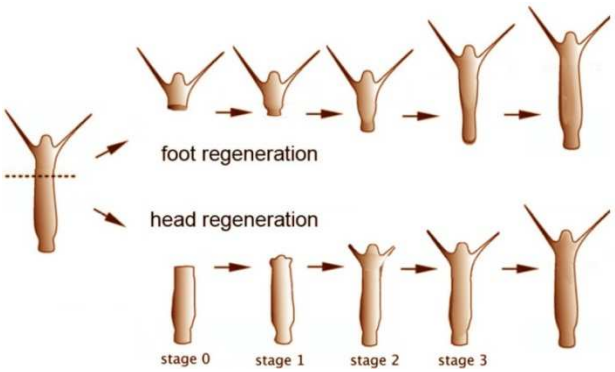

Figure 4-6. The regeneration process in *Hydra vulgaris*. After amputation, the two polyps start immediately an asymmetric process at the wound site: the upper half undergoes foot regeneration in about two days, while the lower half initiates the head regeneration process, which is completed in three days.

The regeneration process can be adversely affected by the presence of organic and inorganic pollutants and specific assays have been developed to quantify this effect.[166, 167] *Hydra* is very sensitive to environmental toxicants and it has been used as a biological indicator of water pollution. The responsiveness to different environmental stressors varies among different species, but it is always quantifiable by standardized protocols in terms of median lethal concentration and median lethal time (LC50 and LT50). For this reason, short term (lethality) and long-term (sub-lethality) tests based on the evaluation of polyp morphology, reproductive activity and regeneration efficiency can be used to test the potential toxicity/teratogenic effect of any kind of medium suspended compound.

Finally, the conservation of the key regulatory genetic pathways in *Hydra* enabled the molecular characterization of QD treated polyps, through the assessment of transcriptional modulation of known or novel toxicity biomarkers associated to QD exposure. In a recent study, aimed to identify the molecular pathways elicited in *Hydra* by exposure to core/shell CdSe/ZnS QDs coated by a positively charged polymer, the authors profiled the transcriptomic changes occurring in two aquatic species (*Hydra* and *Stylophora)* by RNA sequencing (RNA-seq) analysis. The results showed in Hydra 2055 differentially expressed genes (DEGs) in response to QDs and in particular towards those that were highly up-regulated, two DEGs were selected, namely carbonic anhydrase and the serine protease inhibitor antistasin. These two genes showed the highest upregulation as proven by validation step using quantitative reverse transcription polymerase chain reaction PCR (qRTPCR) as well (**Ambrosone et al., submitted**). Therefore, these genes appear to be valid candidates to be analysed upon treatment with QDs of different chemical composition as they likely represent novel biomarkers for toxicity induced by semiconductor QDs.

4.2.3 *In vivo* and *in vitro* analyses to investigate interactions between semiconductor nanocrystals and *Hydra*

4.2.3.1 Hydra exposure to QDs: Impact on morphology, regeneration and reproductive capabilities

Living animals were soaked in culture medium supplemented with increasing doses of InP-based core (**QD510**) and core/shell (**QD530**) NCs (from 50nM to 100nM) and monitored at 24, 48 and 72h of incubation. The QD concentrations were selected according to the results of various experiments. Progressive physical damages were observed, as shown by representative images shown in **Figure 4-7A**. To describe and quantify the morphological alterations induced by NPs, a numerical score originally introduced in the 1980s has been used.[168] This score system, initially developed to monitor and quantify the effects of aquatic pollutants on *Hydra* regenerating potential,[167, 169] has been subsequently adapted and modified by the Nanobiomolecular Group at CNR for nanotoxicology investigations. The scores run from 10 (indicative of healthy conditions) to 0 (animal fully disintegrated).

Median scores recorded at each QD test concentration decreased for treated animals with increasing concentration and incubation time (**Figure 4-7B**). By comparing the median scores of animals exposed to core-only **QD510** and to core/shell **QD530** NCs, lower values were produced at each time point and test concentration for the former, indicating a more toxic effect of the core-only NCs. This is not unexpected as the protective ZnSe/ZnS shell is supposed to prevent In^{3+} ions from leaching out. Moreover, these experiments enabled us also to determinate the doses to assess QD long-term effects; the concentrations of 30 nM and 70 nM were selected.

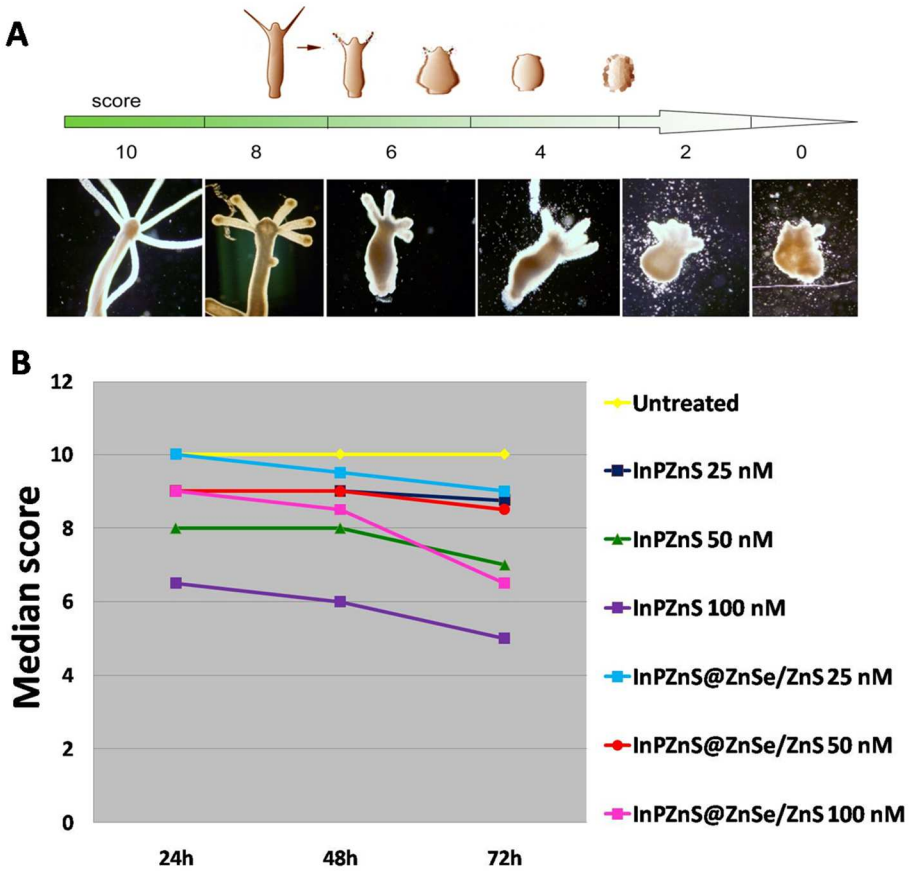

Figure 4-7. A) *Hydra* response to environmental stimuli through a broad range of morphological changes. The green arrow represents the score system[168] used to evaluate progressive morphological changes of polyps exposed to QDs running from 10 (normal) to 0 (disintegrated). **B**) Toxicity curves of Hydra polyps exposed to different concentrations of QDs. 20 polyps without bud were incubated with 25nM, 50nM and 100nM of QDs supplied as core-only InPZnS QDs and core/shell InPZnS@ZnSe/ZnS QDs using incubation times of 24, 48 and 72 h in Hydra medium at pH7.

The QD toxicity screening *in vivo*, at whole animal level, was completed by the assessment of the impact on the regenerative and reproductive capabilities. As mentioned above, *Hydra* polyps are characterized by a remarkable capacity to regenerate amputated body parts: during the first 48h post amputation (p.a.) morphogenetic processes take place, followed by cell proliferation to restore adult size. Healthy polyps were bisected in the upper gastric region and allowed to regenerate (**Figure 4-8A upper panel**) in presence of 30 nM or 70 nM QDs, or in normal medium. At 48h and 72h p.a. animals were inspected for viability and regeneration stage. The regeneration stages are classified like in **Figure 4-6**. Basically, **stage 0** indicates a complete inhibition of regeneration (0 tentacle), while **stage 1** indicates heads with aberrant tentacle (one or two), and finally **stage 2** means normal regeneration (four to six tentacles). Polyp exposure to the **QD530** core/shell NCs slightly impaired patterning during the first 48h, indeed 60% of the polyps are at **stage 1**; on the contrary exposure to core-only **QD510** NCs impaired most of the polyp regeneration.

More precisely, after 72h all the control animals and those treated with 30 nM of **QD530** have completed the regeneration process (100% **Stage2**). The other stumps are still at **stage 1**, namely 15% of the polyps treated with the higher dose of **QD530** as well as 35 % and 10% of the polyps treated with **QD510** (30nM and 70 nM, respectively).

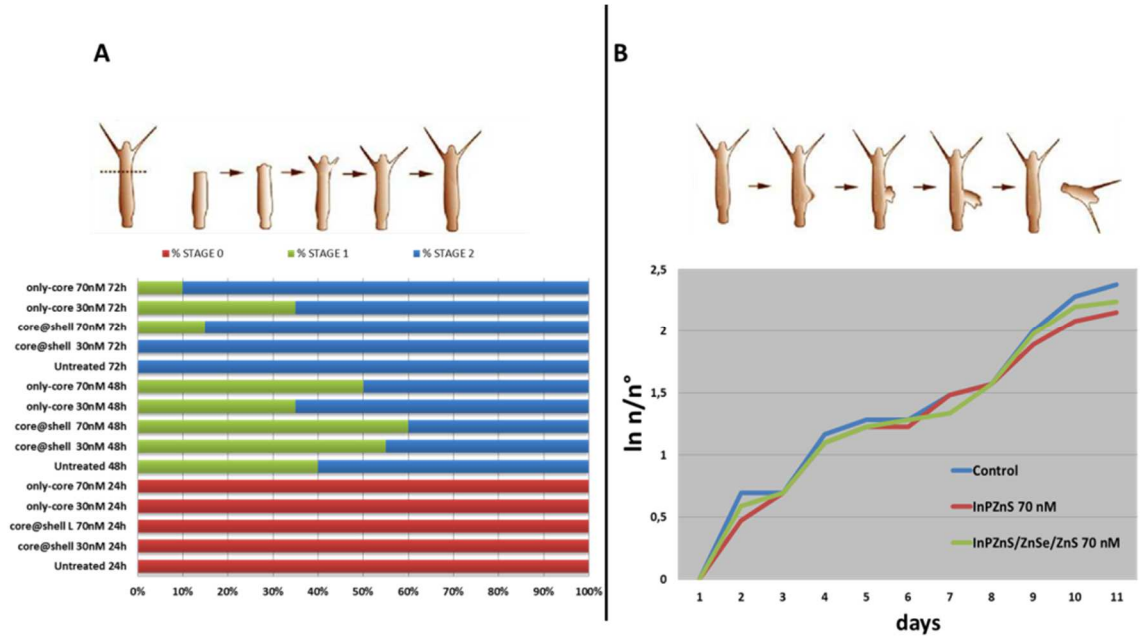

Figure 4-8. Influence of InP-based QDs on *Hydra* regeneration and reproduction. **A)** Impact of the QDs on regeneration. 20 polyps were bisected in the upper gastric region and incubated in presence of 30 nM and 70 nM **core-only** (**QD510**) and **core/shell** (**QD530**) QDs. The regenerating polyps were observed through a stereomicroscope and were grouped in three stages according to their number of tentacles. **B)** Impact of the QDs on reproduction. 5 animals with one bud were treated with 70 nM of **core-only** (**QD510**) and **core/shell** (**QD530**) QDs for 24 h and the following day each animal was washed and placed in a well. Both control and treated *Hydra* were fed once a day during 14 days.

Beside the effect on regeneration, the reproductive capability of QD treated polyps was estimated. In *Hydra*, the epithelial cells structuring its body continuously divide, migrate toward the animal ends, contributing to the formation of new individuals, budding from the gastric region, and detaching from the mother animal in about 3 days (**Figure 4-8B** upper panel).[162] Environmental factors, such as the presence of pollutants or the feeding regime, can affect this process. Thus, the population growth rate is an indirect measure of the *Hydra* tissue growth rate and cell viability. A group of founder animals (n°) either untreated or incubated 24h with 70nM QDs, were monitored over two weeks, and the total number of individuals (n) used to calculate the growth rate constant (k) over the duration of the experiment (t), is defined by the equation ln(n/n°) = kt. In the graph of **Figure 4-8B** the growth rate curve of animals treated show no difference from the others (k values did not evolve significantly).

These results indicate a slowdown in the regenerative process after QDs exposure, except for the polyps exposed to the lowest QD concentrations (30nM) of **QD530 core/shell** NCs, as all these stumps complete the regeneration process as in the case of the untreated animals. In light of these results it is clear that the **core-only** InPZnS NCs **QD510** induce a slight effect on the regenerative capacity, compared to the core/shell system **QD530**, but not on the reproductive capacity of *Hydra*. The same *in vivo* screening was conducted with the Cd-based QDs **QD655** emitting at 655 nm. For simplicity all the other data are not shown, but the behavior of this type of QDs was almost identical as that observed with **QD530**, *i.e*. no significant morphological changes and no impairment of the reproductive capability were found.

In order to evaluate the efficiency of internalization of QDs, polyps were incubated for 24h with 50 nM of all three types of QDs (**QD510**, **QD530** and **QD655**). The process was monitored with phase-contrast and fluorescence microscopy revealing that the QDs were internalized into the *Hydra* tissue, and accumulated into granular-like storage structures. **Figure 4-9** shows the biodistribution of the InP- and CdSe-based core/shell QDs.

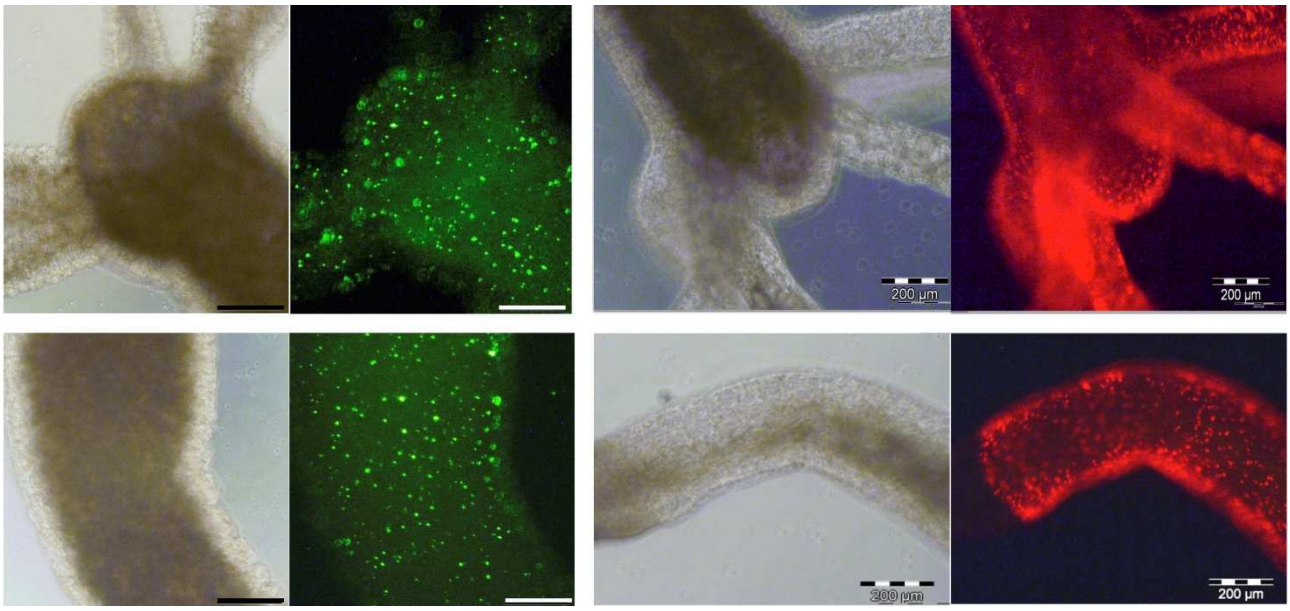

Figure 4-9. **Biodistribution of InP-based (left two columns) and CdSe-based (right two columns) core/shell QDs in *Hydra vulgaris***. For each QD type: left column: images of bright field microscopy; right column: fluorescence microscopy images showing the internalization of the QDs. Upper row: hypostome and tentacles, lower row: body. All scale bars: 200 microns.

The low PL QY of core-only InPZnS QDs did not allow for the determination of the bio-distribution by means of fluorescence microscopy. However, using ICP-AES we measured the intracellular indium concentration of animals treated with core-only and core/shell InP-based QDs.

As shown in **Figure 4-10**, the In content is significantly higher in animals treated with the core-only InPZnS. Further experiments are needed to elucidate this behavior in more detail, but for the moment we ascribe it to either an extracellular degradation (leaching out In from the particles) or to a size effect, as the smaller sized core-only QDs may exhibit a higher degree of internalization. A combination of both effects is of course also possible.

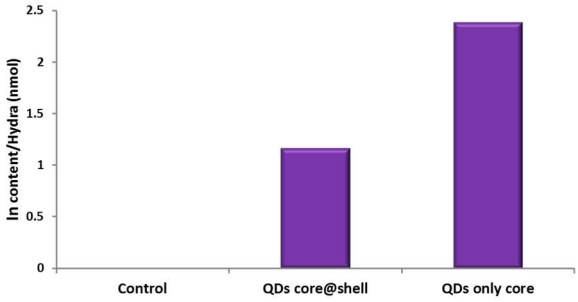

Figure 4-10. The intracellular In amount was evaluated by elemental analysis using ICP-AES. The *Hydra* polyps were incubated with 70 nM of core-only **QD510** NCs or core/shell **QD530** NCs for 24 h.

4.2.3.2 *Hydra* exposure to QDs: effects on the cellular level

The study of the effects of QDs on *Hydra* was completed by the assessment of apoptosis and genotoxic effects. Apoptosis (from the Greek word meaning "falling off", as leaves from a tree), is not a random process but occurs by a programmed sequence of molecular events. This programmed cell death occurs physiologically during the growth, development, and maintenance of multicellular organisms. Indeed, this equilibrium depends not only on the production of cells but also on the mechanisms to destroy them. Cells dying by apoptosis undergo characteristic morphological changes. They shrink and condense, the cytoskeleton collapses, the nuclear envelope disassembles, and the nuclear chromatin condenses (picnotic nuclei) and breaks up into fragments. The cell surface often bulges outward and, if the cell is large, it breaks up into membrane-enclosed fragments called apoptotic bodies.[131] In *Hydra*, apoptosis is a physiological mechanism that keeps the size of the animal constant, as well as being involved in development processes and gametogenesis. To gain deeper insights into the induction of apoptosis by QDs, the detection and quantification of picnotic nuclei was carried out. This was evaluated by 40-6-Diamidino-2-phenylindole (DAPI) staining. Briefly, untreated and QD treated polyps were macerated and the single cell suspension was fixed with 4% of paraformaldehyde and spread on slides.

After extensive washing in PBS, the macerates were stained with DAPI for 2 min and washed in PBS. The DAPI staining of nuclei allows observing the characteristic signs of apoptosis like the nucleus damage. The slides were observed with phase-contrast and fluorescence microscopy to detect picnotic nuclei (**Figure 4-11**). More than 300 cells were counted for each treatment and the percentage of apoptotic nuclei was determined.

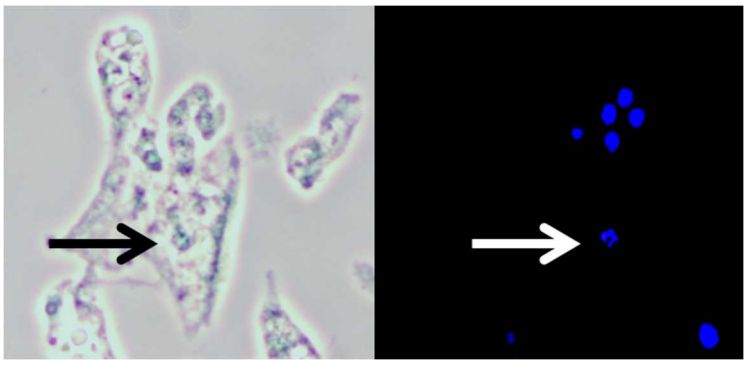

Figure 4-11. Microscope image of single cells prepared from QD treated Hydra. **Left**, an ectodermal epithelial cell in bright field. **Right**, fluorescence imaging following DAPI staining shows a picnotic nucleus (white arrow), typical of apoptosis process, in the epithelial cell.

Figure 4-12 shows that cells treated with Cd-based (**QD655**) QDs for 24h show the highest percentage (18%) of damaged nuclei. Nonetheless, cells treated (using the same dose and time) with core-only InPZnS QDs (**QD510**) also presents 10% of damaged nuclei, compared to 4% induced by core/shell InP-based QDs (**QD530**). The presence of apoptotic nuclei (2-3%) occurring also in untreated polyps is due to the physiological role played by programmed cell death in the maintenance of the steady state in continuously renewing tissues, as reported elsewhere.[170] These results demonstrate both the protective effect of the shell around the InPZnS core NCs and the higher toxic effect of Cd-based QDs.

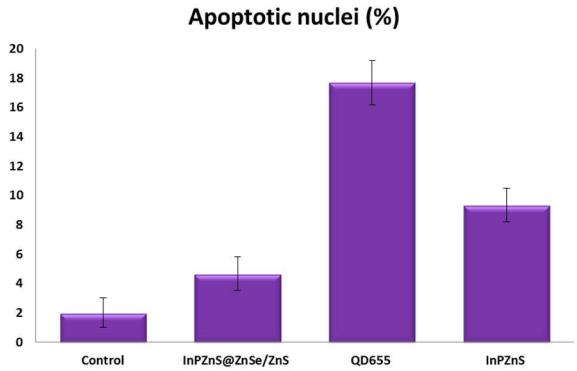

Figure 4-12. Cellular assessment of apoptosis induction by QDs. Following 24h incubation with 50 nM QDs, 20 polyps were macerated in single cells and the percentage of apoptotic cells was determined by counting the DAPI-stained fragmented nuclei.

4.2.3.3 Genotoxic effects

We further investigate the gene expression levels of two genes, antistasin and carbonic anhydrase using Real Time PCR (qRT-PCR). To normalize RNA levels, Elongation 1-alpha (EF1-α), was employed as internal calibrator (**Figure 4-13)**.

Antistasin, a 17kDa serine protease inhibitor –serine protease, belong to a large family of protein-cleaving (proteolytic) enzymes including the digestive enzymes chymotrypsin, trypsin, and elastase, and several proteases involved in blood clotting. Originally isolated from the salivary gland of the Mexican leech (*Haemanteria officinalis*) this protein is a potent anticoagulant by virtue of its ability to inhibit certain factors in the coagulant cascade and it plays a role as inhibitor of metastasis. In *Hydra* this gene may play a role as protector from the digestive enzyme secreted by the polyp itself, similar to some mammalian protease inhibitors.[171]

Carbonic anhydrase (CA) is a metalloprotease - is a zinc-containing enzyme- that catalyzes the reversible hydration of carbon dioxide: $CO_2 + H_2O \leftrightarrow HCO_3^- + H^+$. Its activity is virtually ubiquitous in nature. In the last years the interactions between CA and heavy metals have found a number of applications in environmental and health fields, including the development of biomarkers of pollution exposure, *in vitro* bioassays, and biosensors.[172] Intriguing aspect of the biochemistry of CA is the inhibition by heavy metals. It has been documented for some species and some metals, but the mechanisms behind the inhibition are still unknown. These aspects it's important and open new perspective for biomarker development.

In summary these two genes are involved in cell stress responses and may represent novel biomarker for toxicity induced by semiconductor QDs.

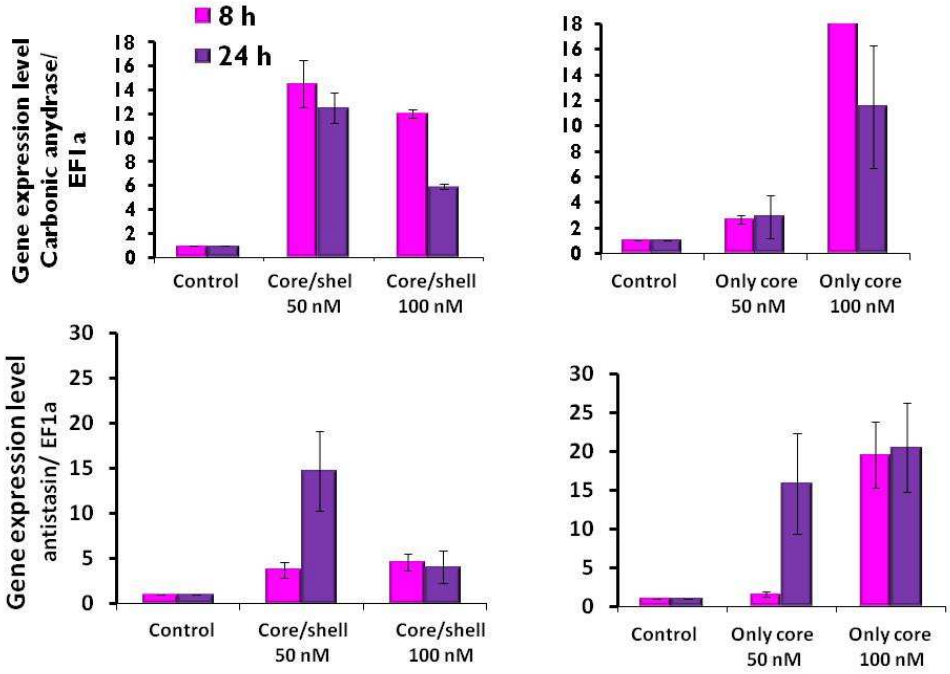

Figure 4-13. Gene expression patterns of selected stress responsive genes in QDs-treated polyps analyzed by qRT-PCR. The Elongation factor 1-alpha (EF-1α) is used as reference gene. The data represent mean of two biological replicates. The value of each biological replicates is the average of three technical repeats.

Animals were incubated with 50 nM and 100 nM of QDs supplied as core/shell and core-only for 8 h and 24h, and then processed for qRT-PCR analysis, using specific primers (see experimental section). Results of **Figure 4-13** show the gene expression level obtained. Overall, the general trend of these genes profiling indicates an enhancement of stress responsive genes more pronounced for the core-only.

In detail the gene antistasin showed increased expression at the doses tested even if this evidence is more pronounced after 24 h for the core/shell at 50 nM. For the core-only this gene appears to be upregulated in all the samples analyzed (except at 50 nM after 8h). The carbonic anhydrase gene result highly overexpressed in all the experimental conditions indicating a great sensitivity of this gene for any type of treatment.

4.2.4 Cytotoxicity study using primary keratinocytes from human skin biopsies

Although this study is still preliminary, we report two representative experiments based on cytotoxicity and proliferation studies in keratinocytes exposed to QDs. Cytotoxicity and the ability of keratinocytes to proliferate following exposure to QDs were evaluated using the same plate with a lactate dehydrogenase assay and a 5-Bromo-2'-deoxy-uridine (BrdU) assay, respectively. **Figure 4-14** shows cytotoxicity after 24h incubation at the highest tested doses (200 nM) for core-only InPZnS (**QD510**) and InPZnS@ZnSe/ZnS core/shell QDs(**QD530**) compared to Cd-based QDs (**QD605**). For all types of QDs, a slight decrease in cell proliferation was found, which started at doses of 50nM and was more pronounced at 200nM. **Figure 4-15** shows the efficient internalization of **QD605** and **QD530** into keratinocytes.

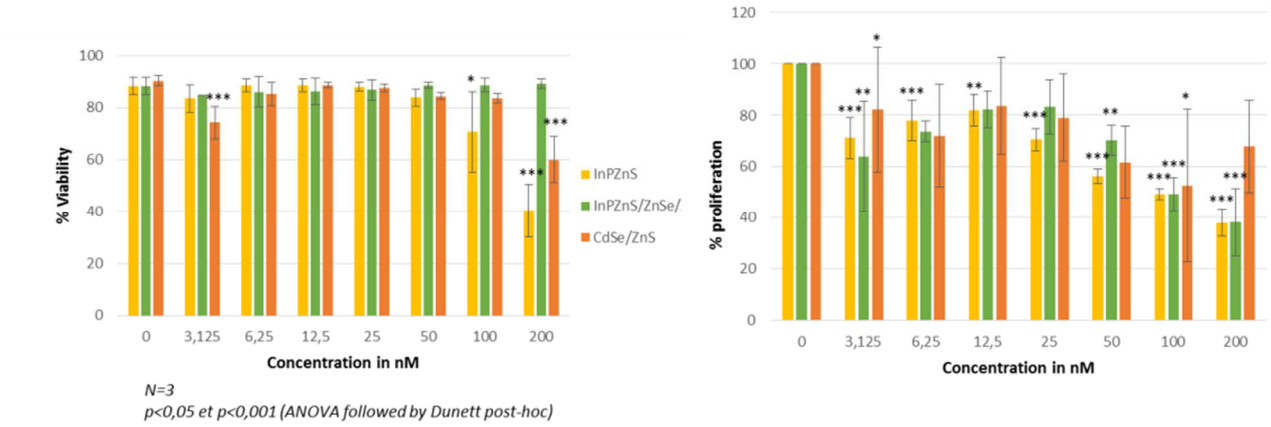

Figure 4-14. Left: cytotoxicity study using the lactate dehydrogenase assay; **right**: proliferation study using the BrdU assay.

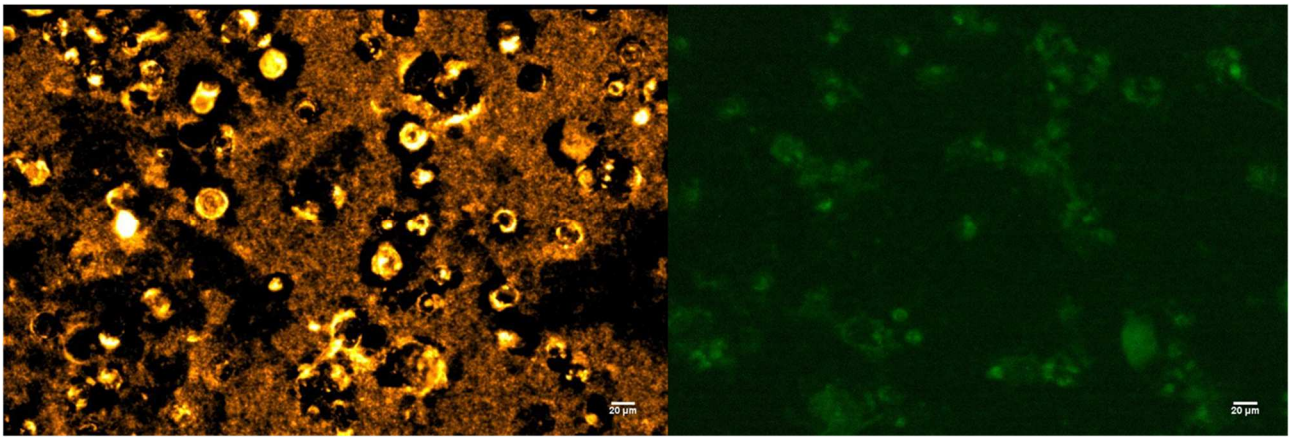

Figure 4-15. Fluorescence microscopy images of keratinocytes exposed to **QD605** (left), and to **QD530** (right).

4.3 Conclusion

The results presented in this chapter are part of toxicological research, aiming at the study of the interactions between nanomaterials and biological systems, which is a prerequisite for the use of novel nanomaterials in biology and medicine for diagnostic and therapeutic purposes. The aim of these studies resides in comparing QDs of different chemical composition but with the same surface coatings to assess the effect of the inorganic core (InP-based *vs.* CdSe-based) and the role played by the protective ZnS outer shell. In particular, here we showed *in vivo* and *in vitro* toxicity studies comparing core-only and core/shell InP-based QDs emitting at 510 nm and 530 nm, respectively and CdSe-based QDs emitting at 605 nm and 655 nm transferred to the aqueous phase by means of ligand exchange with zwitterionic penicillamine (**Pen**). The obtained results represent a significant progress in the field of nanotoxicology of QDs because i) nowadays such studies almost exclusively address Cd-based QDs and ii) the aqueous phase transfer using **Pen** has not yet been validated using *in vivo* and *in vitro* toxicity studies.

By using as toxicity model the freshwater polyp *Hydra vulgaris*, we determined several toxicity endpoints *in vivo* (morphology, reproduction rate, efficiency of regeneration), *ex vivo* (cell apoptosis rate) and at the molecular level (changes in expression levels of two marker genes *i.e.* antistasin and carbonic anhydrase). Overall, the general trend of these genes profiling showed an upregulated pattern after 24h in all the experimental condition. This general trend of gene expression is similar to the one induced by treatment with Cd-based QDs but different compared to other type of NPs*, i.e*. iron oxide, suggesting that these genes are toxicity markers associated to QDs with a semiconductor core. Our studies show that the QDs induce alterations *ex vivo* and *in vitro* at the molecular level while no effects on the *in vivo* behaviour have been detected. In particular, all types of QDs did not affect the morphology and growth rate of *Hydra*. At the cellular level the QD treatment enhances apoptosis pointing at a cytotoxic effect, which increase in the order InPZnS/ZnSe/ZnS core/shell <InPZnS core <CdSe/ZnS core/shell. This order indicates the protective character of the ZnSe/ZnS shell and also demonstrates the higher cytotoxicity of CdSe with respect to InP. However, when we used more sensitive methods, all three types of tested QDs alter the expression of proteinase inhibitor and metal proteases, indicative of genotoxic effects. The occurrence of such subtle genetic variations, in absence of morphological damages, also indicates the importance of genotoxicity studies for QD risk assessment.

Considering that working with primary keratinocytes from human skin biopsies is complicated due to the differences found for different donators, this approach is for the moment still in its preliminary phase.

By consequence these results are still too weak for drawing conclusions of any certainty aiming at correlating the impact of the same type of QDs *in vivo* and *in vitro*. Globally, the results demonstrate the protective effect of the shell around the InPZnS core and the higher toxic effect of Cd-containing nanoparticles, supporting the choice InP as alternative for safer and advanced biological applications. Future experiments on keratinocytes (most of them are already in progress) are needed to better investigate the toxicity induced in these two systems. It remains of intriguing interest to draw correlations between the behaviour of the same QDs in the two systems (*Hydra* and keratinocytes). In fact, the nanotoxicology research community needs not only standardized protocols for measuring the biological response *in vitro* and *in vivo*, but also a database repository to collect large datasets from screening different biosystems, obtained by different laboratories.[173] Therefore our results may constitute a valuable contribution to this field. There are still many doubts about the use of QDs functionalized with active molecules in the biomedical field and in the emerging domain of theranostics, because of the potential risk caused by the heavy metals contained in the core and due to significant discrepancies between conclusions from *in vitro* and *in vivo* studies. For this reason, nanotoxicological studies using rapid, reliable and low-cost methods allowing for the screening of the effects of identical samples *in vivo* and *in vitro*, such as those proposed in in this work, are necessary and indispensable so that new nanomaterials can become integrative part of the nano-bio-medicine of the future.

4.4 Experimental section

Materials and Methods

Culture of test organisms

Hydra vulgaris were cultured in *Hydra* medium comprising 1 mM calcium chloride and 0.1 mM sodium hydrogen carbonate at pH 7.[161] The animals were fed on alternate days with *Artemia nauplii* at 18°C with a 12:12 h light:dark regime. Polyps from homogeneous populations, three-weeks-old and carrying one or two buds, were selected for the experiments.

Culture of human keratinocytes

Human skin samples were obtained immediately after breast plastic surgery from healthy donors. Keratinocytes were isolated from the whole skin and frozen until use.[174] Cells were cultured in Keratinocyte serum-free medium supplemented with 1.5 ng/ml EGF, 25 µg/ml bovine pituitary extract and primocin and maintained at 37°C in a humidified atmosphere. For the experiments, keratinocytes at passages 2 or 3 were seeded in 96 well plates at a density of 10 000 cells/well and incubated overnight before exposure with the QDs. QDs in PBS were diluted in the culture medium of the cells.

Chronic toxicity induced by QDs to individual polyps

Toxicity tests were carried out on groups of 20 polyps, placed into plastic multiwells maintained at a temperature of 18°C in an incubator with a light regime of 12 h light and 12h dark. A range of nominal concentrations was selected for InP-and Cd-based QDs, to assess the progressive effects on the morphology and physiology of individual polyps. Exposure was carried out for 24, 48 and 72h, and new test solution was completely replaced every 24 h. Effects were recorded by microscopic examination of each polyp at 24 h intervals and a score was assigned ranging from 10 for a normal polyp to 0 if it was disintegrated, as described in **Figure 4-7** constructed by Wilby.[167] The median scores were analysed at 24, 48 and 72h for each concentration of the QDs.

Elemental analysis

150 polyps were incubated 12 h with 70 nM of InP-based core-only or core/shell QDs, washed, digested by the addition of concentrated acid (HCl/HNO_3 3:1 (v/v) mixture) and the intracellular In content was measured by means of ICP-AES (Inductively Coupled Plasma Atomic Emission Spectrometry). Similarly, the core-only concentration was also evaluated in the *Hydra* culturing medium used for QD incubation, allowing the estimation of the extracellular In contents.

Hydra growth rates and regeneration

Animals (five *Hydra* with one bud) were treated with 70 nM of QDs for 24h, washed, and the following day placed in 3.5 cm petri dishes (1 *Hydra*/dish). Control polyps at the same developmental stage were not treated. Both treated and untreated *Hydra* were fed once daily for 18 days. The growth rate constant (k) of an exponentially growing group of animals is defined as $ln(n/n_0)= kt$ where n is the number of animals at time t and n_0 the number of animal at t_0. For $n/n_0 = 2$, $t = T_2$, the doubling time of the population. T_2 was determined by linear regression.[162] For regeneration experiments, groups of 20 polyps were bisected in the upper gastric region and incubated in presence of 30 nM and 70 nM QDs. The regenerating polyps, monitored through a stereomicroscope, were grouped in three stages according to their tentacle morphogenetic process.

Assessment of apoptosis

Apoptotic cell death was evaluated by 4'-6-Diamidino-2-phenylindole (DAPI) staining and confirmed by Terminal deoxynucleotidyl Transferase-mediated dUTP nick end labeling (TUNEL) assay.[170] Briefly, untreated and QD treated polyps were macerated and the single cell suspension was fixed with 4% paraformaldehyde and spread on slides. After extensive washing in PBS, macerates were stained with DAPI for 2 min and washed in PBS. Slides were observed with phase-contrast fluorescent microscopy to detect picnotic nuclei. More than 300 cells were counted for each treatment and the percentage of apoptotic nuclei was determined. In Situ Cell Death Detection Kit Fluorescein (Roche) was used for TUNEL assay to confirm the nuclear shrinkage in macerates. In particular, fixed cells were permeabilized for 2 min with 0.1% Triton X-100 / 0.2% sodium citrate solution. Slides were incubated with 50 µl TUNEL reaction mixture in a humid dark chamber for 60 min at 37°C, extensively washed in PBS and counterstained with DAPI solution. The presence of apoptotic cells was confirmed by counting fluorescein-labelled nuclei by fluorescent microscopy.

RNA extraction and qRT-PCR

For each experimental condition RNA was extracted from groups of 25 animals by purification in Trizol Reagent (Life Technologies) according to manufacturer's instructions. RNA was quantified and quality checked by SmartSpec plus spectrophotometer (Biorad, CA, USA) and 2100 Bioanalyzer (Agilent Technologies), respectively.

Before starting the reverse transcription RNA samples were treated with DNaseI *(Amplification Grade, Invitrogen)* according to manufacturer's instruction. The first-strand cDNA was synthesized by High Capacity cDNA Reverse Transcription Kit (Applied Biosystem) using 0.5 µg of DNA-free RNA in a final volume of 20 µL, according to the manufacturer's instructions.

Quantitative real-time reverse transcription-polymerase chain reaction (qRT-PCR) was performed in 25 µL of reaction mixture consisting of 1x Express SybrR GreenER qPCR SuperMix with premixed ROX (Invitrogen), serial cDNA dilutions and 0.3 µM each primer. The reactions were processed using the StepOne Real-Time PCR System (Applied Biosystem) according to the following thermal profile: 95°C for 2 min, one cycle for cDNA denaturation; 95°C for 15 sec and 60°C for 1 min, 40 cycles for amplification.

Specific primers of Hydra homologues genes of antistasin and carbonic anhydrase were designed using Primer3 software (http://frodo.wi.mit.edu/primer3/) and are listed in **Table 4.1**. These primer pairs were chosen to amplify products of 100–200 bp in length. Blast searches against the whole *Hydra* genome were performed to verify primers specificity. The Real Time PCR *(qRT-PCR)* experiment measures the number of cycles needed to attain a threshold concentration of Q-PCR product (C_t). The threshold value is chosen to fall within the exponential amplification phase, before limiting reagents become a factor in the efficiency of each cycle. This method requires a known reference gene with constant expression in all tested samples and whose expression is not changed by the treatment under study. A pair of primers for *Hydra Elongation 1 alpha (HyEF1-α)* housekeeping gene has been used as standard reference. The number of cycles needed for the standard to reach a specified C_t is used to normalize the C_t for the selected genes. A higher C_t for the gene of interest implies a lower initial concentration in the sample, and vice versa. To capture intra-assay variability all qRT-PCR reactions were carried out in triplicate. For triplicate samples, C_t is calculated as the average value among the replicates. The expression of the following genes was assessed by Real time PCR: *antistasin, carbonic anhydrase and Hydra Elongation 1 alpha (HyEF1-α)* as control. Nucleotide sequences and alignments were obtained from Hydra genome database (http://Hydrazome.metazome.net). The expression profiles were analyzed by applying the ΔΔCt method where the values of the gene of interest were normalized for the values of reference control gene *(HyEF1- α).*

Primers	*DNA Sequence*
Ef1α qRTforward	5^{I}-ccaggagacaatgtcggttt-3^{I}
Ef1α qRTreverse	5^{I}-gcttcaatggcaggatcatt-3^{I}
Antistasin qRTforward	5^{I}-actgtgccttggtaagatgc-3^{I}
Antistasin qRTreverse	5^{I}-cacgcaacaatactcctccg-3^{I}
Carbonic anhydrase qRTforward	5^{I}-agctctcaatttcgatcggc-3^{I}
Carbonic anhydrase qRTreverse	5^{I}-ttgtaagtcaacgcccctcc-3^{I}

Table 4-1. Primer sequences used in this study.

Cytotoxicity assay in keratinocytes

Cytotoxicity was evaluated using the lactate dehydrogenase assay (LDH kit from Sigma). It is a colorimetric test which consists in measuring the release of lactate dehydrogenase from damaged or dying cells. Following exposure to the QDs, 50 µl of cell supernatant was collected and transferred to a new 96- well plate. 100 µl of a mix co-factor, substrate, dye (1:1:1) was then added. Following 20 min of reaction, absorbance was measured at a wavelength of 450 nm with correction at 650 nm using a spectrophotometer plate reader. Absorbance values were converted into % mortality by comparing the values to that of the positive control (cells exposed to triton x100 for 24h).

Measurement of 5-Bromo-2'-deoxy-uridine (BrdU) incorporation for the quantification of cell proliferation

The cell proliferation ELISA BrdU kit was from Roche. This assay is a colometric test that measures the incorporation of BrdU, an analogue of thymidine, during DNA synthesis. The cells were incubated for 2h with 100 µM of BrdU solution diluted in the culture medium. Then, they were rinsed with phosphate buffer saline (PBS) and were fixed with a solution (Fixdenat) for 30 min before adding the solution of anti-BrdU antibody conjugated with peroxydase. Following a 45 min incubation, the cells were washed 3 times with PBS and finally, the substrate of peroxydase was added for 20 min. Absorbance was then measured at 370 nm with correction at 492 nm using a spectrophotometer plate reader.

5 Conclusion and perspectives

In this thesis we have focused on the exploration of the interaction between QDs and Lanthanide (Ln) complexes for creating novel probes for biological detection and imaging. One of the biggest challenges to be faced was to render the QDs water-soluble, and biocompatible, while conserving their optical proprieties and functionality. Our main goal was the development of stable and strongly luminescent QD-antibody conjugates for application in Förster resonance energy transfer (FRET) immunoassays aiming at the detection of prostate specific antigen (PSA) in a small volume of serum. Within the huge variety of QD-FRET biosensing application for the analysis of biomolecular interactions, homogeneous sandwich immunoassay, which quantify biomarker via two different antibodies that engage in FRET upon biomarker recognition, range among the most sensitive but also the most challenging systems. Indeed, in this type of immunoassay the relative large dimensions of the biological recognition system that contains antibodies, biomarker, and QD decrease the FRET efficiency. The development of QD-AB conjugates with compact surface functionalization for aqueous phase transfer represents therefore an important progress for the integration of QDs into clinical *in vitro* diagnostics. Using QDs as acceptors and terbium (Tb) complexes as donors, whose long excited-state lifetimes (milliseconds) enable time-gated detection and a concomitant suppression of directly excited QD PL and autofluorescence background, allows for the fast and sensitive detection of biomarkers.

We have designed a novel QD functionalization and bioconjugation approach based on a two-step procedure yielding a compact QD-AB conjugate. In the first step aqueous phase transfer of lab-synthesized InP-based InPZnS/ZnSe/ZnS QDs emitting at 530 nm and of commercial hydrophobic CdSe-based QDs emitting at 605 nm and 705 nm was achieved by surface ligand exchange with penicillamine (**Pen**). In the second step we further functionalized the QD surface with a bifunctional ligand (**Mal1**) containing a lipoic acid anchoring function spaced by three poly(ethylene) glycol (PEG) moieties from a maleimide group, which enables the subsequent coupling to sulfhydryl group of proteins. The obtained Pen- and Mal1-functionalized QDs showed no sign of aggregation after storage of more than two years in aqueous buffer at pH 7.4. This is an outstandingly long shelf-life for QDs with such a compact surface ligand shell and hydrodynamic diameters of 7-9 nm depending on the type of QD used. Furthermore, the QDs conserved between 60 and 80% of their initial fluorescence efficiency. We next demonstrated that the maleimide function maintained its reactivity by the successful conjugation with fragmented antibodies (F(ab)). Although we demonstrated here this bioconjugation strategy only with InPZnS/ZnSe/ZnS (**QD530**), CdSe-based QDs (**QD605** and **QD705**), and F(ab) antibodies, it is applicable to any kind of nanoparticles containing surface atoms with binding affinity for thiolate ligands and biomolecules containing sulfhydryl groups. Our approach yielded the smallest fluorescent QD-AB conjugates reported to date with a hydrodynamic diameter < 13 nm for **QD705**.

The advantages of the obtained compact QD-AB conjugates became visible in Tb-to-QD FRET immunoassays for the detection of PSA on a commercial available clinical fluorescence plate reader (KRYPTOR). The direct applicability of the probes was confirmed by the detection of PSA in 50 µL serum samples with subnanomolar detection limits (LODs). While the spectral overlap integral (QD absorption with Tb emission) of the probe emitting at 530 nm with the Tb donor was too low for practical use, the LOD determined for the probe emitting at 705 nm is significantly lower (0.8 ng/mL) than the clinical cut-off level (4 ng/mL).[175] The LOD of the probe emitting at 605 nm was 3.7 ng/mL. The utilization of our compact QD-AB conjugates also provided a 6.2 and 2.5 fold sensitivity improvement compared to the best study reported for the detection of PSA using the same commercially available QDs but containing already an organic coating for rendering them hydrosoluble. The latter differ from our QDs thus only by their (thicker) surface coating, increasing the D-A distance in FRET assays. It should be noted that the best immunoassay systems combined maximum sensitivity (minimum LOD), minimum antibody modification (no IgG reduction for the Tb conjugates), and maximum separation efficiency.[11] All these parameter were demonstrated in our system. Moreover this assay is performed in serum samples, which means under the same conditions as commercial clinical Tb-based FRET assays. Ongoing works concern the shift of the absorption and emission spectra of the InP-based QDs to the NIR, in order to achieve highly sensitive FRET immunoassays without relying on Cd-based NCs. Alternatively, our team also develops $MInE_2$-based NCs (M: Cu, Ag; E: S, Se), for which efficient NIR absorption and emission can easily be obtained, albeit with a comparably broad PL line width (generally at least 100 nm FWHM).

In this work we also explored the grafting of lanthanide complexes on the surface of QDs with the goal to introduce additional imaging modalities for Magnetic Resonance Imaging (MRI) and fluorescence imaging. In this case, only the InP-based QD (**QD530**) have been used for these studies as they have a high potential as less toxic nanocrystals in biological applications. First of all, the incorporation of a MRI contrast agent (Gd picolinate complex) using different types of organic spacers has been achieved demonstrating that a more rigid linker resulted in a significant increase of the relaxivity, up to 35 $mM^{-1}s^{-1}$ per grafted Gd complex at 20 MHz (*i.e.* 1100 $mM^{-1}s^{-1}$ per QD containing around 30 grafted complexes). This system thus combines the specific advantages of MRI and fluorescence imaging capabilities making it appealing for *in vivo* diagnostics. Additionally, we performed the synthesis of stable hybrid nanoparticles combining **QD530** and grafted luminescent lanthanide complexes (Tb, Eu, Yb). The resulting hybrids exhibit characteristic Ln (Eu and Yb) centered luminescence upon QD excitation at 370 nm, *i.e.* at a wavelength where the organic cage containing the lanthanide does not absorb, suggesting that an energy transfer occurs from the QD to the lanthanide. The obtained QD-Ln conjugates exhibit either dual (QD and Ln) emission or energy transfer depending on the excitation wavelength, showing the potential of using QDs to sensitize both the visible and NIR emission of Ln ions incorporated into QD-grafted complexes.[147] Further experiments are needed to

elucidate the detailed mechanisms behind the energy transfer in these systems and to optimize the transfer through the improved matching of the Ln and QD energy levels. This latter point needs to be addressed in particular for Tb complexes, for which not energy transfer could be achieved.

The last part of this study focused on the assessment of toxicity induced by the used QDs. In the quest for identifying QDs less toxic to human health and the environment, we investigated the impact of InP-based QDs – with and without protective Zn(Se,S) shell – and compared them with commercial Cd-based core/shell QDs using an identical surface functionalization with Pen for aqueous phase transfer. Therefore all types of QDs studied only differ in their inorganic part, making it possible to draw conclusions on the toxic effects of InP or CdSe without being biased by differences in the surface chemistry. Our studies were carried out in two systems: *in vitro* on cells extracted from human skin (primary keratinocytes) and *in vivo* using the freshwater polyp *Hydra vulgaris* as model organism. The decision to combine and investigate *in vivo* systems was also motivated by the fact that, although cultured cells represent valid models to describe basic interactions with nanomaterials, they do not fulfill the *in vivo* response complexity. The results obtained so far *in vitro* are still very preliminary and exhibit relatively large assay-to-assay variations. However, by using as toxicity model *Hydra vulgaris*, we unambiguously determined several toxicity endpoints. This polyp offers several advantages: it has a low cost of rearing and under controlled conditions reproduces itself asexually, has a simple anatomical structure, it is transparent and hence enables the localization of fluorescent QDs on the level of the whole animal as well as cell migration studies under physiological conditions. Moreover, despite the simplicity of its nervous system, organized as a mesh-like network of neurons extending throughout the animal, the complexity of the mechanisms underlying neurotransmission resembles those of higher vertebrates, making *Hydra* an ideal system to study the behavioral response of a whole animal to an external stimulus, *i.e.* bioactive nanomaterials. Using different approaches *in vivo* at the level of whole animal we assessed the short-term impact of the QDs, analyzing the possible induction of morphological changes, and the long-term impact on the reproductive and regenerative capacity of the animal. At the cellular level (*ex vivo*) we assessed the induction of apoptosis and at molecular level (*in vitro*) the induction of the expression of genes involved in cells' stress response. We concluded that the toxicity is not evident at the whole animal level, while clear effects are seen at the cellular level, by induction of the apoptosis process, which increases in the order InPZnS/ZnSe/ZnS core/shell < InPZns core < CdSe/ZnS core shell. This order confirms the protective character of the shell and also demonstrates the higher cytotoxicity of CdSe-based QDs with respect to InP-based QDs. However, when we used more sensitive methods (*i.e.* molecular analysis) we observed that the animal reacts by activating genes involved in the stress response with all types of QD used.

Although the results obtained with primary keratinocytes are still too weak for drawing conclusions of any certainty aiming at the correlation of the impact of the same type of QDs *in vivo* and *in vitro*, globally the

preliminary results demonstrated the same trend, namely the protective effect of the shell around the InPZnS core and the higher toxic effect of Cd-containing NCs. These results support the choice of InP as alternative QD material for safer and advanced biological applications although it is definitively wrong to entitle InP-based QDs as “non toxic”. Experiments are currently underway to backup the *in vitro* toxicity studies. The occurrence of subtle genetic variations in the absence of morphological damages indicates the importance of genotoxicity studies for nanoparticles risk assessment. For this reason, we envisage using integrated techniques available at ESRF (European Synchroton Radiation Facility). These new approaches allowing investigating the biodistribution, intracellular trafficking, the fate of the internalized QDs and the relation to their composition, which to date is not possible to resolve by using different methodologies. It remains of intriguing interest to draw a correlation between the behavior of the same QDs in the two systems (*Hydra* and keratinocytes).

6 References

[1] Brus, L. E. (1984) Electron Electron and Electron-Hole Interactions in Small Semiconductor Crystallites - the Size Dependence of the Lowest Excited Electronic State, *J. Chem. Phys. 80*, 4403-4409.

[2] Ekimov, A.-I., and Onushchenko, A.-A. (1981) Quantum size effect in three-dimensional microscopic semiconductor crystals, *Soviet Journal of Experimental and Theoretical Physics Letters 34*, 345-349.

[3] Efros, A. L. (1982) Interband Absorption of Light in a Semiconductor Sphere, *Soviet Physics Semiconductors USSR 16*, 772-775.

[4] Henglein, A. (1982) Photo-degradation and fluorescence of colloidal-cadmium sulfide in aqueous-solution, *Berichte Der Bunsen-Gesellschaft-Physical Chemistry Chemical Physics 86*, 301-305.

[5] Kovalenko, M. V., Manna, L., Cabot, A., Hens, Z., Talapin, D. V., Kagan, C. R., Klimov, V. I., Rogach, A. L., Reiss, P., Milliron, D. J., Guyot-Sionnnest, P., Konstantatos, G., Parak, W. J., Hyeon, T., Korgel, B. A., Murray, C. B., and Heiss, W. (2015) Prospects of Nanoscience with Nanocrystals, *ACS Nano 9*, 1012-1057.

[6] Gao, X., Yang, L., Petros, J. A., Marshall, F. F., Simons, J. W., and Nie, S. (2005) In vivo molecular and cellular imaging with quantum dots, *Curr. Opin. Biotechnol. 16*, 63-72.

[7] Bruchez, M., M. Moronne, P. Gin, S. Weiss, and A.P. Alivisatos. (1998) Semiconductor Nanocrystals as Fluorescent Biological Labels *Science 281*, 2013-2016.

[8] Chan, W. C. W., and S. Nie. (1998) Quantum Dot Bioconjugates for Ultrasensitive Nonisotopic Detection. , *Science 281*, 2016-2018.

[9] Kattke, M. D., Gao, E. J., Sapsford, K. E., Stephenson, L. D., and Kumar, A. (2011) FRET-Based Quantum Dot Immunoassay for Rapid and Sensitive Detection of Aspergillus amstelodami, *Sensors 11*, 6396.

[10] Zrazhevskiy, P., Sena, M., and Gao, X. (2010) Designing multifunctional quantum dots for bioimaging, detection, and drug delivery, *Chem. Soc. Rev. 39*, 4326-4354.

[11] K. David Wegner, Zongwen Jin, Stina Linden, Travis L. Jennings, and Hildebrandt, N. (2013) Quantum-Dot-Based Förster Resonance Energy Transfer Immunoassay for Sensitive Clinical Diagnostics of Low-Volume Serum Samples, *ACSNANO 7*, 7411-7419.

[12] Algar, W. R., Massey, M., and Krull, U. J. (2013) Semiconductor quantum dots and FRET, *FRET-Förster Resonance Energy Transfer: From Theory to Applications*, 475-605.

[13] Reiss, P., Protiere, M., and Li, L. (2009) Core/Shell Semiconductor Nanocrystals, *Small 5*, 154-168.

[14] Algar, W. R., Massey, M., and Krull, U. J. (2013) Semiconductor Quantum Dots and FRET, In *FRET – Förster Resonance Energy Transfer*, pp 475-605, Wiley-VCH Verlag GmbH & Co. KGaA.

[15] Kim, S., Fisher, B., Eisler, H. J., and Bawendi, M. (2003) Type-II quantum dots: CdTe/CdSe(core/shell) and CdSe/ZinTe(core/shell) heterostructures, *J. Am. Chem. Soc. 125*, 11466-11467.

[16] Tamang, S., Lincheneau, C., Hermans, Y., Jeong, S., and Reiss, P. (2016) Chemistry of InP Nanocrystal Syntheses, *Chem. Mater.*, DOI: 10.1021/acs.chemmater.1025b05044.

[17] Green, M. (2002) Solution routes to III–V semiconductor quantum dots, *Current Opinion in Solid State and Materials Science 6*, 355-363.

[18] Brunetti, V., Chibli, H., Fiammengo, R., Galeone, A., Malvindi, M. A., Vecchio, G., Cingolani, R., Nadeau, J. L., and Pompa, P. P. (2013) InP/ZnS as a safer alternative to CdSe/ZnS core/shell quantum dots: in vitro and in vivo toxicity assessment, *Nanoscale 5*, 307-317.

[19] Chibli, H., Carlini, L., Park, S., Dimitrijevic, N. M., and Nadeau, J. L. (2011) Cytotoxicity of InP/ZnS quantum dots related to reactive oxygen species generation, *Nanoscale 3*, 2552-2559.

[20] Reiss, P., and Philippot, C. (2012) Synthesis of Inorganic Nanocrystals for Biological Fluorescence Imaging, In *Frontiers of Nanoscience* (De la Fuente, J., and Grazu, V., Eds.), pp 81-114, Elsevier, Amsterdam, The Netherlands.

[21] Xu, S., Ziegler, J., and Nann, T. (2008) Rapid synthesis of highly luminescent InP and InP/ZnS nanocrystals, *J. Mater. Chem. 18*, 2653-2656.

[22] Yang, X., Zhao, D., Leck, K. S., Tan, S. T., Tang, Y. X., Zhao, J., Demir, H. V., and Sun, X. W. (2012) Full Visible Range Covering InP/ZnS Nanocrystals with High Photometric Performance and Their Application to White Quantum Dot Light‐Emitting Diodes, *Advanced Materials 24*, 4180-4185.
[23] Li, L., and Reiss, P. (2008) One-pot Synthesis of Highly Luminescent InPZnS Nanocrystals without Precursor Injection., *J. Am. Chem 130*, 11588-11589.
[24] Huang, K., Demadrille, R., Silly, M. G., Sirotti, F., Reiss, P., and Renault, O. (2010) Internal Structure of InP/ZnS Nanocrystals Unraveled by High-Resolution Soft X-ray Photoelectron Spectroscopy, *ACS Nano 4*, 4799-4805.
[25] Ung, T. D. T., Reiss, P., and Nguyen, Q. L. (2010) Luminescence properties of In(Zn)P alloy core/ZnS shell quantum dots, *Appl. Phys. Lett. 97*, 193104.
[26] Kim, S., Kim, T., Kang, M., Kwak, S. K., Yoo, T. W., Park, L. S., Yang, I., Hwang, S., Lee, J. E., Kim, S. K., and Kim, S.-W. (2012) Highly Luminescent InP/GaP/ZnS Nanocrystals and Their Application to White Light-Emitting Diodes, *J. Am. Chem. Soc. 134*, 3804-3809.
[27] Sperling, R. A., and Parak, W. (2010) Surface modification, functionalization and bioconjugation of colloidal inorganic nanoparticles, *Philosophical Transactions of the Royal Society of London A: Mathematical, Physical and Engineering Sciences 368*, 1333-1383.
[28] Wegner, K. D., and Hildebrandt, N. (2015) Quantum dots: bright and versatile in vitro and in vivo fluorescence imaging biosensors, *Chem. Soc. Rev. 44*, 4792-4834.
[29] Susumu, K., H.T. Uyeda, I.L. Medintz, T. Pons, J.B. Delehanty, and Mattoussi, H. (2007) Enhancing the Stability and Biological Functionalities of Quantum Dots via Compact Multifunctional Ligands, *J. Am. Chem. Soc. 129*, 13987-13996.
[30] Alivisatos, A. P., Peng, X., and Manna, L. (2001) Process for forming shaped group III-V semiconductor nanocrystals, and product formed using process, Google Patents.
[31] Algar, W. R., and Krull, U. J. (2009) Quantum Dots for the Development of Optical Biosensors Based on Fluorescence, In *Biosensing Using Nanomaterials*, pp 199-245, John Wiley & Sons, Inc.
[32] Alivisatos, A. P. (1996) Semiconductor Clusters, Nanocrystals, and Quantum Dots, *Science 271*, 933-937.
[33] Michalet, X., Pinaud, F. F., Bentolila, L. A., Tsay, J. M., Doose, S., Li, J. J., Sundaresan, G., Wu, A. M., Gambhir, S. S., and Weiss, S. (2005) Quantum Dots for Live Cells, in Vivo Imaging, and Diagnostics, *Science 307*, 538-544.
[34] Hildebrandt, N. (2011) Biofunctional Quantum Dots: Controlled Conjugation for Multiplexed Biosensors, *ACSNANO 5*, 5286–5290.
[35] Cardoso Dos Santos, M., and Hildebrandt, N. Recent developments in lanthanide-to-quantum dot FRET using time-gated fluorescence detection and photon upconversion, *TrAC, Trends Anal. Chem.*
[36] Hermanson, G. (1996) Bioconjugate Techniques, *Academic Press*
[37] Wegner, K. D., Lanh, P. T., Jennings, T., Oh, E., Jain, V., Fairclough, S. M., Smith, J. M., Giovanelli, E., Lequeux, N., Pons, T., and Hildebrandt, N. (2013) Influence of luminescence quantum yield, surface coating, and functionalization of quantum dots on the sensitivity of time-resolved FRET bioassays, *ACS Appl. Mater. Interf. 5*, 2881.
[38] Jennings, T. L., Becker-Catania, S. G., Triulzi, R. C., Tao, G., Scott, B., Sapsford, K. E., Spindel, S., Oh, E., Jain, V., Delehanty, J. B., Prasuhn, D. E., Boeneman, K., Algar, W. R., and Medintz, I. L. (2011) Reactive semiconductor nanocrystals for chemoselective biolabeling and multiplexed analysis, *ACSNano 5*, 5579.
[39] Min, H., Jo, S. M., and Kim, H. S. (2015) Efficient Capture and Simple Quantification of Circulating Tumor Cells Using Quantum Dots and Magnetic Beads, *small 11*, 2536-2542.
[40] Torchynska, T. V., Vorobiev, Y. V., Makhniy, V. P., and Horley, P. P. (2014) The influence of bio-conjugation on photoluminescence of CdSe/ZnS quantum dots, *Physica B: Condensed Matter 453*, 68-71.
[41] He, X., Gao, L., and Ma, N. (2013) One-step instant synthesis of protein-conjugated quantum dots at room temperature, *Scientific reports 3*.

[42] Montenegro, J.-M., Grazu, V., Sukhanova, A., Agarwal, S., Jesus, M., Nabiev, I., Greiner, A., and Parak, W. J. (2013) Controlled antibody/(bio-) conjugation of inorganic nanoparticles for targeted delivery, *Advanced drug delivery reviews 65*, 677-688.
[43] Pavlickova, P., Schneider, E. M., and Hug, H. (2004) Advances in recombinant antibody microarrays, *Clin. Chim. Acta 343*, 17-35.
[44] Torcello-Gómez, A., Santander-Ortega, M. J., Peula-García, J. M., Maldonado-Valderrama, J., Gálvez-Ruiz, M. J., Ortega-Vinuesa, J. L., and Martín-Rodríguez, A. (2011) Adsorption of antibody onto Pluronic F68-covered nanoparticles: link with surface properties, *Soft Matter 7*, 8450-8461.
[45] Alberts, B. (2008) *Molecular biology of the cell*, Vol. 5th, Garland Science, New York.
[46] Hildebrandt, N., Charbonnière, L. J., Beck, M., Ziessel, R. F., and Löhmannsröben, H. G. (2005) Quantum Dots as Efficient Energy Acceptors in a Time‐Resolved Fluoroimmunoassay, *Angew. Chem. Int. Ed. 44*, 7612-7615.
[47] Geißler, D., Stufler, S., Löhmannsröben, H.-G., and Hildebrandt, N. (2013) Six-color time-resolved Förster resonance energy transfer for ultrasensitive multiplexed biosensing, *J. Am. Chem. Soc. 135*, 1102.
[48] Geissler, D., Charbonnière, L. J., Ziessel, R. F., Butlin, N. G., Löhmannsröben, H.-G., and Hildebrandt, N. (2010) Quantum dot biosensors for ultrasensitive multiplexed diagnostics, *Angew. Chem. 49*, 1396.
[49] Bhuckory, S., Lefebvre, O., Qiu, X., Wegner, K. D., and Hildebrandt, N. (2016) Evaluating Quantum Dot Performance in Homogeneous FRET Immunoassays for Prostate Specific Antigen, *Sensors (Basel, Switzerland) 16*, 197.
[50] Medintz, I., and Hildebrandt, N. (2013) *FRET - Förster Resonance Energy Transfer : From Theory to Applications*, Vol. 1, Wiley-VCH, Hoboken.
[51] Jin, Z., and Hildebrandt, N. (2012) Semiconductor quantum dots for in vitro diagnostics and cellular imaging, *Trends Biotechnol 30*, 394-403.
[52] Sortino, S. (2015) Light-Responsive Nanostructured Systems for Applications in Nanomedicine, Springer.
[53] Myers, M. G., Sun, X. J., and White, M. F. (1994) The IRS-1 signaling system, *Trends Biochem. Sci 19*, 289-293.
[54] Wolf, A., Wender, R. C., Etzioni, R. B., Thompson, I. M., D'Amico, A. V., Volk, R. J., Brooks, D. D., Dash, C., Guessous, I., and Andrews, K. (2010) American Cancer Society guideline for the early detection of prostate cancer: update 2010, *CA: a cancer journal for clinicians 60*, 70-98.
[55] Carroll, P. R. (2005) Operating characteristics of prostate-specific antigen in men with an initial PSA level of 3.0 ng/ml or lower: Thompson IM, Ankerst DP, Chi C, Lucia MS, Goodman PJ, Crowley JJ, Parnes HL, Coltman CA Jr., Department of Urology, University of Texas Health Science Center at San Antonio, TX, *Urologic Oncology: Seminars and Original Investigations 23*, 459.
[56] Adhyam, M., and Gupta, A. K. (2012) A Review on the Clinical Utility of PSA in Cancer Prostate, *Indian journal of surgical oncology 3*, 120-129.
[57] Thévenod, F. (2009) Cadmium and cellular signaling cascades: To be or not to be?, *Toxicol. Appl. Pharmacol. 238*, 221-239.
[58] Jaiswal, J. K., Mattoussi, H., Mauro, J. M., and Simon, S. M. (2003) Long-term multiple color imaging of live cells using quantum dot bioconjugates, *Nature biotechnology 21*, 47-51.
[59] Derfus, A. M., Chan, W. C. W., and Bhatia, S. N. (2004) Probing the Cytotoxicity of Semiconductor Quantum Dots, *Nano Letters 4*, 11-18.
[60] Lovrić, J., Bazzi, H. S., Cuie, Y., Fortin, G. R., Winnik, F. M., and Maysinger, D. (2005) Differences in subcellular distribution and toxicity of green and red emitting CdTe quantum dots, *Journal of Molecular Medicine 83*, 377-385.
[61] Haram, S. K., Quinn, B. M., and Bard, A. J. (2001) Electrochemistry of CdS Nanoparticles: A Correlation between Optical and Electrochemical Band Gaps, *Journal of the American Chemical Society 123*, 8860-8861.

[62] Lovrić, J., Cho, S. J., Winnik, F. M., and Maysinger, D. (2005) Unmodified Cadmium Telluride Quantum Dots Induce Reactive Oxygen Species Formation Leading to Multiple Organelle Damage and Cell Death, *Chemistry & Biology 12*, 1227-1234.

[63] Brunetti, V., Chibli, H., Fiammengo, R., Galeone, A., Malvindi, M. A., Vecchio, G., Cingolani, R., Nadeau, J. L., and Pompa, P. P. (2013) InP/ZnS as a safer alternative to CdSe/ZnS core/shell quantum dots: in vitro and in vivo toxicity assessment, *Nanoscale 5*, 307-317.

[64] Lin, G., Ding, Z., Hu, R., Wang, X., Chen, Q., Zhu, X., Liu, K., Liang, J., Lu, F., and Lei, D. (2014) Cytotoxicity and immune response of CdSe/ZnS Quantum dots towards a murine macrophage cell line, *RSC Advances 4*, 5792-5797.

[65] Nel, A., Xia, T., Mädler, L., and Li, N. (2006) Toxic Potential of Materials at the Nanolevel, *Science 311*, 622-627.

[66] Kahru, A., and Ivask, A. (2013) Mapping the dawn of nanoecotoxicological research, *Acc. Chem. Res. 46*, 823-833.

[67] Kahru, A., and Dubourguier, H.-C. (2010) From ecotoxicology to nanoecotoxicology, *Toxicology 269*, 105-119.

[68] Colvin, V. L. (2003) The potential environmental impact of engineered nanomaterials, *Nat Biotech 21*, 1166-1170.

[69] Fischer, H. C., and Chan, W. C. (2007) Nanotoxicity: the growing need for in vivo study, *Curr. Opin. Biotechnol. 18*, 565-571.

[70] Dubertret, B., P. Skourides, D.J. Norris, V. Noireaux, Brivanlou, A. H., and Libchaber, A. (2002) In Vivo Imaging of Quantum Dots Encapsulated in Phospholipid Micelles, *Science 298*, 1759-1762.

[71] Pellegrino, T., L. Manna, S. Kudera, T. Liedl, D. Koktysh, A.L. Rogach, S.Keller, J. Radler, Natile, G., and Parak, W. J. (2004) Hydrophobic Nanocrystals Coated with an Amphiphilic Polymer Shell: A General Route to Water Soluble Nanocrystals., *Nano Lett. 4*, 703-707.

[72] Pellegrino, T., Kudera, S., Liedl, T., Javier, A. M., Manna, L., and Parak, W. J. (2005) On the development of colloidal nanoparticles towards multifunctional structures and their possible use for biological applications, *Small 1*, 48-63.

[73] Schapotschnikow, P., Hommersom, B., and Vlugt, T. J. (2009) Adsorption and binding of ligands to CdSe nanocrystals, *J. Phys. Chem. C 113*, 12690-12698.

[74] Doty, R. C., T.R. Tshikhudo, M. Brust, and Fernig, D. G. (2005) Extremely Stable Water-Soluble Ag Nanoparticles, *Chem. Mater. 17*, 4630-4635.

[75] Tamang, S., Beaune, G., Texier, I., and Reiss, P. (2011) Aqueous Phase Transfer of InP/ZnS Nanocrystals Conserving Fluorescence and High Colloidal Stability, *ACSNANO 5*, 9392-9402.

[76] Algar, W. R., and Krull, U. J. (2007) Luminescence and Stability of Aqueous Thioalkyl Acid CappedCdSe/ZnS Quantum Dots Correlated to Ligand Ionization, *ChemPhysChem 8*, 561-568.

[77] Algar, W. R., and Krull, U. J. (2006) Adsorption and Hybridization of Oligonucleotides on Mercaptoacetic Acid-Capped CdSe/ZnS Quantum Dots and Quantum Dot-Oligonucleotide Conjugates., *Langmuir, 22*, 11346-11352.

[78] Uyeda, H. T., et al. (2005) Synthesis of Compact Multidentate Ligands to Prepare Stable Hydrophilic Quantum Dot Fluorophores. , *Journal of the Americal Chemical Society 127*, 3870-3878.

[79] Zhang, C., Gao, D., Zhou, G., Chen, L., Zhang, X.-a., Cui, Z., and He, Z. (2012) Label-free homogeneous immunosensor based on FRET for the detection of virus antibody in serum, *Chemistry, an Asian journal U6 - Journal Article 7*, 1764.

[80] Zhou, J., Yang, Y., and Zhang, C.-y. (2015) Toward Biocompatible Semiconductor Quantum Dots: From Biosynthesis and Bioconjugation to Biomedical Application, *Chem. Rev. 115*, 11669-11717.

[81] Wuister, S. F., de Mello Donega, C., and Meijerink, A. (2004) Influence of Thiol Capping on the Exciton Luminescence and Decay Kinetics of CdTe and CdSe Quantum Dots, *J. Phys. Chem. B 108*, 17393-17397.

[82] Breus, V. V., Heyes, C. D., Tron, K., and Nienhaus, G. U. (2009) Zwitterionic biocompatible quantum dots for wide pH stability and weak nonspecific binding to cells, *ACS nano 3*, 2573-2580.

[83] Moloney, M. P., Gun'ko, Y. K., and Kelly, J. M. (2007) Chiral highly luminescent CdS quantum dots, *Chemical Communications*, 3900-3902.
[84] Mohammad‐Rezaei, R., Razmi, H., and Abdolmohammad‐Zadeh, H. (2013) d‐penicillamine capped cadmium telluride quantum dots as a novel fluorometric sensor of copper (II), *Luminescence 28*, 503-509.
[85] Pong, B.-K., Trout, B. L., and Lee, J.-Y. (2008) Modified Ligand-Exchange for Efficient Solubilization of CdSe/ZnS Quantum Dots in Water: A Procedure Guided by Computational Studies, *Langmuir 24*, 5270-5276.
[86] Marrian, D. H. (1949) The Reactions of Substituted Maleimides with Thiols., *J. Chem. Soc.*, 1515.
[87] Yin, Y., and Alivisatos, A. P. (2005) Colloidal nanocrystal synthesis and the organic-inorganic interface, *Nature 437*, 664-670.
[88] Alivisatos, A. P. (1996) Semiconductor Clusters, Nanocrystals, and Quantum Dots, *Science 271*, 933-937.
[89] Li, L., and Reiss, P. (2008) One-pot synthesis of highly luminescent InP/ZnS nanocrystals without precursor injection, *J. Am. Chem. Soc. 130*, 11588-11589.
[90] (11th Edition 2010) Molecular Probes Handbook, A Guide to Fluorescent Probes and Labeling Technologies.
[91] R. Sjoback, J. Nygren, and Kubista, M. (1995) "Absorption and fluorescence properties of fluorescein," *Spectrochim. Acta Mol. Biomol. Spectros., 51*, L7-L21.
[92] Aihua Fu, Christine M. Micheel, Jennifer Cha, Hauyee Chang, Haw Yang, and Alivisatos, A. P. (2004) Discrete Nanostructures of Quantum Dots/Au with DNA, *J. Am. Chem. Soc. 126*, 10832-10833.
[93] Wolcott, A., Gerion, D., Visconte, M., Sun, J., Schwartzberg, A., Chen, S., and Zhang, J. Z. (2006) Silica-coated CdTe quantum dots functionalized with thiols for bioconjugation to IgG proteins, *J. Phys. Chem. B 110*, 5779-5789.
[94] Jennings, T. L., Triulzi, R. C., Tao, G., St Louis, Z. E., and Becker-Catania, S. G. (2011) Simplistic attachment and multispectral imaging with semiconductor nanocrystals, *Sensors (Basel) 11*, 10557-10570.
[95] Pinaud, F., Clarke, S., Sittner, A., and Dahan, M. (2010) Probing cellular events, one quantum dot at a time, *Nature methods 7*, 275-285.
[96] Aldana, J., Wang, Y. A., and Peng, X. (2001) Photochemical instability of CdSe nanocrystals coated by hydrophilic thiols, *J. Am. Chem. Soc. 123*, 8844-8850.
[97] Lim, J., Bae, W. K., Lee, D., Nam, M. K., Jung, J., Lee, C., Char, K., and Lee, S. (2011) InP@ZnSeS, Core@Composition Gradient Shell Quantum Dots with Enhanced Stability, *Chem. Mater. 23*, 4459-4463.
[98] Adam, S., Talapin, D. V., Borchert, H., Lobo, A., McGinley, C., de Castro, A. R. B., Haase, M., Weller, H., and Möller, T. (2005) The effect of nanocrystal surface structure on the luminescence properties: Photoemission study of HF-etched InP nanocrystals, *J. Chem. Phys. 123*, 084706.
[99] Talapin, D. V., Gaponik, N., Borchert, H., Rogach, A. L., Haase, M., and Weller, H. (2002) Etching of colloidal InP nanocrystals with fluorides: photochemical nature of the process resulting in high photoluminescence efficiency, *The Journal of Physical Chemistry B 106*, 12659-12663.
[100] Resch-Genger, U., Grabolle, M., Cavaliere-Jaricot, S., Nitschke, R., and Nann, T. (2008) Quantum dots versus organic dyes as fluorescent labels, *Nature methods 5*, 763-775.
[101] Bünzli, J.-C. G. (2010) Lanthanide Luminescence for Biomedical Analyses and Imaging, *Chem. Rev. 110*, 2729-2755.
[102] Bilan, R., Fleury, F., Nabiev, I., and Sukhanova, A. (2015) Quantum dot surface chemistry and functionalization for cell targeting and imaging, *Bioconjug Chem 26*, 609-624.
[103] Dahan, M., Laurence, T., Pinaud, F., Chemla, D., Alivisatos, A., Sauer, M., and Weiss, S. (2001) Time-gated biological imaging by use of colloidal quantum dots, *Opt. Lett. 26*, 825-827.
[104] Grecco, H. E., Lidke, K. A., Heintzmann, R., Lidke, D. S., Spagnuolo, C., Martinez, O. E., Jares-Erijman, E. A., and Jovin, T. M. (2004) Ensemble and single particle photophysical properties (two-photon

excitation, anisotropy, FRET, lifetime, spectral conversion) of commercial quantum dots in solution and in live cells, *Microsc. Res. Tech. 65*, 169-179.

[105] Yin, Y., and Alivisatos, A. P. (2005) Colloidal nanocrystal synthesis and the organic-inorganic interface, *Nature 437*, 664-670.

[106] Algar, W. R., Wegner, D., Huston, A. L., Blanco-Canosa, J. B., Stewart, M. H., Armstrong, A., Dawson, P. E., Hildebrandt, N., and Medintz, I. L. (2012) Quantum dots as simultaneous acceptors and donors in time-gated Forster resonance energy transfer relays: characterization and biosensing, *J Am Chem Soc 134*, 1876-1891.

[107] Geißler, D., Linden, S., Liermann, K., Wegner, K. D., Charbonnière, L. J., and Hildebrandt, N. (2014) Lanthanides and quantum dots as Förster resonance energy transfer agents for diagnostics and cellular imaging, *Inorg. Chem. 53*, 1824.

[108] Hildebrandt, N., Wegner, K. D., and Algar, W. R. (2014) Luminescent terbium complexes: Superior Förster resonance energy transfer donors for flexible and sensitive multiplexed biosensing, *Coord. Chem. Rev. 273-274*, 125-138.

[109] Zhang, H., Zeng, Q., Liu, X., Kong, X., Zhang, Y., and Tu, L. (2012) Multiple homogeneous immunoassays based on a quantum dots-gold nanorods FRET nanoplatform, *Chem. Commun. 48*, 1781-1783.

[110] Esteve-Turrillas, F. A., and Abad-Fuentes, A. (2013) Applications of quantum dots as probes in immunosensing of small-sized analytes, *Biosens. Bioelectron. 41*, 12-29.

[111] Ge, S., Ge, L., Yan, M., Song, X., Yu, J., and Liu, S. (2013) A disposable immunosensor device for point-of-care test of tumor marker based on copper-mediated amplification, *Biosens. Bioelectron. 43*, 425-431.

[112] Long, F., Gu, C., Gu, A. Z., and Shi, H. (2012) Quantum Dot/Carrier–Protein/Haptens Conjugate as a Detection Nanobioprobe for FRET-Based Immunoassay of Small Analytes with All-Fiber Microfluidic Biosensing Platform, *Anal. Chem. 84*, 3646-3653.

[113] Qian, J., Wang, C., Pan, X., and Liu, S. (2013) A high-throughput homogeneous immunoassay based on Förster resonance energy transfer between quantum dots and gold nanoparticles, *Anal. Chim. Acta 763*, 43-49.

[114] Wei, Q., Lee, M., Lee, E. K., Yu, X., Seong, G. H., Choo, J., and Cho, Y. W. (2006) Development of an open sandwich fluoroimmunoassay based on fluorescence resonance energy transfer, *Anal. Biochem. 358*, 31-37.

[115] Medintz, I. L., Pons, T., Susumu, K., Boeneman, K., Dennis, A., Farrell, D., Deschamps, J. R., Melinger, J. S., Bao, G., and Mattoussi, H. (2009) Resonance Energy Transfer Between Luminescent Quantum Dots and Diverse Fluorescent Protein Acceptors, *The journal of physical chemistry. C, Nanomaterials and interfaces 113*, 18552-18561.

[116] Chen, M.-J., Wu, Y.-S., Lin, G.-F., Hou, J.-Y., Li, M., and Liu, T.-C. (2012) Quantum-dot-based homogeneous time-resolved fluoroimmunoassay of alpha-fetoprotein, *Anal. Chim. Acta 741*, 100.

[117] Chen, Z.-H., Wu, Y.-S., Chen, M.-J., Hou, J.-Y., Ren, Z.-Q., Sun, D., and Liu, T.-C. (2013) A Novel Homogeneous Time-Resolved Fluoroimmunoassay for Carcinoembryonic Antigen Based on Water-Soluble Quantum Dots, *Journal of Fluorescence 23*, 649-657.

[118] Härmä, H., Soukka, T., Shavel, A., Gaponik, N., and Weller, H. (2007) Luminescent energy transfer between cadmium telluride nanoparticle and lanthanide(III) chelate in competitive bioaffinity assays of biotin and estradiol, *Anal. Chim. Acta 604*, 177-183.

[119] Wegner, K. D., Lindén, S., Jin, Z., Jennings, T. L., Khoulati, R. e., van Bergen en Henegouwen, P. M. P., and Hildebrandt, N. (2014) Nanobodies and Nanocrystals: Highly Sensitive Quantum Dot‐Based Homogeneous FRET Immunoassay for Serum‐Based EGFR Detection, *Small 10*, 734-740.

[120] Hildebrandt, N. (2011) Biofunctional quantum dots: controlled conjugation for multiplexed biosensors, *ACSNano 5*, 5286.

[121] Medintz, I. L., H.T. Uyeda, E.R. Goldman, and Mattoussi, H. (2005) Quantum dot bioconjugates for imaging, labelling and sensing, *Nature Material 4* 435-446.

[122] Eliseeva, S. V., and Bunzli, J.-C. G. (2010) Lanthanide luminescence for functional materials and bio-sciences, *Chem. Soc. Rev. 39*, 189-227.
[123] Mathis, G. (1993) Rare earth cryptates and homogeneous fluoroimmunoassays with human sera, *Clinical chemistry 39*, 1953-1959.
[124] Mathis, G. (1999) HTRF® technology, *Journal of biomolecular screening 4*, 309-314.
[125] Hemmilä, I. (1999) LANCEtrade mark: Homogeneous Assay Platform for HTS, *Journal of biomolecular screening 4*, 303.
[126] Charbonnière, L. J., and Hildebrandt, N. (2008) Lanthanide Complexes and Quantum Dots: A Bright Wedding for Resonance Energy Transfer, *Eur. J. Inorg. Chem. 2008*, 3241-3251.
[127] Hildebrandt, N., and Lohmannsroben, H.-G. (2007) Quantum Dot Nanocrystals and Supramolecular Lanthanide Complexes -Energy Transfer Systems for Sensitive In Vitro Diagnostics and High Throughput Screening in Chemical Biology, *Current Chemical Biology 1*, 167-186.
[128] Charbonnière, L. J., Hildebrandt, N., Ziessel, R. F., and Löhmannsröben, H.-G. (2006) Lanthanides to Quantum Dots Resonance Energy Transfer in Time-Resolved Fluoro-Immunoassays and Luminescence Microscopy, *J. Am. Chem. Soc. 128*, 12800-12809.
[129] Jin, Z., Geißler, D., Qiu, X., Wegner, K. D., and Hildebrandt, N. (2015) A Rapid, Amplification-Free, and Sensitive Diagnostic Assay for Single-Step Multiplexed Fluorescence Detection of MicroRNA, *Angew. Chem. Int. Ed. 54*, 10024-10029.
[130] Sukhanova, A., Even-Desrumeaux, K., Kisserli, A., Tabary, T., Reveil, B., Millot, J.-M., Chames, P., Baty, D., Artemyev, M., Oleinikov, V., Pluot, M., Cohen, J. H. M., and Nabiev, I. (2012) Oriented conjugates of single-domain antibodies and quantum dots: toward a new generation of ultrasmall diagnostic nanoprobes, *Nanomedicine : nanotechnology, biology, and medicine 8*, 516.
[131] Alberts, B., Johnson, A., Lewis, J., Morgan, D., Raff, M., Roberts, K., Walter, P., Wilson, J., and Hunt, T. (2015) *Molecular biology of the cell*, Vol. Sixthition., Garland Science, Taylor and Francis Group, New York, NY.
[132] Arruebo, M., Valladares, M., and González-Fernández, Á. (2009) Antibody-Conjugated Nanoparticles for Biomedical Applications, *J. Nanomater. 2009*, 1-24.
[133] Molloy, J. K., Lincheneau, C., Karimdjy, M. M., Agnese, F., Mattera, L., Gateau, C., Reiss, P., Imbert, D., and Mazzanti, M. (2016) Sensitisation of visible and NIR lanthanide emission by InPZnS quantum dots in bi-luminescent hybrids, *Chem. Commun.*
[134] Frullano, L., and Meade, T. J. (2007) Multimodal MRI contrast agents, *JBIC Journal of Biological Inorganic Chemistry 12*, 939-949.
[135] Aime, S., Fasano, M., and Terreno, E. (1998) Lanthanide (III) chelates for NMR biomedical applications, *Chem. Soc. Rev. 27*, 19-29.
[136] Yao, N., Cheung, C., Pang, S., Shek-Kwan Chang, R., Lau, K. K., Suckling, J., Yu, K., Ka-Fung Mak, H., Chua, S. E., Ho, S.-L., and McAlonan, G. M. (2016) Multimodal MRI of the hippocampus in Parkinson's disease with visual hallucinations, *Brain structure & function 221*, 287.
[137] Bünzli, J.-C. G. (2015) On the design of highly luminescent lanthanide complexes, *Coord. Chem. Rev. 293–294*, 19-47.
[138] Bünzli, J.-C. G. (2006) Benefiting from the Unique Properties of Lanthanide Ions, *Acc. Chem. Res. 39*, 53-61.
[139] Faulkner, S., Pope, S. J., and Burton‐Pye, B. P. (2005) Lanthanide complexes for luminescence imaging applications, *Applied Spectroscopy Reviews 40*, 1-31.
[140] Stasiuk, G. J., Tamang, S., Imbert, D., Poillot, C., Giardiello, M., Tisseyre, C., Barbier, E. L., Fries, P. H., de Waard, M., Reiss, P., and Mazzanti, M. (2011) Cell-Permeable Ln(III) Chelate-Functionalized InP Quantum Dots As Multimodal Imaging Agents, *ACS Nano 5*, 8193-8201.
[141] Caravan, P., Ellison, J. J., McMurry, T. J., and Lauffer, R. B. (1999) Gadolinium (III) chelates as MRI contrast agents: structure, dynamics, and applications, *Chem. Rev. 99*, 2293-2352.
[142] Kwon, B.-H., Jang, H. S., Yoo, H. S., Kim, S. W., Kang, D. S., Maeng, S., Jang, D. S., Kim, H., and Jeon, D. Y. (2011) White-light emitting surface-functionalized ZnSe quantum dots: europium complex-capped hybrid nanocrystal, *J. Mater. Chem. 21*, 12812-12818.

[143] Thuy, U. T. D., Maurice, A., Liem, N. Q., and Reiss, P. (2013) Europium doped In (Zn) P/ZnS colloidal quantum dots, *Dalton Transactions 42*, 12606-12610.
[144] Chengelis, D. A., Yingling, A. M., Badger, P. D., Shade, C. M., and Petoud, S. (2005) Incorporating Lanthanide Cations with Cadmium Selenide Nanocrystals: A Strategy to Sensitize and Protect Tb(III), *J. Am. Chem. Soc. 127*, 16752-16753.
[145] Shirazi, R., Kopylov, O., Kovács, A., and Kardynał, B. (2012) Temperature dependent recombination dynamics in InP/ZnS colloidal nanocrystals, *Appl. Phys. Lett. 101*, 091910.
[146] Wild, D. (2013) *The immunoassay handbook: theory and applications of ligand binding, ELISA and related techniques*, Vol. Fourthition.;4th;4;4thition;, Elsevier, Oxford.
[147] Molloy, J. K., Lincheneau, C., Karimdjy, M. M., Agnese, F., Mattera, L., Gateau, C., Reiss, P., Imbert, D., and Mazzanti, M. (2016) Sensitisation of visible and NIR lanthanide emission by InPZnS quantum dots in bi-luminescent hybrids, *Chemical Communications 52*, 4577-4580.
[148] Choi, A. O., Brown, S. E., Szyf, M., and Maysinger, D. (2008) Quantum dot-induced epigenetic and genotoxic changes in human breast cancer cells, *Journal of Molecular Medicine 86*, 291-302.
[149] Oberdörster, G. (2010) Safety assessment for nanotechnology and nanomedicine: concepts of nanotoxicology, *Journal of internal medicine 267*, 89.
[150] Fadeel, B., Feliu, N., Vogt, C., Abdelmonem, A. M., and Parak, W. J. (2013) Bridge over troubled waters: understanding the synthetic and biological identities of engineered nanomaterials, *Nanomedicine and nanobiotechnology 5*, 111.
[151] Ambrosone, A., Mattera, L., Marchesano, V., Quarta, A., Susha, A. S., Tino, A., Rogach, A. L., and Tortiglione, C. (2012) Mechanisms underlying toxicity induced by CdTe quantum dots determined in an invertebrate model organism, *Biomaterials 33*, 1991-2000.
[152] Tino, A., Ambrosone, A., Mattera, L., Marchesano, V., Susha, A., Rogach, A., and Tortiglione, C. (2011) A new in vivo model system to assess the toxicity of semiconductor nanocrystals, *International journal of biomaterials 2011*, 792854.
[153] Alarifi, S., Ali, D., Al-Doaiss, A. A., Ali, B. A., Ahmed, M., and Al-Khedhairy, A. A. (2013) Histologic and apoptotic changes induced by titanium dioxide nanoparticles in the livers of rats, *International journal of nanomedicine 8*, 3937-3943.
[154] Tino, A., Ambrosone, A., Marchesano, V., and Tortiglione, C. (2014) *Molecular bases of nanotoxicology*, Wiley-VCH, Weinheim, Germany.
[155] Tang, L., Zhang, C., Song, G., Jin, X., and Xu, Z. (2013) In vivo skin penetration and metabolic path of quantum dots, *Science China Life Sciences 56*, 181-188.
[156] Wang, L., Qin, G., Geng, S., Dai, Y., and Wang, J.-Y. (2013) Preparation of zein conjugated quantum dots and their in vivo transdermal delivery capacity through nude mouse skin, *Journal of biomedical nanotechnology 9*, 367-376.
[157] Fischer, H. C., and Chan, W. C. W. (2007) Nanotoxicity: the growing need for in vivo study, *Curr. Opin. Biotechnol. 18*, 565-571.
[158] Tortiglione, C. (2011) *An ancient model organism to test in vivo novel functional nanocrystals*, INTECH Open Access Publisher.
[159] Lenhoff, H. M., Muscatine, L., and Davis, L. V. (1968) Coelenterate Biology: Experimental Research, *Science 160*, 1141-1146.
[160] Galliot, B., Miljkovic-Licina, M., de Rosa, R., and Chera, S. (2006) Hydra, a niche for cell and developmental plasticity, *Seminars in Cell & Developmental Biology 17*, 492-502.
[161] Loomis, W. F., and Lenhoff, H. M. (1956) Growth and sexual differentiation of hydra in mass culture, *Journal of Experimental Zoology 132*, 555-573.
[162] Bosch, T. C. G., and David, C. N. (1984) Growth regulation in Hydra: Relationship between epithelial cell cycle length and growth rate, *Developmental Biology 104*, 161-171.
[163] Bode, H. R. (2003) Head regeneration in Hydra, *Developmental Dynamics 226*, 225-236.
[164] Holstein, T. W., Hobmayer, E., and Technau, U. (2003) Cnidarians: An evolutionarily conserved model system for regeneration?, *Developmental Dynamics 226*, 257-267.

[165] Bosch, T. C. G. (2007) Why polyps regenerate and we don't: Towards a cellular and molecular framework for Hydra regeneration, *Developmental Biology 303*, 421-433.
[166] Karntanut, W., and Pascoe, D. (2000) A comparison of methods for measuring acute toxicity to Hydra vulgaris, *Chemosphere 41*, 1543-1548.
[167] Wilby, O. K., Tesh, J. M., and Shore, P. R. (1990) Application of the Hydra regeneration assay: Assessment of the potential teratogenic activity of engine exhaust emissions, *Toxicology in Vitro 4*, 612-613.
[168] Wilby, O. (1988) The Hydra regeneration assay, In *Proceedings of workshop organised by Association Francaise de Teratologie*, pp 108-124.
[169] Johnson, E. M., Gorman, R. M., Gabel, B. E., and George, M. E. (1982) The Hydra attenuata system for detection of teratogenic hazards, *Teratogenesis, carcinogenesis, and mutagenesis 2*, 263.
[170] Gavrieli, Y., Sherman, Y., and Ben-Sasson, S. A. (1992) Identification of Programmed Cell Death in situ via Specific Labeling of Nuclear DNA Fragmentation, *The Journal of Cell Biology 119*, 493-501.
[171] Holstein, T. W., Mala, C., Kurz, E., Bauer, K., Greber, M., and David, C. N. (1992) The primitive metazoan Hydra expresses antistasin, a serine protease inhibitor of vertebrate blood coagulation: cDNA cloning, cellular localisation and developmental regulation, *FEBS Lett. 309*, 288-292.
[172] Lionetto, M. G., Caricato, R., Giordano, M. E., Erroi, E., and Schettino, T. (2012) Carbonic anhydrase as pollution biomarker: an ancient enzyme with a new use, *International journal of environmental research and public health 9*, 3965-3977.
[173] Chan, W. C. W. (2013) Complexities abound, *Nat Nano 8*, 72-73.
[174] Mouret, S., Baudouin, C., Charveron, M., Favier, A., Cadet, J., and Douki, T. (2006) Cyclobutane pyrimidine dimers are predominant DNA lesions in whole human skin exposed to UVA radiation, *Proceedings of the National Academy of Sciences 103*, 13765-13770.
[175] Mattera, L., Bhuckory, S., Wegner, D., Agnese, F., lincheneau, C., Senden, T., Djurado, D., Charbonniere, L. J., Hildebrandt, N., and Reiss, P. (2016) Compact quantum dot-antibody conjugates for FRET immunoassays with subnanomolar detection limits, *Nanoscale*, DOI: 10.1039/C1036NR03261C.

Abbreviations

AB: antibody
AG: antigen
BrdU=5-Bromo-2'-deoxy-uridine
Cys: cysteine
DAPI: 4'-6-Diamidino-2-phenylindole
Dh: hydrodynamic diameter
DHLA: dihydrolipoic acid
DLS: dynamic light scattering
DNA: deoxyribonucleic acid
Eu: Europium
Fab: fragments antibody
FRET= Förster resonance energy transfer
FTIR: Fourier transform infrared spectroscopy
Gd: gadolinium
HEPES: acido 4-2-idrossietil-1-piperazinil-etansolfonico
IgG: immunoglobulin
InP: Indium phosphide
IVD: in vitro diagnostic
LEDs: *Light Emitting Diode*
LLCs= luminescent lanthanide complexes
Ln: Lanthanide
LODs = limits of detection
MAA: mercaptoacetic acid
MRI= Magnetic Resonance Imaging
MSA: mercaptosuccinic acid
NC: nanocrystal
NIR: near infrared
NIR= near infra read
NMR: nuclear magnetic resonance
NMRD: nuclear magnetic resonance dispersion
NPs: nanoparticles
ODE: 1-octadecene
OI= Optical Imaging
P(TMS)3: tris(trimethylsilyl)phosphine
PBS : phosphate buffer saline
PEG : polyethylene glycol
PEG: polyethylene glycol
Pen: penicillamine
pH : potentia hydrogenii
PL : photoluminescence
PSA= prostate specific antigen
QDs: quantum dots
QY: quantum yield
RNA: Ribonucleic acid
rpm: rotaion per minute
SATA: N-succinimidyl-s-acetylthioacetate
SMCC: 4-(N-maleimidomethyl) cyclohexane-1-carboxylate
SNR=signal-to-noise ratio

Tb: Terbium
TCEP: tris(2-carboxyethyl) phosphine hydrochloride
TEM: transmission electron microscopy
TG=time-gated
TGA: thermogravimetric analysis
TGA: thioglycolic acid
TMAH: tetramethylammonium hydroxide
TOP: trioctylphosphine
TPSA: Total prostate specific antigen
TRPL = time resolved photoluminescence
UV-Vis : ultraviolet-visible
Yb: ytterbium

Publications and Communications

Publications:

1. Lucia Mattera, Shashi Bhuckory, K. David Wegner, Xue Qiu, Fabio Agnese, Christophe Lincheneau, Tim Senden, David Djurado, Loïc J. Charbonnière, Niko Hildebrandt, Peter Reiss. *Compact quantum dot-antibody conjugates for FRET immunoassays with subnanomolar detection limits.* ***Nanoscale****, 2016, DOI:* 10.1039/C6NR03261C (ASAP)

2. Jennifer K. Molloy, Christophe Lincheneau, Maria Moula Karimdjy, Fabio Agnese, Lucia Mattera, Christelle Gateau, Peter Reiss, Daniel Imbert and Marinella Mazzanti "*Sensitisation of visible and NIR lanthanide emission by InPZnS quantum dots in bi-luminescent hybrids*" ***Chem. Commun.***, 2016, **52**, 4577-4580

Patent:

Niko Hildebrandt, Loïc J. Charbonnière, Peter Reiss, Shashi Bhuckory, K. David Wegner, Lucia Mattera
Liaison directe d'un anticorps à une nanoparticule. Demande de brevet français 2016

Oral Communications:

Functionalization of quantum dots for use in FRET Immunoassays
Lucia Mattera, Shashi Bhuckory, Tim Senden, David Wegner, Niko Hildebrandt, Peter Reiss
PhD students' annual meeting. May 2015, Grenoble

Quantum dot – antibody conjugates for FRET immunoassays
Lucia Mattera, Shashi Bhuckory, Tim Senden, David Wegner, Niko Hildebrandt, Peter Reiss
E-MRS Spring Meeting. May 2015, Lille

Quantum dot – antibody conjugates for highly sensitive FRET immunoassays
Lucia Mattera, Shashi Bhuckory, Lincheneau Christophe, Tim Senden, David Wegner, Niko Hildebrandt, Peter Reiss
NaNaX7 – Nanoscience with Nanocrystals, April 2016 Marburg (Germany)

Poster Communications:

Functionalization of quantum dots for bioconjugation to antibodies
Lucia Mattera, Peter Reiss.
Ecole thématique « Nanoparticules fonctionnelles, synthèse et applications biomédicales » du CNRS (29/09-04/10/2013 à Porquerolles)

Quantum Dot - Antibody Conjugates for FRET Immunoassays
Lucia Mattera, Tim Senden, David Wegner, Peter Reiss
30 years of quantum dots, May 2014 Paris

Quantum Dot - Antibody Conjugates for FRET Immunoassays
Lucia Mattera, Shashi Bhuckory, Christophe Lincheneau, Tim Senden, K. David Wegner, Niko Hildebrandt, Peter Reiss. European Nanomedicine Meeting (EMN). December 2015, Grenoble

Résumé français : La médecine moderne fait aujourd'hui face à de nombreux défis, comme le diagnostic précis et rapide des maladies. En raison de leurs propriétés photophysiques uniques, les quantum dots (QDs) sont des marqueurs fluorescents prometteurs pour la détection biologique. Le but principal de ce travail est le développement de conjuguées QD-anticorps (AB) en vue de leur utilisation dans des fluoroimmunoassays FRET (Förster Resonance Energy Transfer) pour la détection de la PSA (Antigène Spécifique de la Prostate), biomarqueur du cancer de la prostate. Dans ces systèmes, les QDs agissent comme accepteurs d'énergie en combinaison avec des complexes de terbium agissant comme donneurs. Grâce aux propriétés de luminescence spécifiques de ces deux classes de fluorophores, la mesure résolue en temps du signal de QDs permet la détection rapide et sensible des marqueurs biologiques. Nous avons développé une nouvelle approche en deux étapes pour la fonctionnalisation et la bioconjugaison de QDs qui donne des systèmes QD-AB fortement luminescents, stables et ultra compacts, maximisant ainsi l'efficacité de FRET. Dans une première étape, le transfert en phase aqueuse de QDs de phosphure d'indium (InP) synthétisés au laboratoire, émettant à 530 nm et de QDs commerciaux de CdSe émettant à 605 nm et 705 nm a été réalisé par échange de ligands de surface avec de la pénicillamine. Ensuite, la post-fonctionnalisation avec un ligand hétérobifonctionnel contenant un groupe acide lipoïque et une fonction maléimide permet le couplage ultérieur à des groupes sulfhydryle des protéines, a été effectuée. Après conjugaison des QDs avec des anticorps fragmentés (F(ab)) un très petit diamètre hydrodynamique (<13 nm) et une stabilité colloïdale à long terme (plusieurs années) ont été obtenus. L'applicabilité des sondes obtenues a été confirmée par la détection de PSA dans des échantillons de sérum, avec des limites de détection (LOD) très basses (0,8 ng/mL) pour les sondes émettant à 705 nm, dont l'absorption du spectre montre le plus grand recouvrement spectral avec l'émission du Tb. De plus, le greffage direct de complexes de terres rares sur la surface de QD a également été exploré, donnant accès à des sondes bimodales pour l'imagerie par resonance magnétique et par fluorescence (avec Gd) ou à des sondes biluminescentes (avec Eu, Yb). Dans ce dernier cas, la sensibilisation de la luminescence proche infrarouge de l'Yb par les QDs à base d'InP a été démontrée. Enfin nous avons réalisé des études de nanotoxicologie sur les différents types de QDs utilisés. En particulier, nous avons étudié la toxicité *in vivo* en utilisant l'organisme modèle *Hydra vulgaris* et la toxicité *in vitro* en utilisant des cellules de kératinocytes humains en comparant l'effet de systèmes cœur et cœur-coquille de QDs d'InP et de CdSe.

Résumé anglais : One of the many challenges modern medicine is facing today is the accurate and early diagnosis of diseases. Due to their unique photophysical properties semiconductor quantum dots (QDs) are promising fluorescent labels for biosensing. The major aim of this work is the development of QD-antibody (AB) conjugates to be used in Förster resonance energy transfer (FRET)-immunoassays for the detection of the tumor biomarker PSA (prostate specific antigen). In these assays, the QDs act as FRET acceptors in combination with terbium complex donors. Thanks to the specific luminescence properties of these two classes of fluorophores, time-gated detection of the QD signal allows for the fast and sensitive detection of biomarkers. We developed a novel two-step approach for QD functionalization and bioconjugation which yields ultra compact, stable and highly luminescent QD-AB conjugates maximizing FRET efficiency. In the first step aqueous phase transfer of lab-synthesized InP-based QDs emitting at 530 nm and of commercial CdSe-based QDs emitting at 605 nm and 705nm was achieved by surface ligand exchange with penicillamine. Then, post-functionalization with a heterobifunctional crosslinker, containing a lipoic acid group and a maleimide function, enabled the subsequent coupling to sulfhydryl groups of proteins. This was demonstrated by QD conjugation with fragmented antibodies (F(ab)); the obtained conjugates have a very low hydrodynamic diameter < 13 nm and long-term colloidal stability. The applicability of the obtained probes was confirmed by the detection of PSA in serum samples with detection limits (LODs) down to 0.8 ng/mL for the 705 nm emitting probes, whose absorption spectrum shows the largest overlap integral with the Tb emission. In addition, direct grafting of rare earth complexes on the QD surface has also been explored, giving access to dual-mode imaging agents (with Gd) or to biluminescent (with Eu, Yb) probes. In the latter case, the sensitization of Yb NIR luminescence by InP-based QDs has been firstly demonstrated. Finally, we carried out nanotoxicological studies on the different types of QDs used. In particular we investigated *in vivo* toxicity using the model organism *Hydra Vulgaris* and *in vitro* toxicity using human keratinocyte cells comparing core and core/shell InP-based and CdSe-based QDs.